ISTANBUL TECHNICAL UNIVERSITY ★ GRADUATE SCHOOL OF SCIENCE ENGINEERING AND TECHNOLOGY

PREPARATION AND CHARACTERIZATION OF MAGNETIC NANOPARTICLES WITH ANCHORED ANTIBODIES FOR BIOMARKER SEPARATION FROM BODY FLUIDS

M.Sc. THESIS

Elvan DEMİRBAĞ

Department of Chemical Engineering

Chemical Engineering Programme

JANUARY 2013

ISTANBUL TECHNICAL UNIVERSITY ★ GRADUATE SCHOOL OF SCIENCE ENGINEERING AND TECHNOLOGY

PREPARATION AND CHARACTERIZATION OF MAGNETIC NANOPARTICLES WITH ANCHORED ANTIBODIES FOR BIOMARKER SEPARATION FROM BODY FLUIDS

M.Sc. THESIS

Elvan DEMİRBAĞ
(506081031)

Department of Chemical Engineering

Chemical Engineering Programme

Thesis Advisor: Prof. Dr. Özgül Özcan TAŞPINAR

JANUARY 2013

İSTANBUL TEKNİK ÜNİVERSİTESİ ★ FEN BİLİMLERİ ENSTİTÜSÜ

VÜCUT SIVILARINDAN BİYOGÖSTERGE AYRIMI İÇİN ANTİKOR BAĞLI MAGNETİK NANOPARTİKÜL ÜRETİMİ VE KARAKTERİZASYONU

YÜKSEK LİSANS TEZİ

Elvan DEMİRBAĞ
(506081031)

Kimya Mühendisliği Anabilim Dalı

Kimya Mühendisliği Programı

Tez Danışmanı: Prof. Dr. Özgül Özcan TAŞPINAR

OCAK 2013

Elvan DEMİRBAĞ, a **M.Sc.** student of ITU **Graduate School of Science, Engineering and Technology**, student ID 506081031, successfully defended the **thesis** entitled "**PREPARATION AND CHARACTERIZATION OF MAGNETIC NANOPARTICLES WITH ANCHORED ANTIBODIES FOR BIOMARKER SEPARATION FROM BODY FLUIDS**", which she prepared after fulfilling the requirements specified in the associated legislations, before the jury whose signatures are below.

Thesis Advisor :	**Prof. Dr. Özgül Özcan TAŞPINAR** İstanbul Technical University	**.....**
Thesis Co-advisor :	**Assoc. Prof. Petr Kačer Ph.D** Institute of Chemical Technology, ICT Prague	**.....**
Jury Members :	**Prof. Dr. Güldem ÜSTÜN** İstanbul Technical University	**.....**
	Doç. Dr. Sibel SARGUT Marmara University	**.....**

Date of Submission : 17 December 2012
Date of Defense : 23 January 2013

To my beloved mother,

FOREWORD

I would like to thank Adéla PANKRÁCOVÁ, M.Sc., for her encouragement, advice and support throughout my master of science thesis. I also thank Assoc. Prof. Dr. Petr KAČER for his supervision and helpful discussions in magnetic nanoparticles. Thanks to everyone I have worked alongside during my M.Sc. in the Department of Organic Technology, ICT Prague. In particularly I would like to thank Kateřina ŠIMKOVÁ, M.Sc., Kamila SYSLOVÁ, M.Sc., and Yulia Belyaeva for their helps in the laboratory.

I would also like to thank my supervisor in Turkey, Prof. Dr. Özgül Özcan TAŞPINAR and RNDr. Oldřich BENADA, PhD., from the Academy of Sciences of the Czech Republic, for his helps with the transmission electron microscopy (TEM).

Finally, I would like to thank my beloved mother, Hatice DEMİRBAĞ for her constant support and for always being there.

January 2013

Elvan DEMİRBAĞ
(Chemical Engineer)

TABLE OF CONTENTS

Page

ABBREVIATIONS

8-iso $PGF_{2\alpha}$: 8-iso Prostaglandin $F_{2\alpha}$
8-iso $PGF_{2\alpha}$-d_4 : Deuterium Labelled 8-iso Prostaglandin $F_{2\alpha}$
acac : Acetylacetonate
AOT : Dioctyl Sodium Sulfosuccinate
BSA : Bovine Serum Albumin
ca. : Circa
CID : Collision-Induced Dissociation
Cup : *N*-nitrosophenylhydroxylamine
Cys-LTs : Cysteinyl Leukotrienes
DMSA : 2,3-dimercaptosuccinic Acid
EBC : Exhaled Breath Condensate
EIA : Enzyme Immunoassay
ELISA : Enzyme-Linked Immunosorbent Assay
ESI : Electro-Spray Ionization
Fab : Fragment: Antigen Binding
Fc : Fragment: Crystallizable
fcc : Face-Centered Cubic
FTIR : Fourier Transform Infrared Spectroscopy
GC–MS : Gas Chromatography–Mass Spectrometry
HPLC : High-Performance Liquid Chromatography
I : Ionic Strength
LC–MS : Liquid Chromatography–Mass Spectrometry
LOD : Limit of Detection
LOQ : Limit of Quantification
LTB_4 : Leukotriene B_4
LTC_4 : Leukotriene C_4
LTC_4-d_5 : Deuterium Labelled Leukotriene C_4
LTD_4 : Leukotriene D_4
LTD_4-d_5 : Deuterium Labelled Leukotriene D_4
LTE_4 : Leukotriene E_4
LTE_4-d_5 : Deuterium Labelled Leukotriene E_4
LTs : Leukotrienes
MeOH : Methanol
MN-8-iso $PGF_{2\alpha}$: Magnetic Nanoparticles with Anchored Antibodies Against 8-iso Prostaglandin $F_{2\alpha}$
MN-Cys-LTs : Magnetic Nanoparticles with Anchored Antibodies Against Cysteinyl Leukotrienes
MNPs : Magnetic Nanoparticles
MRI : Magnetic Resonance Imaging
OA : Oleic Acid
PAA : Poly(acrylic acid)
PAHs : Polycyclic Aromatic Hydrocarbons
PBS : Phosphate-Buffered Saline

PEG : Poly(ethylene glycol)
PMAA : Poly(methacrylic acid)
PVA : Poly(vinyl alcohol)
PVP : Poly(vinyl pyrrolidone)
RE : Relative Error
RIA : Radioimmunoassay
ROS : Reactive Oxygen Species
RSD : Relative Standard Deviation
SD : Standard Deviation
SPE : Solid-Phase Extraction
SPIO : Superparamagnetic Iron Oxide
SPION : Superparamagnetic Iron Oxide Nanoparticles
SRM : Selected Reaction Monitoring
TEM : Transmission Electron Microscopy
THF : Tetrahydrofuran
TMAOH : Tetramethylammonium Hydroxide
TRIS : Tris (hydroxymethyl) aminomethane
XRD : X-ray Powder Diffraction

LIST OF TABLES

Page

LIST OF FIGURES

Page

PREPARATION AND CHARACTERIZATION OF MAGNETIC NANOPARTICLES WITH ANCHORED ANTIBODIES FOR BIOMARKER SEPARATION FROM BODY FLUIDS

SUMMARY

In this study, magnetic iron oxide nanoparticles, magnetite (Fe_3O_4) were synthesized through the co-precipitation method of ferrous (Fe^{2+}) and ferric (Fe^{3+}) aqueous solutions by addition of a base (NH_4OH) with the mole ratio of Fe^{2+}/Fe^{3+} : 1/2. To prevent the agglomeration among the particles oleic acid was used, and thus the magnetic nanoparticles were stabilized. Then chitosan was added to coat on the surface of the Fe_3O_4 nanoparticles as a polymeric shell. The amino groups on the chitosan were cross-linked using glutaraldehyde, and finally the magnetic Fe_3O_4–chitosan nanoparticles were obtained. X-ray diffraction pattern indicated that the magnetic nanoparticles were pure Fe_3O_4 with an average diameter of about 5.7 nm. TEM results showed that the magnetic Fe_3O_4–chitosan nanoparticles were quasi-spherical with a mean diameter of about 8.4 nm. The binding of oleic acid, chitosan and glutaraldehyde onto the surface of the magnetic Fe_3O_4 nanoparticles was confirmed by FT-IR.

After synthesizing the magnetic Fe_3O_4–chitosan nanoparticles, the immunomagnetic nanoparticles were prepared by immobilizing antibodies on the surface of the particles by covalent bonding. TEM images demonstrated that the magnetic Fe_3O_4–chitosan nanoparticles were successfuly anchored with antibodies. These immunomagnetic nanoparticles were used to separate cysteinyl leukotrienes (Cys-LTs: LTC_4, LTD_4, and LTE_4) and 8-iso Prostaglandin $F_{2\alpha}$ (8-iso $PGF_{2\alpha}$), which are essential biomarkers of asthma and oxidative stress present in exhaled breath condensate (EBC), respectively. The principle of separation method was based on forming an antibody-antigen (antibody-biomarker) interaction owing to antibody's ability to form a specific complex with antigens and isolating targeted molecules by applying an external magnetic field.

The Cys-LTs and 8-iso $PGF_{2\alpha}$ biomarkers, which were treated like antigens in the study, were then uncoupled from the resulting antibody-antigen complexes by glycine solution through magnetic separation. The amount of separated molecules was measured by a highly selective and sensitive detection method: high performance liquid chromatography–mass spectrometry (HPLC-MS).

The analytical procedure was optimized, validated and analytically tested on real EBC samples collected from patients diagnosed with two sub-types of bronchial asthma (occupational asthma and hard-to-treat asthma) and on the control group of healthy subjects.

VÜCUT SIVILARINDAN BİYOGÖSTERGE AYRIMI İÇİN ANTİKOR BAĞLI MAGNETİK NANOPARTİKÜL ÜRETİMİ VE KARAKTERİZASYONU

ÖZET

Bronşiyal astım, tüm dünyada çocukları ve yetişkinleri etkileyen halk sağlığı sorunlarının başında gelmektedir. Astımın dünyada yaklaşık 300 milyon, ülkemizde ise 3.5 milyon kişiyi etkilediği düşünülmektedir. Solunum yolu enflamasyonu ve duyarlılığı astım oluşumunda anahtar rol oynayan temel mekanizmalardır. Bu enflamasyon, gece ve sabah erken saatlerde sık görülen öksürük ile beraber tekrarlayan hırıltılı solunum, nefessiz kalma ve göğüs sıkışmasına sebep olur. Bir astım atağı esnasında, solunum yolları kasların büzülmesi sebebiyle aşırı derecede daralır, iç katmanlar şişer ve mukus üretir. Bu tekrarlayan ataklar, limitli hava geçişine sebebiyet vererek beklenmeyen ölümlere yol açabilir. Bronşiyal astımın tetikleyicileri üç gruba ayrılabilir: 1) genetik yatkınlık ve bağışıklık sistemi gibi içsel faktörler, 2) alerjenler (polen, küf sporları, toz ya da hayvan tüyü), kapalı ve açık mekanlardaki kirleticiler ve tahriş edici maddeler (sigara, parfüm, temizlik maddeleri, vb.) gibi dış faktörler, 3) fiziksel faktörler (özellikle egzersiz ve soğuk hava) ve stres, gastroözofageal reflü hastalığı (GERD) ya da viral ve bakteriyel üst solunum yolu enfeksiyonu gibi fizyolojik faktörlerdir.

Astımın görülme sıklığı, 1995-2010 yılları arasında % 95, yine aynı süreçte 5 yaş altı çocuklarda ise % 190'dan fazla artış göstermiştir. 2025 yılına kadar astımlı insan sayısının 100 milyon kişi daha artacağı tahmin edilmektedir. Bu sebeplerden ötürü, doğru ve erken astım teşhisi ve tedavisi önem kazanmaktadır. Bununla beraber, astım hastalığında teşhis koymak zordur. Günümüzde, astım teşhisi için kesin bir fizyolojik, immünolojik ya da histolojik bir test bulunmamaktadır. Astım teşhisinde, olası aynı semptomları gösteren diğer hastalıkları bertaraf etmek için, genellikle ilk olarak akciğer fonksiyonları test edilir. Akciğer fonksiyonlarını ölçmede kullanılan testler içerisinde spirometre testi, metakolin ya da histamin zorlama testi ve azot oksit testi yer almaktadır. Halihazırda, akciğerlerdeki enflamasyonun ölçümü açık akciğer biyopsisi, bronkoalveoler lavaj sıvısının incelenmesi gibi girişimsel (invasive), indüklenmiş sputum metodu gibi yarı-girişimsel ya da plazma ve idrardaki enflamatuvar göstergelerin ölçümü gibi girişimsel olmayan yöntemlere dayanmaktadır.

Biyolojik gösterge (biyogösterge), biyolojik ya da patofizyolojik proseslerin fiziksel bir göstergesidir. Biyogöstergeler teşhis koyma, hastalık evrelendirme ve hastalık aktivitesi/ilerleyişini görüntüleme gibi çeşitli amaçlar için kullanılabilir. Özellikle, küçük çocuklarda, güvenilir ve girişimsel olmayan biyogöstergeler çok önemli olabilmektedir. Ayrıca, biyogöstergeler klinik belirti ve semptomlar ya da patofizyolojik ölçümler gibi geleneksel hastalık göstergelerine tamamlayıcı bilgiler sağlayabilirler. Astımla ilişkili çok sayıda biyogöstergenin olduğu ve bunların solunum yollarındaki karmaşık enflamasyonu yönettikleri bilinmektedir. Bu biyogöstergeler girişimsel olmayan ya da yarı-girişimsel solunum yolu örnek

toplama yöntemleriyle elde edilebilir. Alt solunum yollarından, yoğunlaştırılmış soluk havasının (EBC; exhaled breath condensate) eldesi tamamen girişimsiz (non-invasive) bir örnek toplama tekniğidir. EBC, akciğerler ve solunum yollarının durumunu direkt olarak yansıtan bronkoalveoler ekstrasellüler sıvısının belirli bir bileşimini gösterir ve soluk havasının soğutulup yoğunlaştırılması ile elde edilir. EBC, akciğerlerdeki asit stresin, oksidatif stresin ve enflamasyonun biyogöstergeleri olan sisteinil lökotrienler (Cys-LTs: LTC_4, LTD_4, LTE_4), prostaglandinler (8-iso Prostaglandin $F_{2\alpha}$), histamin, adenozin gibi molekülleri içerir. Literatürdeki birçok çalışmada, EBC'deki bu çeşitli enflamatuvar moleküller, olası astım biyogöstergesi olarak araştırılmış ve araşidonik asit türevlerinin (lökotrienler, prostaglandinler) astımlı hastaların EBC'sinde yüksek seviyelerde olduğu gözlemlenmiştir. Bu nedenle, bu biyogöstergelerin klinik tespit ve ölçümlerinin astım teşhisinde kullanılabileceği düşünülmüştür.

Lökotrienler, bronş mukozasında eozinofil, bazofil ve mast hücresi gibi enflamatuvar hücrelerinde sentezlenen ve astım oluşumunda önemli rolleri olan biyogöstergelerdir. Lökotrienlerin bir alt grubu olan sisteinil lökotrienler çok güçlü bronş daraltıcı maddeler olup astım hastalarının solunum yollarında akut ve kronik yapısal bozukluklara neden olabilirler. Son dönemlerde, astım hastalarının bronkoalveoler lavaj sıvısı ve balgamlarında yüksek sisteinil lökotrien (LTC_4, LTD_4, LTE_4) seviyelerine rastlanmıştır.

8-iso Prostaglandin $F_{2\alpha}$ (8-isoprostan, 8-iso $PGF_{2\alpha}$), araşidonik asitin hücre yüzeyinde oksijen radikalleri aracılığıyla enzimatik olmayan direkt oksidasyonu ile üretilen bir moleküldür. 8-iso Prostaglandin $F_{2\alpha}$, genellikle oksidatif stresin ve antioksidan eksikliğinin önemli bir biyogöstergesi olarak kabul edilir. EBC'deki 8-isoprostan seviyesi, yetişkin astım hastalarında artış göstererek hastalığın şiddeti ve enflamasyonun derecesi hakkında bilgi verir.

Bu çalışmada, kompleks biyolojik matriksler içerisinden astım biyogöstergelerini ayırmada kullanılabilecek antikor bağlanmış magnetik demir oksit (Fe_3O_4: magnetit) nanopartikülleri sentezlenmiştir. Sentez aşamasında, molce 1'e 2 oranında demir (II) sülfat ve demir (III) klorür çözeltileri ile amonyum hidroksit (NH_4OH) reaksiyona sokulmuştur. Nanopartiküllerin stabilizasyonu için oleik asit, yüzey işlevselleştirilmesi için kitosan (chitosan) ve çapraz bağlama reaksiyonu için de glutaraldehid kullanılmıştır. Sentezlenen nanopartiküllerin karakterizasyonu FT-IR, XRD ve TEM kullanılarak gerçekleştirilmiş ve magnetit nanopartiküllerinin kitosan ve glutaraldehid ile birlikte başarılı bir şekilde sentezlendiği saptanmıştır.

Sonraki aşamada, üretilen bu nanopartiküllere antikor (*anti*-Cys-LTs ya da *anti*-8-iso $PGF_{2\alpha}$) eklenmiş ve bu şekilde işlevselleştirilen nanopartiküller, Cys-LTs ve 8-iso $PGF_{2\alpha}$ moleküllerini bulundukları ortamdan ayırmada kullanılabilecek hâle getirilmiştir. Nanopartiküllerin antikor ile işlevselleştirilmiş bu formları "immünomagnetik nanopartikül", bu partiküllerle gerçekleştirilen ayırma işlemi de "immünomagnetik ayırma yöntemi" olarak adlandırılmaktadır.

Çalışmadaki ayırma prensibi, magnetik nanopartiküllere bağlanmış olan antikorlar ile matrikste (EBC) bulunan antijenler (biyogösterge) arasında spesifik bir kompleks oluşturma ve bu kompleksin güçlü bir mıknatıs yardımıyla bulunduğu ortamdan ayrılmasına dayanmaktadır.

Oluşturulan kompleksten biyogöstergelerin ayrılması glisin çözeltisi ve mıknatıs yardımıyla gerçekleştirilir. EBC'de bulunan bu biyogöstergeler (Cys-LTs, 8-iso $PGF_{2\alpha}$) çok düşük konsantrasyonlarda (pg/ml) olduğundan bu moleküllerin miktar

tayinlerinde oldukça hassas ve seçici analitik yöntemlere ihtiyaç duyulmaktadır. Bu nedenle, bu biyogöstergelerin miktarları yüksek performanslı sıvı kromatografisi ile birleştirilmiş kütle spektrometre cihazı (HPLC-MS) ile saptanmıştır.

Bu çalışmada uygulanan analitik prosedür optimize edilmiş ve optimum koşullar doğrulanmıştır. Daha sonra bu yöntem, astım teşhisi konmuş hastalardan ve kontrol grubunu oluşturan sağlıklı bireylerden alınan gerçek EBC örnekleri üzerinde analitik olarak da test edilmiştir.

1. INTRODUCTION

Asthma is one of the most common chronic pulmonary diseases with 300 million people suffering from it and 250,000 attributed annual deaths. It is characterized by reversible airflow obstruction, airway remodeling, and inflammation which is biased toward Th2 cytokine production and involves mast cells, eosinophils, lymphocytes, macrophages and neutrophils [1,2].

Bronchial asthma, defined as a chronic inflammatory disorder of the airways, is one of the top public health problems globally affecting both children and adults [2]. The chronic inflammation is associated with airway hyperresponsiveness that leads to recurrent episodes of wheezing, breathlessness, chest tightness, and coughing, particularly at night or in the early morning [3].

The prevalence of asthma increased by 95 % from 1995 to 2010 and the asthma rates in children under the age of five increased by more than 190 % from 1995 to 2010. It is estimated that the number of people with asthma will grow by more than 100 million by 2025. Therefore proper and early diagnostics and treatment is necessary. However, the diagnostics can be rather difficult. Currently, there is no precise physiological, immunological, or histological test for diagnosing asthma. In order to rule out other possible conditions, the lung functions are generally tested first in an asthma diagnosis process. Tests to measure the lung functions include spirometry test, peak expiratory flow rate test, methacholine or histamine challenge tests and nitric oxide test. At present, quantification of inflammation in the lungs is based on invasive (open lung biopsy, bronchoalveolar lavage) or semi-invasive methods (method of induced sputum) and the measurement of inflammatory markers in plasma and urine, which are likely to reflect systemic rather than lung inflammation [2].

A biological marker (biomarker) is a physical sign or laboratory measurement that can serve as an indicator of biological or pathophysiological processes or as a response to a therapeutic intervention. Biomarkers can be employed for various

purposes, including diagnosis, staging and monitoring of disease activity/progression or predictors c.q. monitors of a treatment response. Especially in (young) children, reliable, non-invasive biomarkers would be valuable. In addition, they can provide complementary information to traditional disease markers, such as clinical signs and symptoms or pathophysiological measures [4].

Presently, there are several biomarkers for asthma that can be obtained by non-invasive or semi-invasive airway sampling methods. Collection of exhaled breath condensate (EBC) is a fully non-invasive sampling technique of the lower airways [4]. EBC is a liquid matrix that reflects the particular composition of the bronchoalveolar extracellular lung liquid, which replicates the conditions proceeding directly in the lungs and airways. The substances are contained in the exhaled breath in both gaseous and liquid phases (aerosol form). The aerosol particles (non-volatile components, including various water-soluble inflammatory markers) and the substances present in the gaseous phase (volatile substances such as nitric oxide (NO) and carbon dioxide (CO_2)) could be condensed by breathing over a condenser, which is readily available at specialized clinical facilities. In the obtained liquid, typically known as EBC, more than 1000 compounds have been identified so far, out of which a substantial number are considered to represent sensitive biomarkers of lung diseases [5,4].

EBC contains many biomarkers of oxidative and nitrative stress (8-iso Prostaglandin $F_{2\alpha}$, thiobarbituric acid, 3-nitrotyrosine, S-nitrosothiols, etc.) as well as mediators of inflammation processes (leukotriene B_4: LTB_4, cysteinyl leukotrienes (Cys-LTs): LTC_4, LTD_4, LTE_4, prostaglandins, histamine, adenosine, interleukins, etc.) [6]. Oxidative stress -an imbalance between increased exposure to reactive oxygen species (ROS) and antioxidant defences- is thought to contribute to the chronic inflammatory process that characterises asthma [7]. It can result in a free radical-induced damage of cell membranes, proteins or structures with genetic significance that are oxidized by ROS. Among them the most prominent are superoxide anion (O_2^-) and the hydroxyl radical (OH^-). Their natural physiological role is to defend the organism against a microbial attack. ROS are generated in large concentrations by activated granulocytes and can potentially damage any cellular structure. 2-5 % of the oxygen amount, typically exchanged during respiration, is used to produce ROS in mitochondria. Their activity is under standard conditions well balanced by the

antioxidant system. However, this system can be impaired or exhausted by a disease or environmental conditions. Uncontrolled ROS activity leads to the organism damage by oxidative stress in a target organ (such as lungs), or a systemic damage in many organs, caused by atherosclerosis or diabetes. It can harm important bio-macromolecules as lipids, proteins, enzymes, DNA and thus affect physiological processes and/or cause cell death [8].

Various inflammatory markers present in EBC have been investigated as possible asthma biomarkers and several independent studies have indicated the presence of elevated levels of arachidonic acid derivatives (Cys-LTs, LTB_4, 8-iso Prostaglandin $F_{2\alpha}$) in EBC of asthma patients. Therefore, measurements of these mediators are considered potentially effective in the establishment of asthma diagnosis in a large cohort [2].

Leukotrienes, a family of lipid mediators derived from arachidonic acid through the 5-lipoxygenase pathway, are potent constrictors and proinflammatory mediators that have been shown to have a role in asthma pathophysiology [9], (Fig. 1.1).

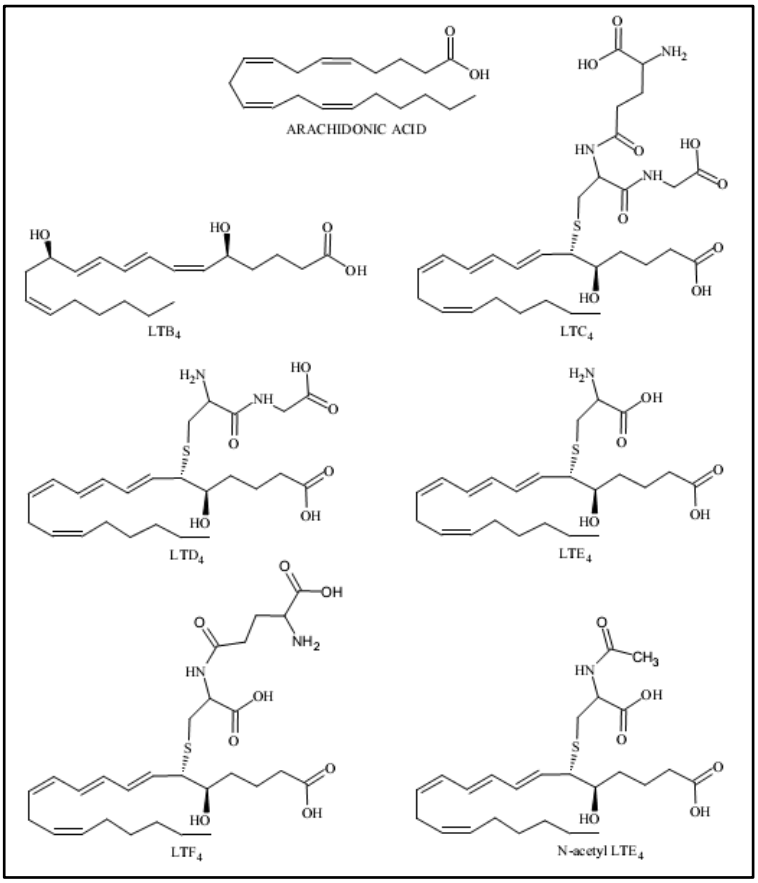

Figure 1.1 : Arachidonic acid derivatives - potential biomarkers of bronchial asthma [2].

The cysteinyl leukotrienes (Cys-LTs: LTC_4, LTD_4, and LTE_4) are generated mainly by mast cells and eosinophils and are able to contract airway smooth muscle and increase mucus secretion and vascular permeability and recruit eosinophils. Increased levels of Cys-LTs have been found in bronchoalveolar lavage and induced sputum of asthmatic patients. Recently, higher levels of leukotrienes have also been found in EBC of asthmatic adults and children [9].

8-iso Prostaglandin $F_{2\alpha}$ (=8-isoprostane) is produced *in vivo* by non-enzymatic direct oxidation of arachidonic acid on the cell surface by oxygen radicals (Fig. 1.2). It is generally accepted as a significant biomarker of oxidative stress [6] and antioxidant deficiency [10].

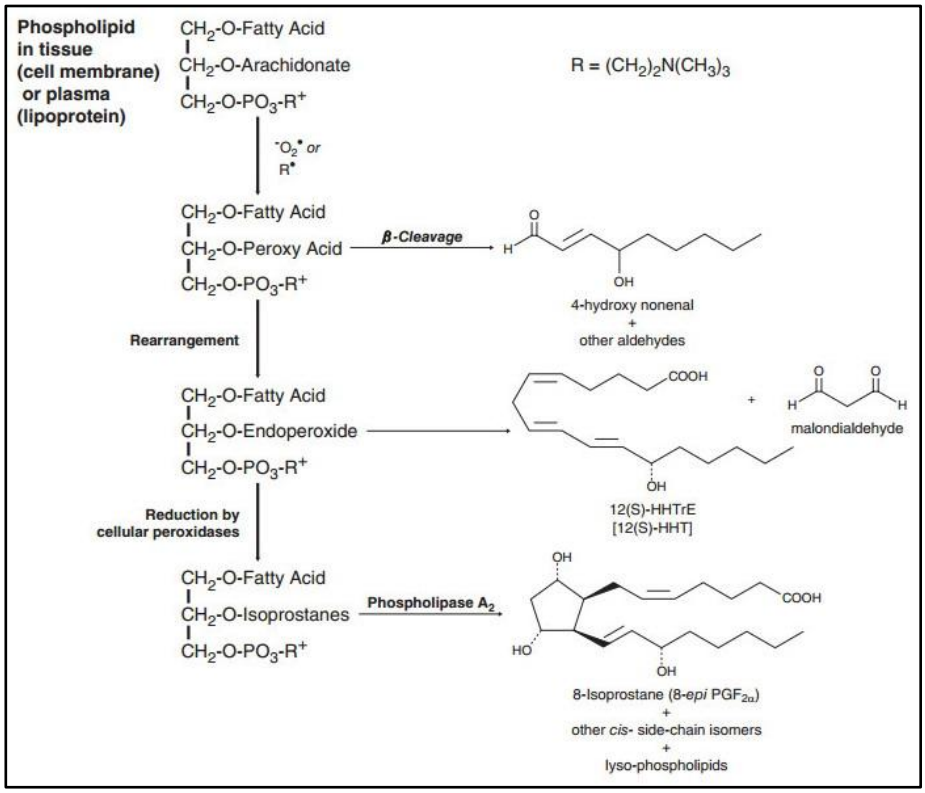

Figure 1.2 : The formation of 8-isoprostane [10].

Concentrations of 8-isoprostane in EBC are increased in adults with stable asthma, reflecting the severity of the disease and the degree of inflammation [11]. 8-isoprostane levels are also a relative indicator of sample integrity for lipid-containing samples such as serum, plasma, and whole cell preparations. Plasma from healthy volunteers contains modest amounts of 8-isoprostane (40-100 pg/ml) that increase with the age of the test subject. Normal human urinary levels range from 10-50 ng/mmol creatinine, which is an order of magnitude higher than many enzymatically

derived eicosanoids [10]. Isoprostanes have different biological effects within the respiratory system, suggesting that they may also function as pathophysiological mediators of oxidant injury in asthma (Fig. 1.3) [7].

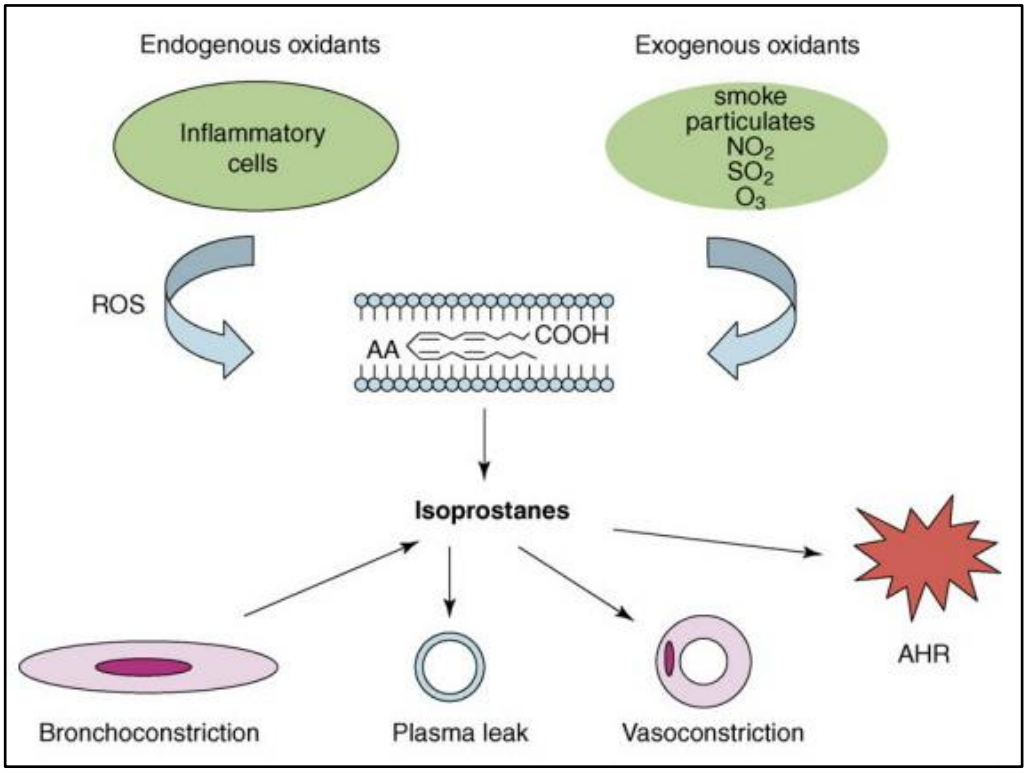

Figure 1.3 : Biological effects of the isoprostanes in the respiratory system [7][1].

In patients with asthma, airway inflammatory cells including eosinophils, Th2 lymphocytes, neutrophils and macrophages release increased amounts of reactive oxygen species (ROS). These, in turn, cause peroxidation of arachidonic acid in the plasma membrane phospholipids with subsequent production of isoprostanes. Environmental oxidants can contribute to isoprostane production. Biological effects of isoprostanes are compound, species and tissue specific [7].

8-iso Prostaglandin $F_{2\alpha}$ as well as the other biomarkers are often detected in EBC at levels as low as picograms per milliliter. However, the quantification of extraordinarily low concentrations of 8-iso Prostaglandin $F_{2\alpha}$ and leukotrienes in EBC requires highly sensitive analytical methods. In the past, RIA (Radioimmunoassay), EIA (Enzyme Immunoassay), ELISA (Enzyme Linked Immunosorbent Assay) and GC–MS (Gas chromatography–mass spectrometry) analytical techniques had been used for this task [6,5].

[1] ROS: reactive oxygen species; AA: arachidonic acid; AHR: airway hyperresponsiveness; NO_2: nitrogen dioxide; O_3: ozone; SO_2: sulfur dioxide.

During the last decade, LC-MS/MS has become the technique of choice for the trace analysis of various compounds contained in complex biological matrices (plasma, urine, cerebrospinal fluid, bronchoalveolar lavage fluid, etc.). It has been successfully applied for the detection and quantification of EBC markers. In comparison with biochemical methods, connecting liquid or gas chromatography to mass spectrometry not only offers precise quantitative data but also structural information (qualitative information) [6,5].

In this study, biomarker (8-iso $PGF_{2\alpha}$ and Cys-LTs) extraction from samples was provided by magnetic Fe_3O_4–chitosan nanoparticles with anchored antibodies. Highly specific reactions between antigens (8-iso $PGF_{2\alpha}$ and Cys-LTs) and antibodies were formed and the resulting antigen-antibody complexes were separated from the solution by using an external magnetic field. For the quantification and detection of biomarkers, a highly selective and sensitive method by LC-ESI-MS/MS was applied. For its extremely high degree of selectivity, the selected reaction monitoring (SRM) mode with collision-induced dissociation (CID) was used. The analytical procedure of immunomagnetic separation was tested on real EBC samples collected from patients diagnosed with two sub-types of bronchial asthma (occupational asthma and hard-to-treat asthma) and on the control group of healthy subjects.

2. THEORETICAL PART

2.1 Magnetic Nanoparticles

Nanotechnology is the understanding and control of matter at the nanoscale, at dimensions between approximately 1 and 100 nanometers, where unique phenomena enable novel applications. A nanometer is one billionth of a meter [12], (Fig. 2.1).

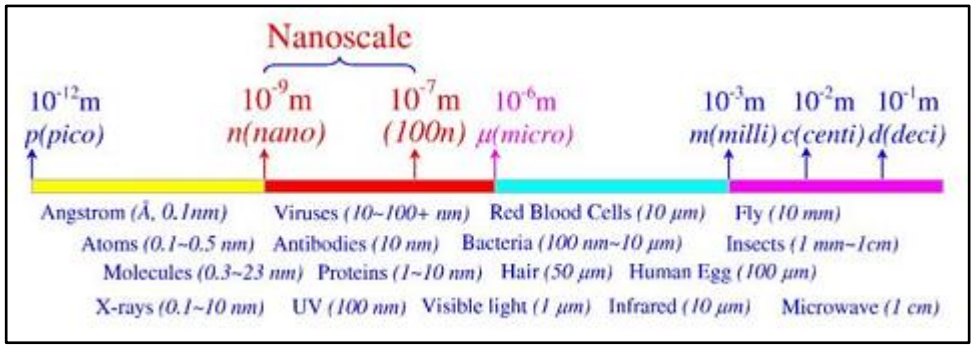

Figure 2.1 : Nanoscale and typical materials whose dimension ranges are comparable to nanoscale [13].

At the nanometer scale, the physical, chemical, and biological properties of materials differ in fundamental and valuable ways from the properties of individual atoms and molecules or bulk matter [14].

Nanoparticles are essential part of our natural environment, modern science, and high technology. Magnetic nanoparticles are most common and very promising for applications [15]. Magnetic nanoparticles will rotate under an external uniform magnetic field, and will make translational movements under an external magnetic field gradient. Therefore, magnetic nanoparticles, or magnetically tagged molecules, can be manipulated by applying an external magnetic field [16].

Among a wide range of the magnetic nanomaterials, nanoparticles of magnetic metals (Fe, Co, Ni), simple and complex magnetic oxides (Fe_3O_4, Fe_2O_3, FeO, FeOOH, Co_3O_4, NiO), and alloys (Fe-Co, Fe-Ni, Fe-Pt, Co-Pt) may be separated. Most magnetic materials used in today's technology are either metals or metal oxides. Iron is a ferromagnetic material with high magnetic moment density (about

220 emu/g) and is magnetically soft [15]. Highly magnetic materials such as cobalt and nickel are toxic, susceptible to oxidation and hence are of little interest [17].

Iron oxides are composed of Fe together with O and/or OH. The iron oxides are common compounds which are widespread in nature and readily synthezised in the laboratory. They are present in almost all of the different compartments of the global system: from atmosphere to lithosphere [18]. The iron oxides are also present in living organisms (e.g. plants, bacteria, molluscs, birds and humans). Fe(II) complexes are the active center of haemoglobin and ferredoxins, and various biomineralization processes involve Fe(II) and Fe(III) species for the regulation of iron concentration in organism (ferritin) or, in various occurrences, to produce different oxides, such as goethite, magnetite, lepidocrocite [19].

Iron oxide magnetic nanoparticles tend to be either paramagnetic or superparamagnetic, with particles approximately 20 nm being classed as superparamagnetic. In most cases superparamagnetic particles (usually Fe_2O_3 and Fe_3O_4) are of interest for *in vivo* applications, as they do not retain any magnetism after removal of the magnetic field. This is important as large domain magnetic and paramagnetic materials aggregate after exposure to a magnetic field [20].

Magnetic particles with suitable surface characteristics have potential applications both *in vitro* and *in vivo*. In almost all applications, the preparation and surface modification of magnetic particles present significant challenges in determining the particle size and shape, the size distribution, the surface chemistry and consequently the magnetic properties of the particles, all important for application in biomedicine [17]. Magnetic nanoparticles can bind to drugs, proteins, enzymes, antibodies, or nucleotides and can be directed to an organ, tissue, or tumour using an external magnetic field or can be heated in alternating magnetic fields for use in hyperthermia [21].

Though magnetic nanoparticles with different compositions, sizes and shapes have been developed for biomedical applications, the most frequently used magnetic materials are two types of iron oxide particles, magnetite (Fe_3O_4) and maghemite (γ-Fe_2O_3) [16].

2.1.1 Magnetite (Fe_3O_4)

Magnetite, Fe_3O_4 ($FeO.Fe_2O_3$), is a black, ferrimagnetic mineral containing both Fe^{II} and Fe^{III} [18], (Fig. 2.2).

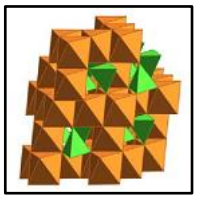

Figure 2.2 : Magnetite (Fe_3O_4) [22].

Magnetite is a common magnetic iron oxide that has a cubic inverse spinel structure with oxygen forming an fcc closed packing and Fe cations occupying interstitial tetrahedral sites and octahedral sites [21], (Fig. 2.3).

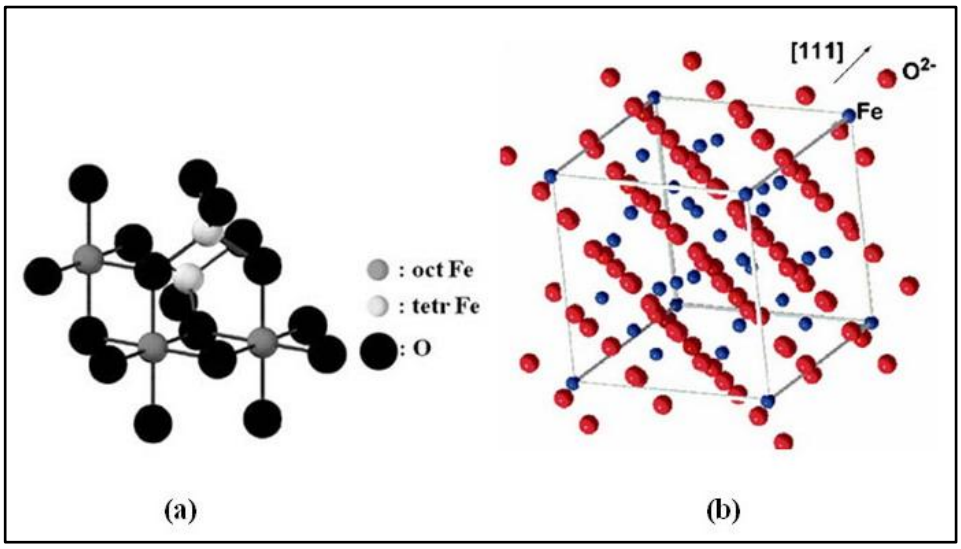

Figure 2.3 : Crystal structures of magnetite [23,24].

In magnetite (Fe_3O_4), iron ions are distributed into the octahedral (O_h) and tetrahedral (T_d) sites of the fcc stacking of oxygen according to ($[Fe^{3+}]_{Td}[Fe^{3+}Fe^{2+}]_{Oh}O_4$) [19], Formula 1:

$$Fe_3O_4 : [Fe^{3+}]_{Td}[Fe^{3+}\,Fe^{2+}]_{Oh}O_4$$

Formula 1: Structure of magnetite [25].

Magnetite is characterized by a fast electron hopping between the iron cations (Fe^{2+} and Fe^{3+} ions) on the octahedral sublattice [19]. It is frequently non-stoichiometric in which case it has a cation deficient Fe^{III} sublattice. In stoichiometric magnetite Fe^{II}/Fe^{III} = 0.5 [18]. At the stoichiometry Fe^{2+}/Fe^{3+} = 0.5, crystallisation of spinel

phase is quasi-immediate at room temperature [26] and electron transfer between Fe^{2+} and Fe^{3+} ions plays a fundamental role in the process [19]. Table 2.1 shows the physical and magnetic properties of magnetite.

Table 2.1 : Physical and magnetic properties of magnetite [18,23]**.**

Property	**Magnetite**
Molecular formula	Fe_3O_4
Density (g/cm^3)	5.18
Melting point (°C)	1583-1597
Boiling point (°C)	2623
Hardness	5.5
Type of magnetism	Ferrimagnetic
Curie temperature (K)	850
M_S at 300 K ($A\text{-}m^2/kg$)	92-100
Standard free energy of formation $\Delta G_f°$ (kJ/mol)	-1012.6
Crystallographic system	Cubic
Structural type	Inverse spinel
Space group	Fd3m
Lattice parameter (nm)	a = 0.8396

2.2 Synthesis of Magnetic Nanoparticles

Numerous chemical methods can be used to synthesize magnetic nanoparticles for medical imaging applications: microemulsions, sol-gel syntheses, sonochemical reactions, hydrothermal reactions, hydrolysis and thermolysis of precursors, flow injection syntheses, and electrospray syntheses. However, the most common method for the production of magnetite nanoparticles is the chemical coprecipitation technique of iron salts [25].

2.2.1 Classical synthesis by coprecipitation

Precipitation or coprecipitation of cations in aqueous solutions is an easy and cheap route of synthesis of metal oxide particles [26].

Iron oxides (either Fe_3O_4 or γ-Fe_2O_3) can be synthesized through the co-precipitation of ferrous (Fe^{2+}) and ferric (Fe^{3+}) aqueous salt solutions by addition of a base. Conventionally, magnetite is prepared by adding a base to an aqueous mixture of Fe^{2+} and Fe^{3+} chloride at a 1:2 molar ratio. The precipitated magnetite is black in colour. The overall reaction may be written as eq (2.1a) [21] and eq (2.1b) [27]:

$$Fe^{2+} + 2Fe^{3+} + 8OH^{-} \rightarrow Fe_3O_4 + 4H_2O \quad \textbf{(2.1a)}$$

$$FeCl_2 + 2FeCl_3 + 8NH_4OH \rightarrow Fe_3O_4 + 8NH_4Cl + 4H_2O \quad \textbf{(2.1b)}$$

According to the thermodynamics of this reaction, complete precipitation of Fe_3O_4 should be expected at a pH between 8 and 14, with a stoichiometric ratio of 2:1 (Fe^{3+}/Fe^{2+}) in a non-oxidizing oxygen environment [25].

Magnetite, Fe_3O_4 is easily obtained by coprecipitating aqueous Fe^{3+} and Fe^{2+} ions with x = 0.66 ($x = Fe^{3+}/(Fe^{2+} + Fe^{3+})$, the system composition). With x = 0.66, corresponding to stoichiometric magnetite, the mean particle size is monitored in the range 2–12 nm by the conditions of the medium (precipitation), pH and ionic strength (I) imposed by a salt [19].

However, magnetite (Fe_3O_4) is not very stable and is sensitive to oxidation due to the high electron mobility in the bulk and transformed into maghemite (γ-Fe_2O_3) in the presence of oxygen [22,25], eq (2.2) [27]:

$$4Fe_3O_4 + O_2 \rightarrow 6\gamma\text{-}Fe_2O_3 \quad \textbf{(2.2)}$$

Maghemite (γ-Fe_2O_3) has a structure similar to that of magnetite. It differs from magnetite in that all or most Fe is in the trivalent state. Cation vacancies compensate for the oxidation of Fe^{II} [18], Formula 2:

γ-$Fe_2O_3 : 0.75[Fe^{3+}]_{Td}[Fe_{5/3}{}^{3+}\,V_{1/3}]_{Oh}O_4$ (where V stands for a cationic vacancy)

Formula 2: Structure of maghemite [25].

In effect, maghemite does not form directly in solution by precipitation of ferric ions, but a small proportion of Fe^{2+} ($\geq$ 10 mol %) induces the crystallization of all the iron into spinel [19]. It is generally considered to result from the oxidation of stoichiometric or nearly stoichiometric magnetites [28].

Due to the oxidative instability of Fe^{2+} ions, it is required in some cases to execute the co-precipitation of iron ions in inert atmosphere (introduction of nitrogen gas into the reaction system). Despite this, several authors report about the successful synthesis of magnetite in the presence of oxygen [29].

Oxidation in air is not the only way to transform magnetite (Fe_3O_4) into maghemite (γ-Fe_2O_3) [25]. Jolivet and Tronc have shown that Fe_3O_4 can be transformed into γ-Fe_2O_3 without an oxidizing agent. It likely involves electron trapping in octahedral

surface sites [30]. Different mechanisms involving ionic and/or electronic interfacial transfers are implicated, depending on the pH of the suspension [26], according to eq (2.3) [25]:

$$Fe_3O_4 + 2H^+ \rightarrow \gamma\text{-}Fe_2O_3 + Fe^{2+} + H_2O \quad \textbf{(2.3)}$$

In basic medium, the oxidation of magnetite proceeds by oxygen reduction at the surface of particles (electron transfer only) and coordination of oxide ions, while in acidic medium and anaerobic conditions, surface Fe^{2+} ions are desorbed as hexaaquo complexes in solution (electron and ion transfer) according to eq (2.4) [22]:

$$[Fe^{3+}]_{Td}[Fe_2^{2.5+}]_{Oh}O_4 + 2\,H^+ \rightarrow 0.75[Fe^{3+}]_{Td}[Fe_{5/3}^{3+}V_{1/3}]_{Oh}O_4 + Fe^{2+} + H_2O \quad \textbf{(2.4)}$$

In both cases, the oxidation of Fe^{2+} ions is correlated with the migration of cations through the lattice framework, creating cationic vacancies in order to keep the charge balance [22], explaining the structure of maghemite [25].

Fe_3O_4 might also be oxidized as eq (2.5) [21]:

$$Fe_3O_4 + 0.25\,O_2 + 4.5\,H_2O \rightarrow 3Fe(OH)_3 \quad \textbf{(2.5)}$$

Oxidation would critically affect the physical and chemical properties of the nanosized magnetic particles. In order to prevent them from possible oxidation in air as well as from agglomeration, Fe_3O_4 nanoparticles produced by reaction (2.1b) are usually coated with organic or inorganic molecules during the precipitation process [21].

Magnetite nanoparticles, prepared by coprecipitation of Fe^{2+} and Fe^{3+} with NH_4OH, can be stabilized with silica to form well-dispersed magnetic silica nanospheres. The addition of chelating organic anions (carboxylate or α hydroxy carboxylate ions, such as citric, gluconic, or oleic acid) or polymer surface complexing agents (dextran, carboxydextran, starch, or polyvinyl alcohol) during the formation of magnetite can help to control the size of the nanoparticles [25].

The major advantage of precipitation reactions is that large quantities of particles can be synthesised. However, it is difficult to tailor the particle size as only kinetic factors are available to control growth [31].

Particles prepared by co-precipitation unfortunately tend to be rather polydisperse. It is well known that a short burst of nucleation and subsequent slow controlled growth is crucial to produce monodisperse particles [32].

Controlling these processes is therefore the key in the production of monodisperse iron oxide magnetic nanoparticles [32]. The properties of finely divided magnetic materials closely depend on the size of the particles and their state of dispersion and aggregation. It is therefore very important to carefully control the synthesis of particles and their surface state. In these conditions, well-defined materials regarding the crystal structure, the mean particle size, the size distribution, the morphology and the state of dispersion appear very difficult to obtain, because it is difficult to control the reactions [26].

Size, shape and composition of magnetic nanoparticles are dependent on;

- type of salts used (e.g. chlorides, sulphates, nitrates, etc.),
- ratio of Fe^{2+} and Fe^{3+},
- pH value,
- ionic strength of the reaction system [29].

The mean size is strongly dependent on the acidity and the ionic strength of the precipitation medium, and clearly decreases with increasing pH and I [26].

Another disadvantage of these bulk solution synthesis is that the pH value of the reaction mixture has to be adjusted in both the synthesis and purification steps. As a result, the production of significant quantities of narrowly dispersed, nanometer sized magnetic particles remains a significant challenge through these methods [21].

A wide variety of factors can be adjusted in the synthesis of iron oxide nanoparticles to control size, magnetic characteristics, or surface properties. A number of studies have dealt with the influence of these different factors [25].

Khalafalla and Reimers (1980) described a method to prepare dilution-stable aqueous magnetic fluids. The preparation method involved precipitation of mixed ferrous and ferric hydroxides followed by peptization of the colloidal magnetite particles with dodecanoic acid. In the method, $FeCI_2.4H_2O$, $FeCl_3.6H_2O$ and ammonium hydroxide (NH_4OH) were used. The mixture represented an initial molar ratio of Fe(III) to Fe(II) of 3:2. Dodecylamine was then added to the precipitate, and the mixture heated at 90°C for 4 minutes while stirring. The resulting magnetic fluid had a saturation magnetization of 200 gauss [33].

The first controlled preparation of superparamagnetic iron oxide particles using alkaline precipitation of $FeCl_3$ and $FeCl_2$ was performed by Massart (1981). The

Massart process described the coprecipitation without molecules for stabilization [25]. In this process, an aqueous mixture of ferric chloride and ferrous chloride were added to ammonia solution. The gelatinous precipitate was isolated from the solution by centrifugation or magnetic decantation without washing with water. There were two ways of treating this precipitate: alkaline sol and acidic sol. In these alkaline or acidic magnetic sols, iron concentrations higher than one molar could easily be obtained. A very peculiar observance was that a sol could be obtained only if the Fe(III)/Fe(II) ratio was larger than two (as in Fe_3O_4). It was observed that the size decreases when the pH and/or the initial ratio Fe(III)/Fe(II) increase [34].

In another study of E. Tronc et al. (1982), aqueous solutions of ferrous and ferric chloride were added to NH_3 in excess, at fixed pH and temperature. Various samples were obtained by varying only the Fe^{2+}/Fe^{3+} relative concentration at the initial step of the reaction. Electron micrographs confirmed that the particles were roughly spherical. All samples, as long as the Fe^{2+} initial concentration was not too low, exhibited X-ray diffraction patterns characteristic of the spinel structure. The cell parameters were in the range 8.375 - 8.36 Å [35].

After pioneer work being reported by Massart and Khalafalla, coprecipitation was widely studied in preparing magnetite nanoparticles for its extraordinary advantages, such as gram-scale production and facility. In fact, almost all the magnetite nanoparticles used in clinical research nowadays are prepared by classical coprecipitation, because their surface can be easily modified to be hydrophilic, which is suitable for biomedical applications [36].

Jolivet et al. reported an investigation of magnetite as a function of the initial Fe(II) level ($0.10 < x \leq 0.50$). Aqueous mixtures of $FeCl_3$ and $FeCl_2$ in various proportions were added to an NH_3 solution with vigorous stirring at room temperature. At any x value, all stable products exhibited the structure of (oxidized) magnetite [37].

Babes et al. have studied the influence of different parameters such as media composition, iron media, injection fluxes, Fe and tetramethylammonium hydroxide (TMAOH) concentrations, temperature, and oxygen on size, magnetic and magnetic resonance relaxometric properties, and colloidal stability of particles. They have determined the relative importance of these parameters as well as the optimal conditions for obtaining uncoated stable particles with an average size of 5 nm and

interesting relaxivities. Among the parameters, TMAOH concentration (0.25-2 M) and synthesis temperature (20–50°C) showed little or no influence in the experimental setup. Only the difference of the sizes of the particles prepared at 20 and 65°C was statistically significant, with lower relaxivities and sizes with increasing temperature [38].

The particle size or shape can be varied easily by controlling the pH and the ionic strength in the medium of synthesis [39]. The higher the pH and ionic strength, the smaller the particle size and size distribution width will be, because these parameters determine the chemical composition of the crystal surface and consequently the electrostatic surface charge of the particles [25].

Qiu et al. investigated that the size of the magnetic particles was dependent on both temperature and the ionic strength of the iron ion solutions. Magnetic nanoparticles with average diameter in the range of 6.4–8.3 nm have been synthesized by a chemical co-precipitation of Fe(II) and Fe(III) salts in NH_4OH solution. The magnetic particles formed at higher temperature or lower ionic strength were slightly larger than those formed at lower temperature or higher ionic strength respectively. In spite of the different reaction conditions, all the resultant nanoparticles were nearly spherical and had a similar crystalline structure. At 300 K, such prepared nanoparticles were superparamagnetic [40].

Some other factors have an influence on the size of the nanoparticles. For example, an increase of the mixing rate tends to decrease the particle size. The different studies also show that the formation of magnetite particles decreases with an increase in the temperature. Bubbling nitrogen gas through the solution not only protects against critical oxidation of the magnetite but also reduces the particle size when compared to methods without oxygen removal [25].

2.2.2 Thermal decomposition (High-temperature reactions)

Nanoparticles with a high level of monodispersity and size control can be obtained by high-temperature decomposition of iron organic precursors, such as $Fe(Cup)_3$, $Fe(CO)_5$, or $Fe(acac)_3$ (acac = acetylacetonate) using organic solvents and surfactants [25]. Fatty acids, oleic acid, and hexadecylamine are often used as surfactants [32].

The size and morphology of the nanoparticles can be controlled by controlling the reaction times and the temperature but also the concentration and ratios of the

reactants, nature of the solvent, precursors, complexing strength, and addition of seeds. The adsorption of a surfactant onto the surface of the iron nanoparticle stabilizes the colloid solution [25].

K. Woo et al. prepared hydrophobic magnetite nanoparticles with a narrow size distribution by thermal decomposition of $Fe(CO)_5$ in octyl ether solution of oleic acid and by consecutive aeration. The nanoparticles were converted into magnetite core/silica shell (magnetite@silica) structured particles with hydrophilic and processible aminopropyl groups on their surfaces [41].

Sun et al. reported a convenient organic phase process for making monodisperse Fe_3O_4 nanoparticles through the reaction of $Fe(acac)_3$ and a long-chain alcohol [42]. They demonstrated that high-temperature (265°C) reaction of iron (III) acetylacetonate, $Fe(acac)_3$, in phenyl ether in the presence of alcohol, oleic acid, and oleylamine could be used to make size-controlled monodisperse magnetite nanoparticles (Fig. 2.4) [43].

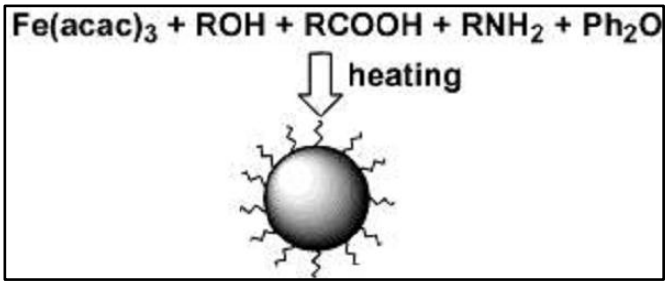

Figure 2.4 : High-temperature reaction of iron (III) acetylacetonate [43].

According to the Figure 2.4, the 4-nm Fe_3O_4 nanoparticles were made as follows: $Fe(acac)_3$ (2 mmol) was mixed in phenyl ether (20 mL) with 1,2-hexadecanediol (10 mmol), oleic acid (6 mmol), and oleylamine (6 mmol) under nitrogen and was heated to reflux for 30 min. After cooled to room temperature, the dark-brown mixture was treated with ethanol under air, and a dark-brown material was precipitated from the solution. The product was dissolved in hexane in the presence of oleic acid and oleylamine and reprecipitated with ethanol to give 4 nm Fe_3O_4 nanoparticles [43].

As magnetic nanoparticles synthesized in an organic environment often have better crystallinity and monodispersity than those synthesized in an aqueous environment, a method of transferring organically synthesized particles to aqueous conditions is clearly desirable [44]. Therefore, it is very important to further develop the thermal decomposition method to directly synthesize water-soluble magnetic nanoparticles

by using strong polar molecules to modify the magnetic nanoparticles [45]. Li et al. reported a one-pot reaction to achieve water-soluble iron oxide nanocrystals by thermal decomposition of $Fe(acac)_3$ in 2-pyrrolidone (Fig. 2.5) and results of surface coordination of the magnetic nanocrystals obtained. In the one-pot reaction, 2-pyrrolidone was chosen as solvent and stabilizer because it has strong polarity, a high boiling point, and coordination capacity with transition metal ions [45].

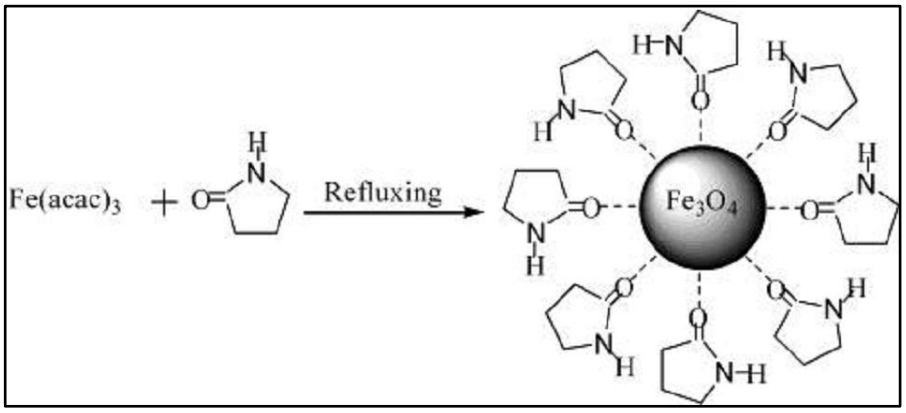

Figure 2.5 : Synthetic route of water-soluble magnetite nanocrystals [45].

Li et al. have also presented a simple route to synthesize water-soluble magnetite nanocrystals by refluxing inexpensive $FeCl_3.6H_2O$ as iron source instead of costly [$Fe(acac)_3$]. In addition, the mechanism leading to Fe_3O_4 in 2-pyrrolidone was discussed. Differently sized (average particle sizes were 4, 12, and 60 nm) and shaped (from spherical to cubic with increasing reflux time) magnetite nanocrystals could be obtained simply by varying the reaction time. In accordance with the results, a possible mechanism leading to magnetite nanocrystals is proposed in Fig. 2.6 [46].

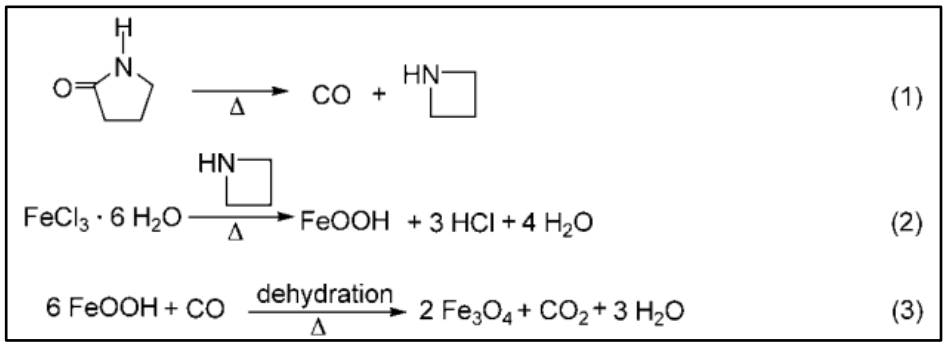

Figure 2.6 : Chemical reactions involved in the formation of magnetite nanoparticles [46].

In Fig. 2.6, the equation (2) is a process involving dissolution of $FeCl_3.6H_2O$ in 2-pyrrolidone and azetidine-catalyzed hydrolysis of $FeCl_3$. In fact, the thermal

decomposition of 2-pyrrolidone is rather complex. Therefore, Fig. 2.6 does not depict all decomposition reactions that take place. Only those related to the formation of magnetite nanocrystals are shown [46].

Jun et al. reported the synthesis of magnetic Fe_3O_4 nanocrystals through thermal decomposition of $Fe(acac)_3$ in a hot organic solvent. The size of these nanocrystals was controlled from 4 to 6, 9, and 12 nm with high monodispersity. It was necessary to develop a multifunctional ligand system that allows one to transfer the nanocrystals from the organic to the aqueous phase, a simple but highly effective 2,3-dimercaptosuccinic acid (DMSA) ligand was exchanged onto the nanocrystal surface. Obtained Fe_3O_4 nanocrystals with the DMSA ligand were fairly stable in water and phosphate-buffered saline (PBS) without any aggregation [47].

2.2.3 Hydrothermal reactions

Hydrothermal reactions are aqueous reactions carried out using autoclaves or high pressure reactors where the pressure can be over 2000 psi at temperatures above 200°C. Water acts as a reactant at these supercritical conditions, accelerating the kinetics of the hydrolysis reactions. At increased temperatures, the solubility of most ionic species increases and, with the lower viscosity of water, exhibits greater mobility. The increased mobility allows Ostwald ripening to continue at a faster rate increasing the uniformity of the precipitates [31].

Hydrothermal method has many advantages: the use of organic reagents are waived, relatively cost-effective, high yield of products and excellent particle crystallinity with controllable size and good morphology of particles can be easily obtained. In addition, no post-heat treatment is required for the produced nanoparticles which makes this method highly desirable as heat treatment might result in particle agglomeration [48].

Hydrothermal synthesis of Fe_3O_4 nanoparticles in organic solvent-free system is useful because of simplicity of the process and relatively low environmental impact. In normal hydrothermal synthesis technique, a mixed aqueous solution of ferrous and ferric ions is used as the starting solution, and precipitates of ferrous hydroxide ($Fe(OH)_2$) and goethite (α-FeOOH) are formed as the precursor via coprecipitation in an alkaline solution [49].

There are two main routes for the formation of ferrites via hydrothermal conditions: hydrolysis and oxidation, and neutralisation of mixed metal hydroxides. Some lesser routes involve the hydrothermal treatment of mixed metal oxides, or the use of other solvents such as ethylene glycol at supercritical conditions. Hydrolysis and oxidation reactions are very similar to neutralisation reactions where the former uses ferrous salts as opposed to ferric salts in the latter [31].

During the hydrothermal process of preparing magnetite, several factors such as temperature, pH values, and the amount of iron powder should be considered [50]. Size and morphological control in hydrothermal reactions is achieved by controlling time and temperature. The reaction conditions of precursor material and pH have an impact on phase purity of the nanoparticles [31]. Indeed, it was observed that the particle size of Fe_3O_4 powders increased with a prolonged reaction time and that higher water content resulted in the precipitation of larger Fe_3O_4 particles [25].

Under hydrothermal conditions a broad range of nanostructured materials can be formed. Li et al. reported a generalized hydrothermal method for synthesizing a variety of different nanocrystals by a liquid–solid–solution reaction. The system consists of metal linoleate (solid), an ethanol–linoleic acid liquid phase, and a water–ethanol solution at different reaction temperatures under hydrothermal conditions [32].

Konishi et al. hydrothermally prepared Fe_3O_4 powders from Fe(III) carboxylate using alcohol as the solvent (this method is known as the solvothermal method) [51]. In the absence of water, the heat treatment of the iron carboxylate solution at 245°C (0.45 MPa) led to the formation of magnetite alone. The resulting magnetite was crystalline particles with size ca. 0.1 μm and was free from contamination by the organic starting material [52].

D. Chen and R. Xu hydrothermally synthesized Fe_3O_4 particles from iron(II) 2-methoxyethoxides ($Fe(OMOE)_2$), using 2-methoxyethanol (MOE)–water mixed solvent as the medium. Their experiments showed that the borderline synthesis conditions were a reaction temperature of about 140°C, a reaction time from 42 to 64 h, and a volume ratio of MOE/H_2O in the range 1.4 –2.0 [51].

Si et al. have reported a facile method to produce monodisperse magnetite nanoparticles via the reaction between Fe powder and $FeCl_3.6H_2O$. The solvethermal

reaction was carried out at 180°C in *n*-hexane in the presence of oleic acid and laurylamine. Fe_3O_4 nanocrystals with sizes of 5.2, 7.9, 9.8, 11.7, and 12.7 nm were synthesized through the sealed reaction in 3, 6, 12, 18, and 24 h, respectively. These Fe_3O_4 nanocrystals were soluble in oil phases such as hexane. Comparing the experiments of aqueous syntheses through different processes, the system of organic-surfactant in this solvothermal process has important roles in slowing the nucleation rate and preventing the particle aggregation [53]. Though this method has been proved to be effective in increasing the crystallinity, the magnetite nanoparticles obtained exhibit poor water solubility, which limits their application in biomedical fields [54].

S. Xuan et al. reported the preparation of water-soluble magnetite nanoparticles by a hydrothermal method. In this work, hydrated ferric salt was employed as a single iron precursor and ascorbic acid as a reducing agent to synthesize superparamagnetic Fe_3O_4 nanocrystals, which capped with $C_6H_6O_6$ (the oxidation state of ascorbic acid) [54].

A possible formation mechanism of the magnetite nanocrystals was suggested as follows [54]:

$$2Fe^{3+} + 3CO_3^{2-} + 6H_2O \rightarrow 2Fe(OH)_3 + 3H_2CO_3 \quad \textbf{(2.6)}$$

$$2Fe(OH)_3 + C_6H_8O_6 \rightarrow 2Fe(OH)_2 + C_6H_6O_6 + 2H_2O \quad \textbf{(2.7)}$$

$$2Fe(OH)_3 + Fe(OH)_2 \rightarrow Fe_3O_4 + 4H_2O \quad \textbf{(2.8)}$$

C.Y. Haw et al. synthesized Fe_3O_4 nanoparticles using hydrothermal method. The black precipitate of Fe_3O_4 nanoparticles is then transferred into an autoclave and heated to 200°C for 1 h. Earlier studies suggest that if hydrothermal temperature is greater than 160°C, it would possibly result in bigger particles size. Lower hydrothermal temperatures of 120 or 80°C have a tendency to produce smaller size distribution of Fe_3O_4 nanoparticles. Besides, the duration of heating process may also play important role in the production of Fe_3O_4 nanoparticles. Mao et al. synthesized Fe_3O_4 nanoparticles at 180°C for 24 h and their results indicate that the Fe_3O_4 nanoparticles produced are of well-defined crystal shape and bigger due to the recrystallization. Contrastingly, in the study of C.Y. Haw et al., the obtained Fe_3O_4 nanoparticles are of spherical shape with average diameters of 17.12 nm [48].

N. Mizutani et al. carried out the hydrothermal synthesis of Fe_3O_4 nanoparticles by using the starting solution containing lactate and sulfate ions at various concentrations in order to control the particle size. Under the experimental conditions in this work, the median particle size could be varied from 9.5 to 38.6 nm. Therefore, it has been demonstrated that the particle size is controlled by means of the coexistence effects of lactate and sulfate ions. The size control can be carried out precisely by adjusting their concentration in the starting solution properly as the operating factor [49].

Y. Qian et al. prepared homogeneous ultrafine magnetite particles by means of a hydrothermal procedure in the temperature range of 130°-150°C, starting from a solution of iron chloride ($FeCI_3.6H_2O$) and iron powder, using urea as precipitant. No iron powder remained in the products, and the yield of magnetite was above 95 % [50].

A mechanism of the formation of magnetite in the hydrothermal process can be proposed as follows [50]:

$$Fe + 2H_2O \rightarrow Fe(OH)_2 + H_2 \quad \textbf{(2.9)}$$

$$Fe^{3+} + 3NH_3.H_2O \rightarrow Fe(OH)_3 + 3NH_4^+ \quad \textbf{(2.10)}$$

$$Fe^{3+} + 3NH_3.H_2O \rightarrow Fe(OH)_3 + 3NH_4^+ \quad \textbf{(2.11)}$$

$$Fe(OH)_2 + 2Fe(OH)_3 \rightarrow Fe_3O_4 + 4H_2O \quad \textbf{(2.12)}$$

R. Fan et al. have synthesized nanocrystalline magnetite successfully by hydrothermal reaction of aqueous ferrous sulfate ($FeSO_4$), sodium hydroxide and sodium thiosulfate ($Na_2S_2O_3$). They were homogenous with an average size of 50 nm and the yield of the magnetite was above 90 %. The total reaction was related as follows [55]:

$$3Fe^{2+} + 2S_2O_3^{2-} + O_{2(aq)} + 4OH^- \rightarrow Fe_3O_{4(s)} + S_4O_6^{2-} + 2H_2O \quad \textbf{(2.13)}$$

2.2.4 Microemulsion

A microemulsion is a thermodynamically stable dispersion of two relatively immiscible liquids stabilized by surfactant molecules [56]. Surfactant (also known as stabilizer or emulsifier) is an amphiphilic molecule that possesses both polar and non-polar moieties, consisting of hydrophilic (likes water) and hydrophobic (fears

water) components [57]. Microemulsions should not be regarded as emulsions with very small droplet size; micro- and macroemulsions are fundamentally different (Table 2.2) [58].

Table 2.2 : Characteristic differences between emulsions and microemulsions [58].

Emulsion	Microemulsion
Unstable, will eventually separate	Thermodynamically stable
Relatively large droplets (1-10 μm)	Small aggregates (~10 nm)
Relatively static system	Highly dynamic system
Moderately large internal surface, moderate amount of surfactant needed	High internal surface, high amount of surfactant needed
Small oil/water curvature	The oil/water interfacial film can be highly curved

Depending on relative concentrations, surfactant molecules self-assemble into a variety of structures in the solvent mixture, such as micelles, bilayers and vesicles. Most commonly used structures in nanoparticle synthesis are micelles, either as reverse (water-in-oil) or normal (oil-in-water) form. In both cases, the dispersed phase consists of monodispersed droplets in the size range of 2–100 nm. This dispersed phase provides a confined environment for synthesizing nanoscale particles [56].

In water-in-oil microemulsions, the aqueous phase is dispersed as microdroplets (typically 1–50 nm in diameter) surrounded by a monolayer of surfactant molecules in the continuous hydrocarbon phase. The size of the reverse micelle is determined by the molar ratio of water to surfactant. By mixing two identical water-in-oil microemulsions containing the desired reactants, the microdroplets will continuously collide, coalesce, and break again, and finally a precipitate forms in the micelles. By the addition of solvent, such as acetone or ethanol, to the microemulsions, the precipitate can be extracted by filtering or centrifuging the mixture. In this sense, a microemulsion can be used as a nanoreactor for the formation of nanoparticles [32].

A common way to achieve a uniform particle size is to carry out the synthesis in the interior of small microemulsion liquid droplets. For example, metallic nanoparticles were produced in microemulsions by combining adequate amounts of organic solvent, water and surfactant, a precursor of metal ions and reducing agents [57]. The most widely used approach is shown in Fig. 2.7. This involves the preparation of two separate microemulsions, incorporating the different reactants. Upon mixing,

nucleation occurs on the micelle edges as the water inside them becomes supersaturated with reactants. Growth then occurs around this nucleation point, with the arrival of more reactant fed via intermicellar exchange [59].

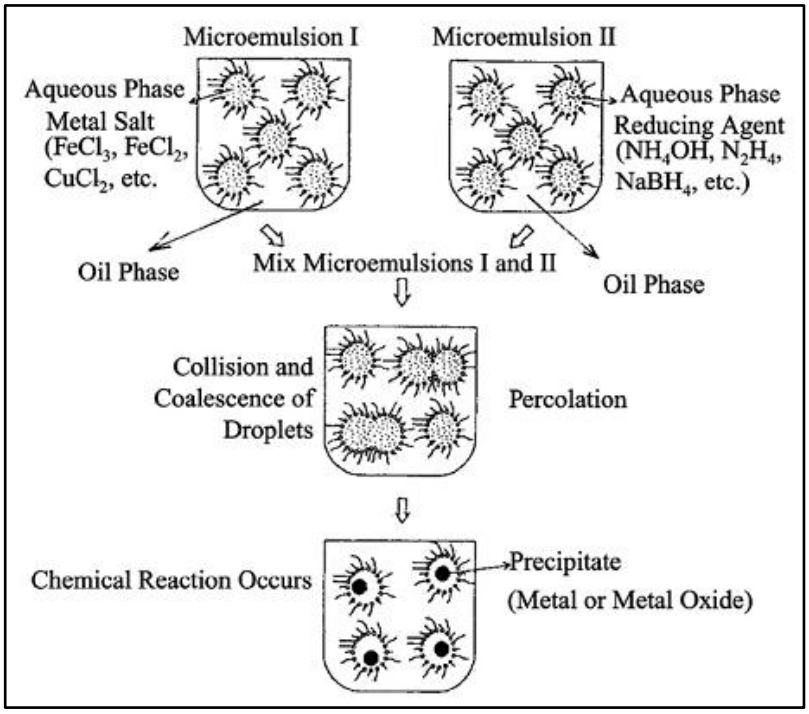

Figure 2.7 : Proposed mechanism for the formation of nanoparticles by the microemulsion approach [59].

The water-in-oil emulsions are currently being used to synthesize superparamagnetic iron oxide nanoparticles with a narrow size range and uniform physical properties because of the ability to control the size and shape of the nanoparticles. The main advantage of using this type of emulsion system is that the size of the nanoparticles can be controlled by modulating the size of the aqueous droplets core [25].

Gupta and Wells reported an approach to prepare magnetic polymeric nanoparticles with magnetic core and polymeric shell using inverse microemulsion polymerization process. Poly(ethyleneglycol) (PEG) modified superparamagnetic iron oxide nanoparticles with specific shape and size have been prepared inside the aqueous cores of AOT/n-Hexane reverse micelles. The inverse microemulsion polymerization of a polymerizable derivative of PEG and a cross-linking agent resulted in a stable hydrophilic polymeric shell of the nanoparticles. The results showed that the particles are spherical in shape with core–shell structure. The average size of the PEG-modified nanoparticles was found to be around 40–50 nm with narrow size distribution [60].

The inexpensive large-scale synthesis of uniform and highly crystalline magnetite nanoparticles using reverse micelles as nanoreactors under reflux conditions has been recently described by Y. Lee et al. (2005). The key feature of this synthetic procedure was the maintenance of the micelle structure during the formation of the nanoparticles at high reaction temperature. In the study, the particle size could be controlled from 2 nm to 10 nm by varying the relative concentrations of the iron salts, surfactant, and solvent [61].

J. Vidal-Vidal et al. presented a one-pot microemulsion method to produce both coated and uncoated magnetic nanoparticles. A water-in-oil microemulsion (cyclohexane/Brij-97/aqueous phase) was chosen because it is stable at moderated temperatures and uses a non-ionic surfactant. The nanoparticles were formed by the coprecipitation reaction of ferrous and ferric salts with two organic bases, cyclohexylamine and oleylamine, into a water-in-oil microemulsion. The results showed that when oleylamine was used as precipitant agent, a stable colloidal dispersion of maghemite nanoparticles coated with oleylamine was obtained. In contrast, cyclohexylamine did not avoid the aggregation of the particles during the synthesis. It was shown that the oleylamine adsorbed at particle surface could be easily replaced by oleic acid, due to its strong chemisorption when carboxilate bonded to Fe^{3+} at the particle surface. The obtained particles coated with oleylamine (or oleic acid) showed a narrow size distribution of 3.5 ± 0.6 nm; were spherical shaped and well crystallized; had high saturation magnetization; and were strong protected by a monolayer coating [62].

J. Zhi et al. have suggested a new method of in situ preparation of magnetic chitosan/Fe_3O_4 composite nanoparticles in microreactors of tiny water pools of water-in-oil microemulsion. Tiny water pools of water-in-oil microemulsion are ideal nano-sized microreactors for the preparation of nanoparticles, such as GeO_2, CdS and $BaSO_4$. Chitosan solution was prepared by dissolving chitosan powder in hydrochloric acid. Cyclohexane, *n*-hexanol, hydrochloric acid (HCl) solution containing chitosan and ferrous salt solutions were mixed at the volume ratio of 55:30:8:8. The microemulsion was formed by adding Triton X-100 (surfactant) into the mixture. Through adding the basic solution of NaOH into the microemulsion containing chitosan and ferrous salt, the magnetic Fe_3O_4 and chitosan nanoparticles were precipitated from the system. The magnetic iron oxide nanoparticles were

surrounded by the chitosan nanoparticles. The size of the magnetic chitosan nanoparticles ranged from 10 nm to 80 nm [63].

Another method to synthesise nanoparticles is from a single microemulsion. One of the desired reactants is solubilised inside reverse micelles, and a second reactant (often a reductant) added directly to the system. This is a common way to produce metal nanoparticles [59].

A novel approach to prepare magnetic polymeric nanoparticles by synthesis of the magnetite core and polymeric shell in a single inverse microemulsion was reported by Dresco et al. The particle size was varied in the range 80-320 nm by changing of the monomer concentration and water/surfactant ratio. The technique of synthesizing a core and a shell in a single microemulsion has improved the particle structure and size distribution [64].

Microemulsion-based syntheses are typically carried out at low temperatures. They are easy to be scaled up to an industrial level, but they suffer from some disadvantages [56]:

- extensively agglomerated nanoparticles are often generated [61].
- particles are sometimes less crystalline and more polydispersed because of the slow nucleation rate at low reaction temperatures [56].
- it is an expensive method due to the large amounts of surfactant (as much as 20–30%) and solvent added to the system [57,32].
- the yield of nanoparticles is often very low compared to other methods, such as thermal decomposition and co-precipitation. In other words, a large amount of solvent is used to synthesize a very small amount of nanoparticles [61,32].
- although many types of magnetic nanoparticles have been synthesized in a controlled manner using the microemulsion method, the particle size and shapes usually vary over a relative wide range, and the working window for the synthesis in microemulsions is usually quite narrow [32].
- the surfactant ensuring colloidal stability is adsorbed on the surface of the nanoparticles, thereby decreasing their usability [57].

2.3 Stabilization of Magnetic Nanoparticles

Magnetic nanoparticles contain hundreds to thousands of single atoms/ions and have extremely large surface energy and magnetic interactions [65]. In the absence of any surface coating, magnetic iron oxide particles have hydrophobic surfaces with a large surface area to volume ratio. Due to hydrophobic interactions between the particles, these particles agglomerate and form large clusters, resulting in increased particle size [21]. Dependent upon the pH of the solution, the surface of the magnetite will be positive or negative [25]. The principal cause of aggregation is the short-range forces-van der Waals attraction between the two particles. To counteract these attractive interactions and promote stability, equally short-range repulsive forces are required. They are enforced either by electrostatic repulsion between the particles or by coating the particles with organic long-chain molecules [66], as indicated in Fig. 2.8 [65]. The stabilization of nanoparticles seems to result from thermodynamics rather than kinetics [67].

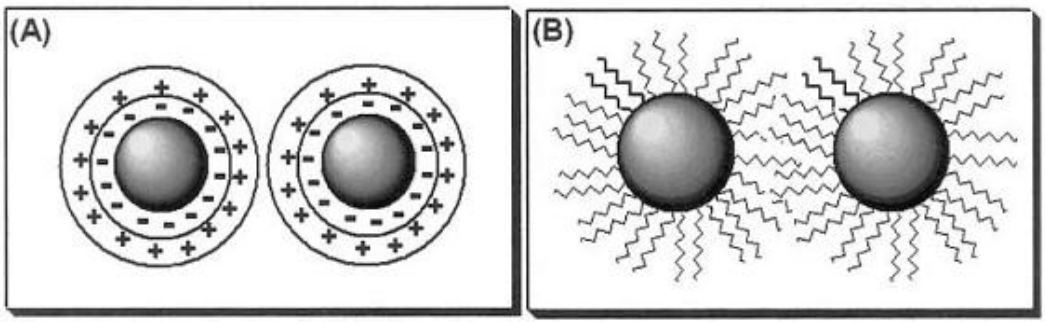

Figure 2.8 : Schematic illustration of particle stabilization via (a) electric double layer and (b) steric effect [65].

Electrostatic stabilization (see Fig. 2.8a) is based on the Coulombic repulsion between the particles caused by the electrical double layer formed by ions adsorbed at the particle surface (e.g. sodium citrate) and the corresponding counterions. This is exemplified by the gold sols prepared by the reduction of $[AuCl_4]^-$ with sodium citrate. Steric stabilization (see Fig. 2.8b) is achieved by the coordination of sterically demanding organic molecules that act as protective shields on the metallic surface. In this way, nanometallic cores are separated from each other and agglomeration is prevented. The main classes of protective groups selected from the literature are: polymers and block copolymers; P, N, and S donors (e.g. phosphanes, amines, thioethers); solvents such as THF, THF/MeOH, and propylene carbonate; long-chain

alcohols; surfactants; and organometallics [68]. Oleic acid ($C_{18}H_{34}O_2$) is a commonly used surfactant to modify the magnetic nanoparticles synthesized by the traditional co-precipitation method compared to other surfactants [69].

The surfactants can form the single layer or bilayer coated structure on the surface of nanoparticles. When Fe_3O_4 nanoparticles were coated by single layer oleic acid, the two oxygen atoms of COO in oleic acid provided two coordination positions to form the chemical interaction with Fe atom. The studies showed that the primary layer in the bilayer coated structure was chemically absorbed on the surface of nanoparticles (Fig. 2.9), and the secondary layer was physically absorbed on the primary layer through the interpenetration of the tails of the primary and secondary surfactants at their interface (Fig. 2.10) [70].

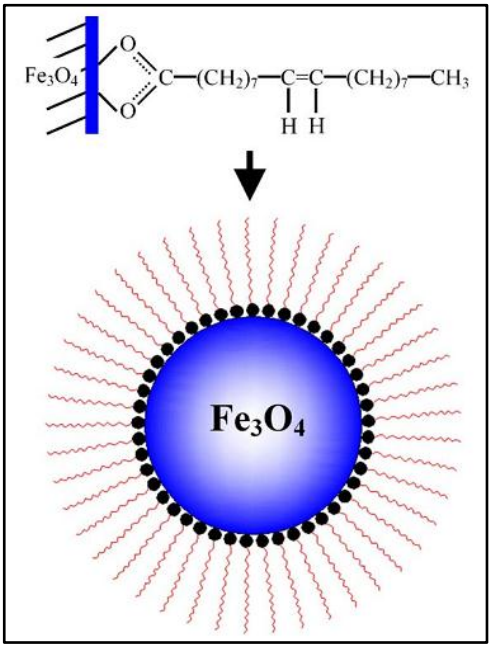

Figure 2.9 : Schematic representation of single layer oleic acid-coated Fe_3O_4 nanoparticles [70].

The long hydrocarbon chains of the surfactants are responsible for the hydrophobicity. These long aliphatic chains also cause the nanoparticles to be immiscible in the aqueous solution, and the biological applications of these nanoparticles are greatly restricted because of their poor solubility in aqueous solution [71]. Bilayer oleic acid-coated Fe_3O_4 nanoparticles can be applied in more areas than single layer oleic acid-coated ones because they can be well dispersed not only in nonpolar carrier liquids but also in polar carrier liquids, while the single layer oleic acid-coated ones can be dispersed only in nonpolar carrier liquids [70].

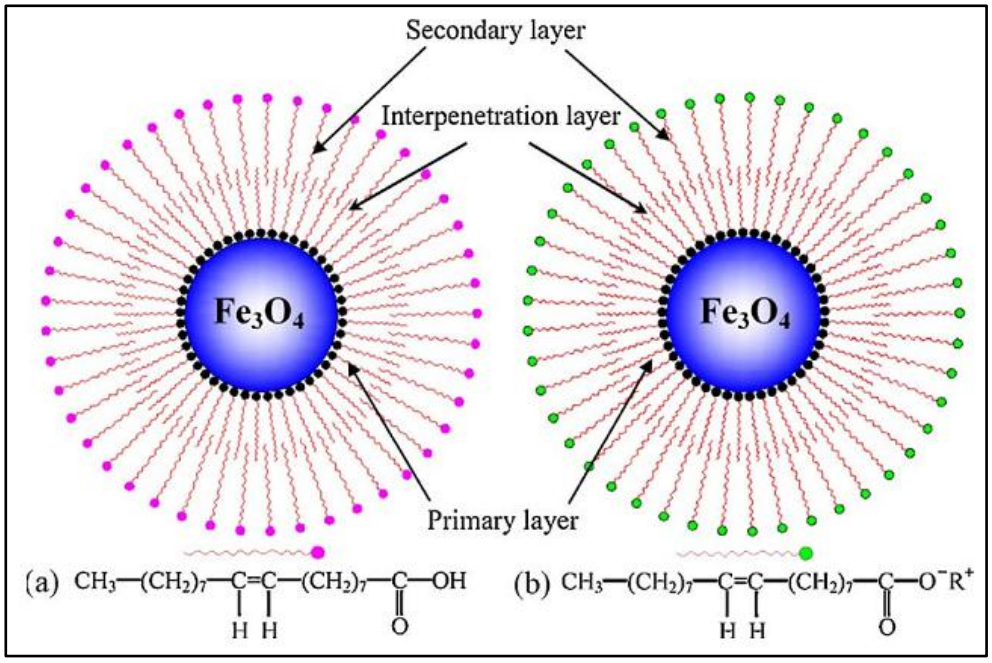

Figure 2.10 : Schematic representation of bilayer oleic acid-coated Fe_3O_4 nanoparticles: (a) oleic acid as the secondary layer; (b) oleate as the secondary layer [70].

Both in the single layer and bilayer oleic acid-coated Fe_3O_4 are contributed to be the strong chemical bond formed between the carboxylic acid and the amorphous iron oxide nanoparticles. However, too much oleic acid will make nanoparticles reunite into spherical, and too little oleic acid is also not sufficient to coat all of the nanoparticles completely, therefore it is critical to coat appropriate amount of oleic acid. Though K. Yang et al. have found the FTIR bound at 1710 cm^{-1} was the characteristic band for the secondary layer in bilayer oleic acid-coated Fe_3O_4, but there is still no suitable determination method to judge the optimum amount of oleic acid coated in Fe_3O_4 nanoparticles [69].

While some research has focused on the synthesis of magnetic particles stabilized by surfactant bilayers, little is known about the stabilization mechanisms underlying such systems in terms of the interfacial interactions that might exist. Indeed, the concept of surfactant bilayer stabilization has not yet progressed beyond being a reasonable hypothesis. Quantitative experimental characterizations of such systems are still rare and the results are inconsistent with each other [72].

Ferrofluids or magnetic fluids are stable colloidal homogeneous suspensions of magnetic nanoparticles (around 10 nm in diameter) in an appropriate carrier (aqueous or non-aqueous) liquid. D. Maity and D.C. Agrawal have prepared iron oxide

nanoparticles using Fe^{3+}/Fe^{2+} = 1.5/1, stabilized in oil (dodecane and kerosene) and water media. The particles have been suspended in non-aqueous and aqueous media by coating the particles with a single layer and a bilayer of oleic acid, respectively. The particle size of the powder was found to be much reduced when a surfactant (oleic acid) was used during the preparation. Particles coated with a single layer of surfactant could be stabilized in kerosene and dodecane while the bilayer coating was necessary to obtain the water-based ferrofluids [73].

Yan Wei et al. developed an efficient modification method using sodium citrate and oleic acid for the synthesis of Fe_3O_4 magnetic nanoparticles (MNPs) with narrow size distribution and excellent dispersion in fluids. Fe_3O_4 MNPs were synthesized by a co-precipitation method at different temperatures, and modified with sodium citrate and oleic acid respectively. Phase composition and microstructure analysis indicated that the sodium citrate and oleic acid have been successfully grafted onto the surface of Fe_3O_4 MNPs by chemical bond. Sodium citrate and oleic acid modified Fe_3O_4 MNPs showed excellent dispersion capibility in aqueous or inaqueous solution [74].

Sahoo et al. reported the surface derivatization of magnetite (Fe_3O_4) by oleic acid (OA), lauric acid (LA), dodecylphosphonic acid (DDP), hexadecylphosphonic acid (HDP), and dihexadecyl phosphate (DHDP) and compared the properties of carboxylic acid coated particles to colloidal nanoparticles coated with phosphonate or phosphate ligands. Coated magnetite nanoparticles with a 6-8 nm average diameter were prepared. Transmission electron microscopy analyses of the aggregation of the coated particles suggested that carboxylate surfactants provided the particles with better isolation and dispersibility as compared with phosphonate surfactants. Magnetic nanoparticles coated with oleic acid were easily dispersed in a nonpolar solvent like hexane, while the ones coated with lauric acid were not [75].

Another way to prepare stable magnetite particles is to coat magnetite particles with a polymeric material. Various techniques are used for preparing polymer encapsulated iron oxide particles. Some of those techniques are based on, first, precipitating iron oxide particles, and then coating the precipitated particles with polymers [76].

Polymers containing functional groups, such as carboxylic acids, phosphates, and sulfates, can bind to the surface of magnetite. Suitable polymers for coating include

poly(pyrrole), poly(aniline), poly(alkylcyanoacrylates), poly(methylidene malonate), and polyesters, such as poly(lactic acid), poly (glycolic acid), poly(ε-caprolactone), and their copolymers [32].

H. Zhang et al. have reported a method to prepare poly(methacrylic acid) (PMAA)-capped Fe_3O_4 nanoparticles by coprecipitation with PMAA in aqueous solution. Transmission electron micrographs and selected area electron diffraction pattern revealed the Fe_3O_4 nanoparticles to be approximately 8 nm in diameter with a cubic phase structure [77].

J. Lee et al. presented ultrafine magnetite particles of average diameter 4-7 nm prepared by precipitation in a poly (vinylalcohol) (PVA) aqueous solution. PVA is a hydrophilic polymer and serves as a protective agent to stabilize colloidal dispersions of magnetite. The results showed that the crystallinity of the particles decreased with increasing PVA concentration, while the morphology and particle sizes remained almost unchanged. The dispersion of the magnetite particles prepared at 1 wt % PVA was particularly stable [78].

Various methods have been reported for the preparation of stable dispersions of iron oxide in organic solvents (organosols), including hexane and decane. However, for these organosols, the biological applications are greatly restricted because of their poor solubility in aqueous solutions. For biomedical applications, it is essential to develop nanoscale magnetite with a narrow size distribution and surface coating with biocompatibility materials, i.e., nonimmunogenic, nonantigenic, and protein-resistant [66].

A.L. Andrade et al. have reported a direct reduction–precipitation method to prepare ferrofluids containing chemically stabilized nanoparticles of magnetite (Fe_3O_4) with tetramethylammonium hydroxide (TMAOH). To ensure that the Fe_3O_4 nanoparticles were monodispersed, their surfaces were modified by adsorbing TMAOH. TMAOH was used as protective agent to decrease particle aggregation, due interparticle interaction; the electrostatic repulsion effect was mainly caused by charges of the tetramethylammonium cations adsorbed on the particle surface, in the water medium. The post-synthesis autoclave-heating promoted the decrease of the mean particle size and TMAOH tended to satisfactorily keep particles well dispersed, making the resulting primary material suitable for many technological applications [79].

Santra et al. reported a water-in-oil microemulsion method for the preparation of silica-coated iron oxide nanoparticles. Three different nonionic surfactants (Triton X-100, Igepal CO-520, and Brij-97) have been used for the preparation of microemulsions, and their effects on the particle size, crystallinity, and the magnetic properties have been studied. All the particles showed magnetic behavior close to that of superparamagnetic materials. By use of this method, magnetic nanoparticles as small as 1-2 nm and of very uniform size (percentage standard deviation was less than 10 %) have been synthesized [80].

2.4 Functionalization of Magnetic Nanoparticles

The aim of surface functionalization of magnetic composite particles, such as polymer-coated magnetic particles and silica-coated magnetic particles, is to introduce some functional groups on the surface for immobilizing various biomolecules and biological ligands [17].

Functionalization of magnetic nanoparticles (MNPs) with amino group, silica, polymer, various surfactans or other organic compounds is usually provided in order to achieve better physical and chemical properties. Moreover, the core/shell structure of MNPs have the advantages of good dispersion, high stability against oxidation. Furthermore, lots of functional groups from polymers on the surface can be used for further functionalization to get various properties [81].

Apart from enabling the selective binding of different bioactive molecules, the functionalized nanoparticles must exhibit appropriate magnetic properties; they have to be non-toxic, hydrophilic, and biocompatible, and they have to remain stable in aqueous colloidal suspensions. One of the preferred functional groups for bonding different bioactive molecules to nanoparticles is the amino group [82].

Several groups of coating materials are used to modify MNP surface chemistry:

a) organic polymers, such as dextran, chitosan, polyethylene glycol, polysorbate, polyaniline,
b) organic surfactants, such as sodium oleate and dodecylamine,
c) inorganic metals, such as gold,
d) inorganic oxides, such as silica and carbon,
e) bioactive molecules and structures (liposomes, ligands/receptors) [83].

2.4.1 Polymer coating

Coating organic polymers on the surface of MNPs endows the particles some important properties that the bare particles lack. Polymer coating could enhance the compatibility between nanoparticles and aqueous medium, prevent particles from oxidation, reduce toxicity, extend storage life and facilitate transport, etc. Polymers for coating can be classified into natural and synthetic substances. Natural polymers include dextran, chitosan, gelatin, etc. Synthetic polymers include poly (ethyleneglycol) (PEG), poly (vinylpyrrolidone) (PVP), poly (vinyl alcohol) (PVA) and polyacrylic acid (PAA), etc. [84].

2.4.1.1 Chitosan

Chitosan, poly(1→4)-2-amino-2-deoxy-ɒ-glucan, is a poly(amino saccharide) with many significant biological (biodegradable, biocompatible, bioactive) and chemical properties (polycationic, hydrogel, reactive groups such as OH and NH_2) [85], (Fig. 2.11). Chitosan is the alkaline deacetylated product of chitin [63].

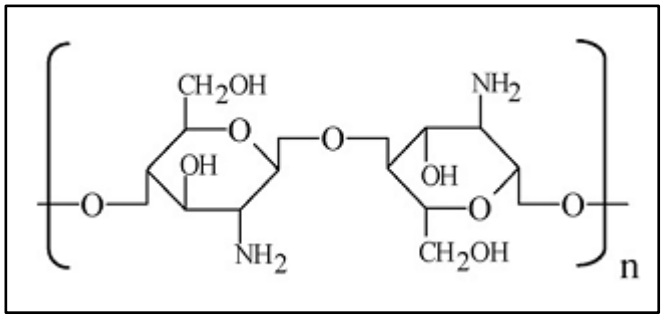

Figure 2.11 : Molecular structure of chitosan [87].

Chitin, poly(1→4)-2-acetamido-2-deoxy-β-ɒ-glucan is a naturally occurring polymer extracted from crustacean shells, such as prawns, crabs, krill, insects and shrimps. It is the second most abundant biopolymer next to cellulose. By partially deacetylating the acetamido groups in its side chain with a strong alkaline solution, chitin is converted to chitosan, which is non-toxic, hydrophilic and anti-bacterial [86].

Chitosan has both hydroxyl and amine groups that can be chemically modified [88]. The amino groups on the chitosan can also be used for further functionalization with specific components, such as various drugs, specific binding sites, or other functional groups. Chitosan is a suitable kind of polymer to be used to modify the Fe_3O_4 nanoparticles [89].

The presence of the amino groups indicates that pH substantially alters the charged state and properties of chitosan. At low pH, these amines get protonated and become positively charged and that makes chitosan a water-soluble cationic polyelectrolyte. On the other hand, as the pH increases above 6, chitosan's amines become deprotonated and the polymer loses its charge and becomes insoluble (Fig. 2.12) [90].

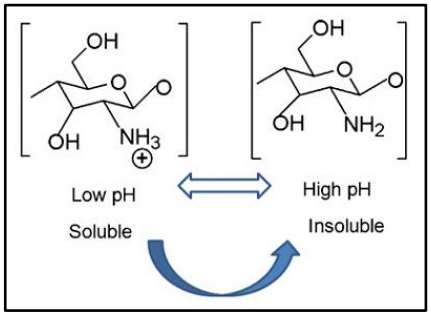

Figure 2.12 : Schematic illustration of chitosan's versatility [90].

Several methods have been used to modify raw chitosan flake either physical or chemical modifications [88]. Sungwook Hong et al. synthesized iron oxide (Fe_3O_4) nanoparticles coated with biocompatible chitosan for use as an MRI (magnetic resonance imaging) contrast agent. The average diameter of the coated particles was 67 nm. As can be seen from the Fig. 2.13, the amino group (NH_2) of chitosan is bonded to the particle. However, the hydroxyl group (-OH) of chitosan remains unbonded. Consequently, the coated particles are slightly positively charged. Due to the Coulomb repulsion between these positively charged particles, the aqueous solution of the coated particles remains in a state of colloidal suspension when no organic solvent or surfactant is used [91].

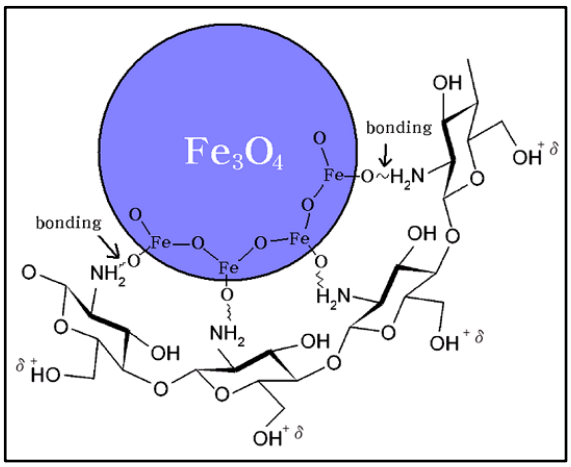

Figure 2.13 : Chitosan bonded to Fe_3O_4 [91].

Chitosan is often crosslinked, using a variety of agents, including glutaraldehyde and sodium tripolyphosphate. The glutaraldehyde forms a bridge between the NH_3^+ groups of the chitosan [92], (Fig. 2.14).

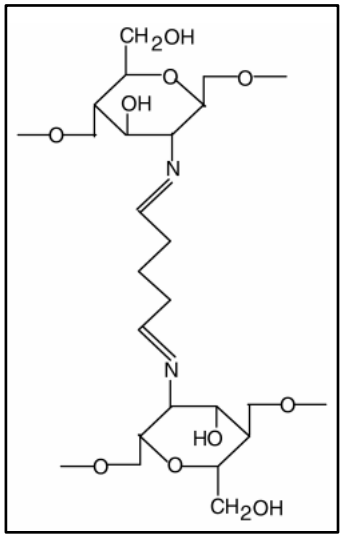

Figure 2.14 : Schematic representation of the chitosan-glutaraldehyde [93].

The aldehyde groups of the glutaraldehyde form covalent imine bonds with the amino groups of chitosan, due to the resonance established with adjacent double ethylenic bonds via a Schiff reaction (Fig. 2.15) [94].

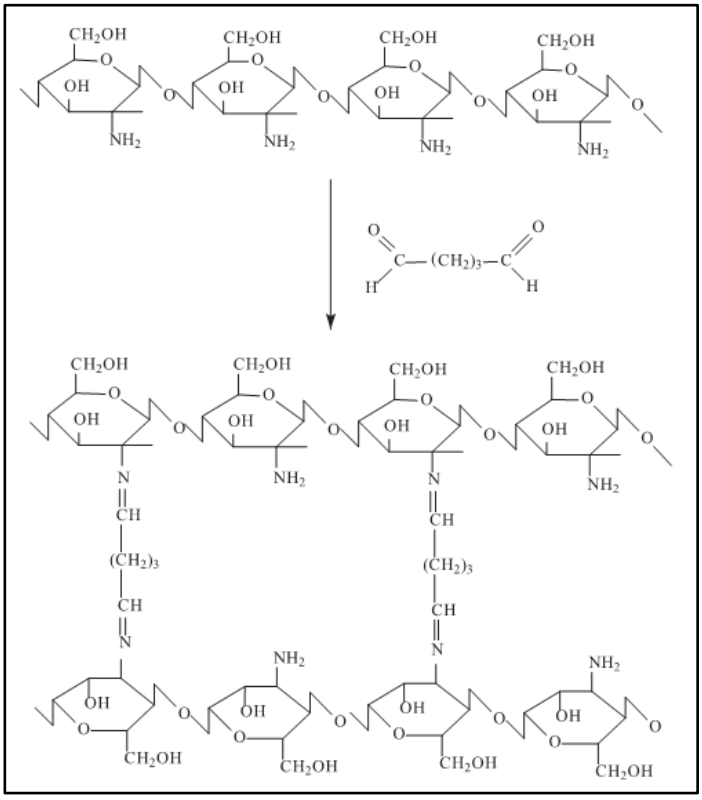

Figure 2.15 : Crosslinking process of chitosan treated with glutaraldehyde [94].

Gui-yin Li et al. synthesized magnetic Fe_3O_4–chitosan nanoparticles by the covalent binding of chitosan onto the surface of magnetic Fe_3O_4 nanoparticles. Firstly, Fe_3O_4 were prepared by hydrothermal method using H_2O_2 as an oxidizer, then chitosan and Fe_3O_4 aqueous slurry were mixed by appropriate proportion with reverse-phase suspension cross-linking method to form the magnetic nanoparticles with amine group. The formation process of magnetic Fe_3O_4–chitosan nanoparticles was shown in Fig. 2.16. TEM results showed that Fe_3O_4 particles and Fe_3O_4–chitosan nanocomposites were regular sphere with a mean diameter of 23 nm and 25 nm, respectively [95].

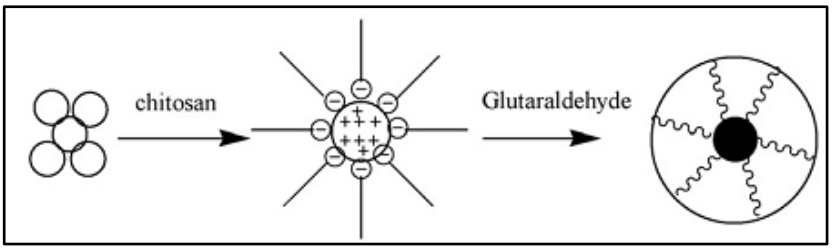

Figure 2.16 : The formation process of magnetic Fe_3O_4–chitosan nanoparticles with core-shell [95].

J. Qu et al. prepared Fe_3O_4–chitosan nanoparticles with core-shell structure by crosslinking method. Oleic acid modified Fe_3O_4 nanoparticles were firstly prepared by co-precipitation then chitosan was added to coat on the surface of the Fe_3O_4 nanoparticles by physical absorption. The Fe_3O_4–chitosan nanoparticles were obtained by crosslinking the amino groups on the chitosan using glutaraldehyde. The particle size of the composite nanoparticles was 10.5 nm and the size distribution was narrow. The Fe_3O_4–chitosan nanoparticles exhibited high saturation magnetization (30.7 emu/g) and superparamagnetic property [89].

Zhao et al. synthesized Fe_3O_4–chitosan magnetic composite nanoparticles with a core–shell structure with a diameter of 30–50 nm by two steps via a suspension cross-linking method. The potential of Fe_3O_4–chitosan composite nanoparticles was evaluated for localized hyperthermia treatment of cancers and it was found that the Fe_3O_4–chitosan composite nanoparticles would be good thermoseeds for localized hyperthermia cancer therapy [96].

E.H. Kim et al. developed microspheres composed of superparamagnetic iron oxide (SPIO; Fe_3O_4; magnetite) nanoparticles and chitosan as a novel MRI-detectable embolic material. They prepared spherical SPIO nanoparticles about 15 nm in radius

by sonochemistry, and embedded them in chitosan to synthesize a ferrofluid. To make an embolic material, the synthesized ferrofluid was sprayed on the surface of an alkali solution so that the ferrofluid in microsphere form was dispersed in the solution. Considering their uniform size and shape, the SPIO particles were suitable to prepare ferrofluids for medical applications. In this study, the SPIO-chitosan microspheres showed a strong enhancement of MR image contrast similar to the ferrofluid *in vitro* [97].

B. Feng et al. demonstrated a novel approach to synthesis monodisperse magnetite nanoparticles (3–5 nm in diameter) by using a chitosan–polyacrylic acid (CS–PAA) template. The results revealed that the Fe_3O_4 nanoparticles were 3–5 nm in size with excellent dispersibility. The particles exhibited superparamagnetic property with saturation magnetizations of 40.7 emu/g. In addition, the current samples were chosen to perform on MRI, the results indicated that the nanoparticles prepared by current synthetic approach could be potential used as T2-type contrast agents in MR imaging [98].

2.4.1.2 Dextran

Dextran is a polymer $(C_6H_{10}O_5)_n$, of anhydroglucose having mainly alpha-D(1-6) linkages with some unusual 1,3 glucosidic linkages at branching points [99], (Fig. 2.17). It is a natural polysaccharide that finds wide use in the pharmaceutical field. It is water soluble, inert in biological systems and does not affect cell viability [100].

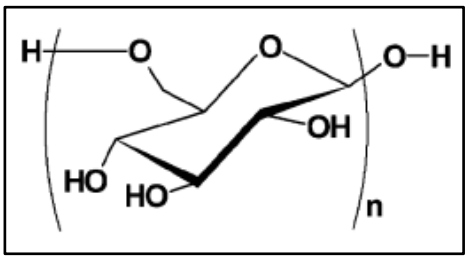

Figure 2.17 : Schematic representation of dextran [101].

Dextran is a good stabilizer for nanoscale magnetite owing to its excellent biocompatibility and water-solubility, and has been utilized in both laboratory products and some commercial MNPs [102].

H. Bai et al. reported a new method of synthesizing a kind of dextran coated Fe_3O_4 magnetic nanoparticles draw solute to technologically integrate the good solubility of dextran, which can generate sufficient osmotic pressure for brackish water

desalination, and the strong magnetism of Fe_3O_4 magnetic nanoparticles, which is beneficial for the easy separation of the draw solutes by an external magnet. They concluded that the dextran coated Fe_3O_4 magnetic nanoparticles used as draw solutes would bring benefits to the clean water production via promoting the forward osmosis system in an environmental friendly and energy saving manner. A schematic diagram to show the difference between pure Fe_3O_4 magnetic nanoparticles and the dextran coated Fe_3O_4 magnetic nanoparticles is shown in Fig. 2.18 [103].

J. Hradil et al. prepared dextran-modified iron oxide nanoparticles by precipitation of Fe(II) and Fe(III) salts with ammonium hydroxide by two methods. Iron oxide was precipitated either in the presence of dextran solution, or the dextran solution was added after precipitation. In the second method, the iron oxide particle size and size distribution could be controlled depending on the concentration of dextran in the solution. The dextran/iron oxide ratio 0–0.16 used in precipitation of iron salts could be recommended for synthesis of nanoparticles suitable for biomedical applications, as the colloid did not contain excess dextran and did not coagulate [104].

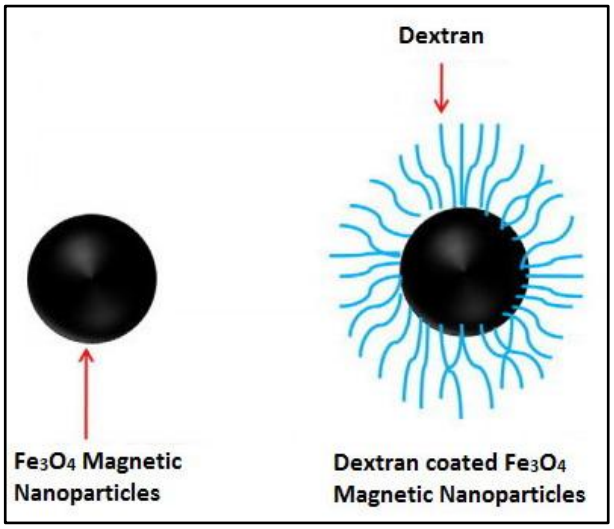

Figure 2.18 : Schematic diagram showing the Fe_3O_4 magnetic nanoparticles and the dextran coated Fe_3O_4 magnetic nanoparticles [103].

When magnetite/dextran nanocomposite was prepared by a one-step method, dextran was linked with MNPs through van der Waals force and hydrogen bond. In this case, when magnetic fluid was injected into veins, the magnetic fluid will be diluted, leading to the precipitation of the magnetic nanoparticles. In order to resolve the problem, a two-step method was proposed to bond dextran onto the surface of MNPs through chemical linkage [84].

R.Y. Hong et al. presented a one-step method for preparing biocompatible ferrofluid based on dextran-coated Fe_3O_4 magnetic nanoparticles. The biocompatible ferrofluid was intravenously injected into rabbits, bio-distribution of ferrofluid in organs and blood was investigated. The MRI of the rabbit liver, marrow and lymph were analyzed after the ferrofluid was injected. The results showed that the tumor could easily be identified, which indicated a potential application of the as-prepared magnetic nanoparticles in functional molecular imaging for biomedical research and clinical diagnosis [105].

G. Liu et al. synthesized superparamagnetic nanoparticles functionalized with carboxymethyl dextran (CM-dextran) by a two-step method, as shown in Fig. 2.19. First, the magnetic nanoparticles (MNPs) coated with dextran were prepared by co-precipitation of Fe^{2+} and Fe^{3+} ions. Then, dextran on the surface of MNPs reacted with monochloroacetic acid (MCA) in alkaline condition. The MRI experiment indicated that the CM-dextran MNPs could potentially be used as MRI contrast agents for magnetic resonance molecular imaging [106].

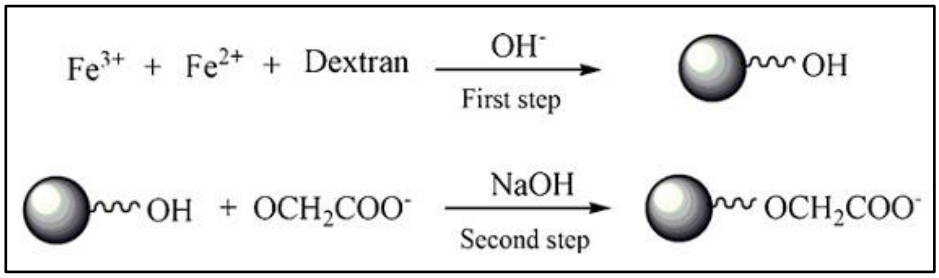

Figure 2.19 : Synthesis route for the carboxymethyl dextran coated magnetic nanoparticles [106].

2.4.1.3 Other polymers

Polyethylene glycol (PEG) is a polymer widely used for its hydrophilicity and low antigenicity. In addition to steric stabilization of MNPs, PEG prevents their plasma opsonization and uptake by macrophages, increasing MNP circulation *in vivo*. PEG-coated MNPs are efficiently internalized by cells via fluid-phase endocytosis and through amphiphilic affinity to lipid bilayers on plasma membranes. These qualities, however, increase their potential to overload cells with iron and become toxic [83].

Gupta and Curtis prepared poly(ethyleneglycol) (PEG) modified superparamagnetic iron oxide nanoparticles and studied their influence on human fibroblasts. The aim of the study was to modify the surfaces of the magnetic nanoparticles with PEG to

improve the biocompatibility of the nanoparticles by resisting protein adsorption and increasing their intracellular uptake. The results showed that the PEG coated nanoparticles did not affect the cell adhesion behaviour and morphology and their internalisation into endosomes offer the opportunity to label a variety of cells with high efficiency [107].

Polyvinyl alcohol (PVA) is a synthetic, water soluble polymer with excellent film forming, emulsifying, and adhesive properties [108]. It is a biocompatible polymer that is also attractive due to its high functionality and hydrogel-like properties, and is widely used as a dispersing agent for preventing particle coagulation and contributing to their stability and monodispersity [109].

A. Petri-Fink et al. developed functionalized superparamagnetic iron oxide nanoparticles (SPION) for interaction with human cancer cells. SPION (mean diameter 9 nm) were coated with various ratios to iron oxide of either polyvinyl alcohol (PVA), carboxylate-functionalized PVA, thiol-functionalized PVA and amino-functionalized PVA (amino-PVA). The interaction with cells and cytotoxicity of the SPION preparations were determined using human melanoma cells. From the four functionalized SPION preparations, only the amino-PVA SPION demonstrated the capacity to interact with, and were not cytotoxic to, human melanoma cells [110].

Polyvinylpyrrolidone (PVP), a polymer widely used in pharmaceutical formulations, forms covalent adducts with drugs containing nucleophilic functional groups [111]. In synthetic conditions, PVP molecules not only prevent the aggregation of the Fe_3O_4 nanoparticles, but also restrict their size by utilizing the interaction between the carbon atoms in carbonyl groups and the Fe atoms on the Fe_3O_4 nanoparticles. Y. Zhang et al. synthesized PVP-coated ultra-small Fe_3O_4 nanoparticles as MRI contrast agent. The as-prepared Fe_3O_4 nanoparticles with diameter from 6.5 to 1.9 nm were homogeneous and well dispersed. *In vivo* results for MRI and magnetic targeting showed that the PVP coated Fe_3O_4 particles could be concentrated at the target area and obviously exhibited negative contrast enhancement for the whole body [112].

Xu et al. reported a simplified method for synthesis of polyacrylic acid-bound iron oxide magnetic nanoparticles (Fe_3O_4@PAA NPs) on the basis of the amine-functionalized magnetite nanoparticles which were synthesized by a facile one-pot hydrothermal method without templates. The Fe_3O_4@PAA NPs had been utilized as

environment friendly adsorbent for the removal of rhodamine 6G (R6G) (as a model basic dye pollutant from aqueous solution) added to the aqueous sample from the Yellow River due to the high efficiency and fast adsorption process, as well as simple and convenient magnetic separation [113].

2.4.2 Inorganic materials coating

Iron oxide nanoparticles can be coated with silica, gold or gadolinium(III). These coatings not only provide stability to the nanoparticles in solution but also help in binding various biological ligands to the nanoparticle surface. These nanoparticles have an inner iron oxide core with an outer metallic shell of inorganic materials [25].

2.4.2.1 Silica

Silica is known to be biocompatible but not biodegradable. Amorphous silica coating on magnetite NPs was first reported by Philipse et al. with a sol–gel approach. As silica is hydrophilic in nature, the silica-coated core–shell particles were reported to be well dispersed in aqueous suspensions. The silica-coated SPIONs can be negatively charged above the isoelectric point of silica (pH∼2); hence, they have been used for separation of biomolecules through electrostatic interactions. In addition, silica has hydroxyl groups (silanol group: Si-OH) useful for the attachment of further functionalities through covalent bonding with organosilanes [114]. Such a capability opens the door to the design and synthesis of magnetic carriers that can be used to deliver drugs to targeted organs via highly specific recognition (e.g. antibody–antigen interaction) [115].

Organosilanes are bifunctional molecules with the general formula $X\text{-}(CH_2)_n\text{-}SiR_n(OR')_{3\text{-}n}$, where X represents the headgroup functionality, $(CH_2)_n$ a flexible spacer, and $Si(OR)_n$ the anchor groups by which (after hydrolysis of the alkoxy group) they can attach to free Si-OH surface groups. Alkoxysilanes with a variety of X functionalities are commercially available, amino groups being one of the most frequently used for biological applications. These can be employed in silanization of surfaces via a range of procedures including organic phase, aqueous phase, and chemical vapor deposition of the silane. Silanization in solution is the most common approach since it does not restrict the use of volatile compounds and is not required to be performed under vacuum [116].

Silica coated iron oxide nanoparticles are commercially available as contrast agents for MRI (Lumirem®). The protocol to obtain silica coated nanoparticles involves the synthesis of the magnetic nanoparticles and a series of reactions to grow the coating layer based on the Stöber method. Finally the functionalization of the coating is undertaken [117]. In Stöber process, silica is formed in situ through the hydrolysis and condensation of a sol-gel precursor [118].

J.H. Chang et al. developed molecularly assembled silica coated magnetic nanoparticles for protein separation such as bovine serum albumin (BSA) and lysozyme (LSZ) at different pH conditions. After the process of silica coating on the magnetic nanoparticle, the monolayers of organosilanes were grafted on the silica coated magnetic nanoparticles to enforce the covalent bonding and to capture the target proteins as the anchored probes. Work on using these amino functionalized silica coated magnetic nanoparticles for protein purification indicated that they have many advantages such as easy preparation, low cost, easy handling and rapid purification [119].

K. Ashtari et al. prepared silica-encapsulated magnetic nanoparticles (MNPs) via microemulsion method. MNPs with no observed cytotoxic activity against human lung carcinoma cell and brine shrimp lethality were used as suitable support for glucose oxidase (GOD) immobilization. The results demonstrated potential biocompatible applicability of the silica-encapsulated MNPs for biomedical applications [120].

Kang et al. described a simple and convenient process for highly efficient and direct DNA separation with functionalized silica-coated magnetic nanoparticles. The efficiency of the DNA separation was explored via the function of the amino-group numbers, particle size, the amount of the nanoparticles used, and the concentration of NaCl salt. The adsorption efficiency of aminofunctionalized nanoparticles was the 4-5 times (80-100 %) higher compared to silica-coated nanoparticles only (10-20 %) [121].

Yu et al. reported a synthesis of silica encapsulated magnetic nanosize particles (4–11 nm) as a magnetic separable carrier based on a simple microemulsion technique. The silica coating surface is shown to isolate and protect the magnetic core from reactive environment where a range of conditions for magnetic separation can be

made possible. Thus, it is demonstrated that the relatively smaller size coated magnetic nanoparticle can carry bulky protein, the bovine serum albumin (BSA) on the silica overlayer surface [122].

2.4.2.2 Gold

Precious metals, such as gold, have been used to protect iron oxide cores against oxidation, as they form highly stable particles of low reactivity. Nanogold is known for its superior optical properties, biocompatibility and outstanding capacity for functionalization. These properties make gold a particularly attractive surface chemistry for MNPs. One limitation is that gold coating can weaken magnetic properties of iron oxide MNPs and is considered difficult to achieve due to the dissimilar nature of the two surfaces. When achieved, gold-coated MNPs are stable under neutral and acidic conditions. Engineering a continuous gold shell over an MNP core is a challenge, but it can provide an extremely effective barrier against oxidizing agents [83].

Goon et al. reported a facile method of synthesizing 50-150 nm magnetite-gold composites via the use of a biocompatible polyelectrolyte, polyethyleneimine (PEI), for the dual function of attaching gold seeds and preventing the formation of large aggregates. They demonstrated the importance of having a saturated surface of gold seeds in obtaining gold shells and also showed that this shell imparts resistance to chemical attack [123].

Kim et al. prepared monodispersed gold coated superparamagnetic iron oxide nanoparticles (Au@SPION) in water-in-oil reverse microemulsion. The reverse micelle microreactor was prepared with CTAB (cetyltrimethyl–ammonium bromide), octane, and varying the water to surfactant ratio and molar ratio between cosurfactant and surfactant. Morphological analysis by TEM showed that Au@SPION, with average sizes 9 nm and narrow size distribution [124].

Salgueirino-Maceira et al. reported a method for the development of bifunctional magnetic and optically tunable nanoparticles with a structural design involving a magnetic iron oxide core (Fe_3O_4/γ-Fe_2O_3) surrounded by a thick silica shell and further covered with an outer shell of gold. These gold-coated magnetic silica spheres take advantage of the strong resonance absorption they show in the visible and near-infrared (NIR) range and can be controlled by using an external magnetic

field, which makes them very promising in biomedical applications. They can be controlled through the blood stream using an external magnetic field, therefore favoring their selective accumulation at the targeted pathologic tissue [125].

2.4.2.3 Carbon

One way to protect metal nanoparticles is to encapsulate the particles with a chemically stable species, such as graphite. Carbon is one of the best solutions for encapsulation as it is light, cheap and highly stable under extreme chemical and physical environments. The carbon coatings immunize the nanoparticles against environmental degradation and therefore retain their intrinsic nanocrystalline properties. Furthermore, carbon coatings can endow these nanoparticles with biocompatibility and a clear potential for further functionalization. It is enormously significant for prospective biomedical applications [126].

Carbon-encapsulated magnetic nanoparticles (CEMNs) possess wide promising applications in magnetic recording media, seal liquid, magnetic inks for bank cheques, and biomedical applications such as magnetic resonance imaging (MRI) contrast agent, separation and concentration agent of biological samples [127].

S. Zhang et al. synthesized carbon coated Fe_3O_4 nanoparticles (Fe_3O_4/C) by a simple hydrothermal reaction and the particles were applied as solid-phase extraction (SPE) sorbents to extract trace polycyclic aromatic hydrocarbons (PAHs) from environmental water samples. The Fe_3O_4/C sorbents possess high adsorption capacity and extraction efficiency due to strong adsorption ability of carbon materials and large surface area of nanoparticles, and only 50 mg of sorbents are required to extract PAHs from 1000 mL water samples. Large surface area of nanomaterial and strong adsorption ability of carbon material result in high adsorption capacity and extraction efficiency to target compounds, therefore, satisfactory results were achieved using lower amount of Fe_3O_4/C nanoparticle sorbents than common sorbents [128].

P. Hojati-Talemi et al. prepared Fe_3O_4/carbon composite nanoparticles using polystyrene as the carbon source, with a household microwave oven providing the required energy to produce plasma in a partially-evacuated reaction vessel, leading to the high temperatures required for carbonization of the carbon source and formation of nanoparticles. In this process, magnetite nanoparticles actively catalyzed the

formation of carbon nanofibers. The resulting composite retained the magnetic properties after this process, which is potentially very useful for producing new additives for electromagnetic shielding nanocomposites [129].

2.5 Characterization of Magnetic Nanoparticles

2.5.1 Fourier transform infrared spectroscopy (FT-IR)

FT-IR stands for Fourier Transform InfraRed, the preferred method of infrared spectroscopy. In infrared spectroscopy, IR radiation is passed through a sample. Some of the infrared radiation is absorbed by the sample and some of it is passed through (transmitted) (Fig. 2.20). FT-IR can identify unknown materials, determine the quality or consistency of a sample and the amount of components in a mixture [130].

Figure 2.20 : FT-IR mechanism [131].

Two types of interactions -absorption and transmission- are important in the typical IR experiment. When the molecule in the sample compartment of the spectrometer is exposed to a source of continuous IR radiation, the photons of discrete energy units that are absorbed by the molecule do not reach the detector. The IR spectrum reveals these missing photons, or absorptions, as a series of well-defined, characteristic, and reproducible absorption bands. Photons that are not absorbed by the sample are transmitted to the detector essentially unaltered. For a given wavelength or frequency of IR radiation striking a sample, these two interactions are inversely related through the following equation [132]:

$$A = \log 1 / T \qquad \textbf{(2.14)}$$

where: A = absorbance and T = transmittance (% T/l00).

The resulting spectrum represents the molecular absorption and transmission, creating a molecular fingerprint of the sample. Like a fingerprint no two unique molecular structures produce the same infrared spectrum. This makes infrared spectroscopy useful for several types of analysis [130]. Absorption bands in the range of 4000 - 1500 wavenumbers are typically due to functional groups (e.g., -OH, C=O, N-H, CH_3, etc.). The region from 1500 - 400 wavenumbers is referred to as the fingerprint region. Absorption bands in this region are generally due to intramolecular phenomena and are highly specific to each material. The specificity of these bands allows computerized data searches within reference libraries to identify a material [133].

The FT spectrometer works by splitting an IR beam into two. When these recombine, the light waves interfere constructively or destructively, creating the "interferogram" which is the time domain signal obtained from the detector. The interferogram must be analyzed with a computer using Fourier transforms to obtain a single-beam infrared spectrum that can be interpreted [134,133]. An IR spectrum displays detector response as percent transmittance (% T) on the y-axis, and IR frequency in terms of wavenumber (cm^{-1}) on the x-axis. The detector response indicates the extent of interaction of the IR electromagnetic radiation with the sample as it is proportional to the resultant intensity of IR radiation that reaches the detector after passing through the sample [132]. From the Fig. 2.21, a simple spectrometer layout can be seen.

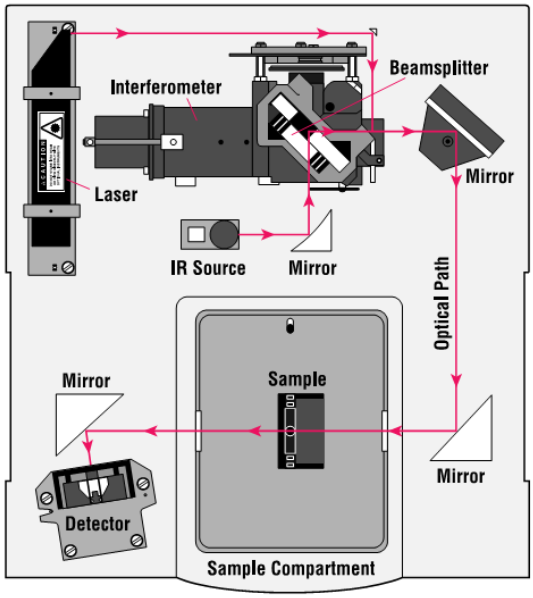

Figure 2.21 : A simple spectrometer layout [130].

2.5.2 X-ray powder diffraction (XRD)

X-ray crystallography is a powerful and unambiguous method for the structural determination and characterization of crystalline substances: from simple salts and small molecules to complex proteins. There is no technique that can match the speed and reliability of single crystal X-ray diffraction for determining the structure of molecules in the solid state. It provides fast, reliable, secure access to small molecule crystal structure determination. Bragg's law refers to the simple equation [135]:

$$n\lambda = 2\,d\sin\theta \qquad \textbf{(2.15)}$$

English physicists Sir W.H. Bragg and his son Sir W.L. Bragg developed this relation in 1913 to explain why the cleavage faces of crystals appear to reflect X-ray beams at certain angles of incidence (theta, θ). The variable 'd' is the distance between atomic layers in a crystal, and the variable lambda 'λ' is the wavelength of the incident X-ray beam; 'n' is an integer. This observation is an example of X-ray wave interference, commonly known as X-ray diffraction (XRD), and was direct evidence for the periodic atomic structure of crystals postulated for several centuries [135].

About 95 % of all solid materials can be described as crystalline. When X-rays interact with a crystalline substance (phase), one gets a diffraction pattern. The X-ray diffraction pattern of a pure substance is like a fingerprint of the substance [136].

An electron in an alternating electromagnetic field will oscillate with the same frequency as the field. When an X-ray beam hits an atom, the electrons around the atom start to oscillate with the same frequency as the incoming beam. In almost all directions destructive interference will be had, that is, the combining waves are out of phase and there is no resultant energy leaving the solid sample. However the atoms in a crystal are arranged in a regular pattern, and in a very few directions constructive interference will be had. The waves will be in phase and there will be well defined X-ray beams leaving the sample at various directions. Hence, a diffracted beam may be described as a beam composed of a large number of scattered rays mutually reinforcing one another [136].

Fig. 2.22 and 2.23 show the schemes for the basic XRD mechanism and X-ray scattering.

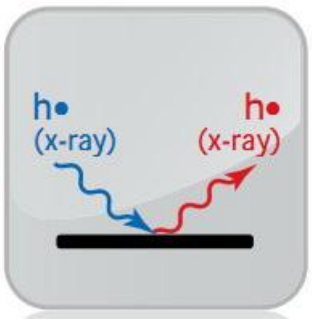

Figure 2.22 : XRD mechanism [131].

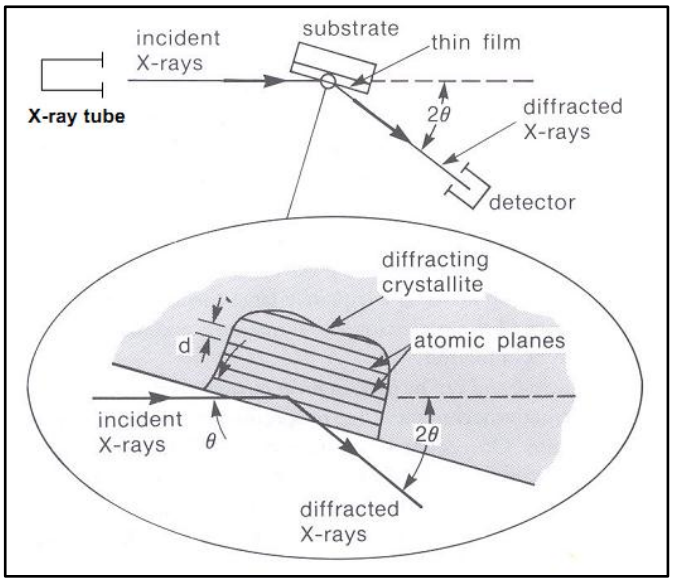

Figure 2.23 : Scattering of X-rays by a crystallite [137].

2.5.3 Transmission electron microscopy (TEM)

Transmission electron microscopy is used to reveal sub-micrometre, internal fine structure in solids [138]. It operates on the same basic principles as the light microscope but uses electrons instead of light [139] (Fig. 2.24).

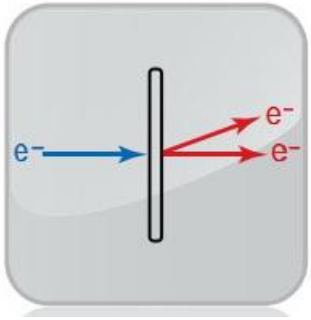

Figure 2.24 : TEM mechanism [131].

What you can see with a light microscope is limited by the wavelength of light. TEMs use electrons as "light source" and their much lower wavelength makes it

possible to get a resolution a thousand times better than with a light microscope. You can see objects to the order of a few angstrom (10^{-10} m). For example, you can study small details in the cell or different materials down to near atomic levels. The possibility for high magnifications has made the TEM a valuable tool in both medical, biological and materials research [139].

Electrons are one type of ionizing radiation, which is the general term given to radiation that is capable of removing the tightly bound, inner-shell electrons from the attractive field of the nucleus by transferring some of its energy to individual atoms in the specimen. One of the advantages of using ionizing radiation is that it produces a wide range of secondary signals from the specimen and some of these are summarized in Fig. 2.25 [140].

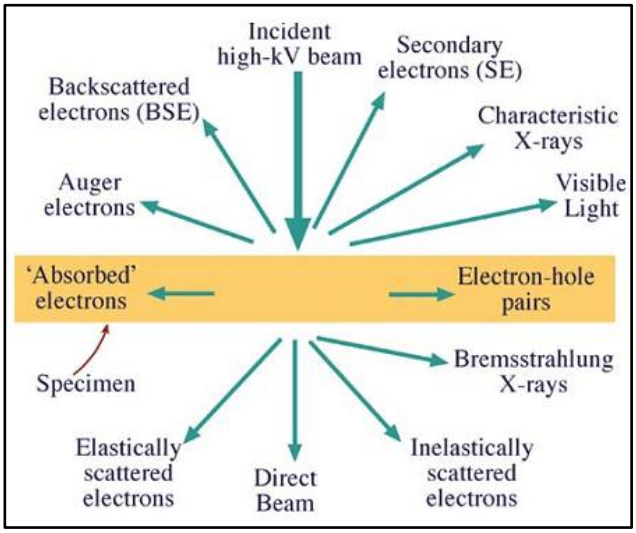

Figure 2.25 : Interaction of a high-energy beam of electrons with a thin specimen and the resulting secondary signals [140].

As can be seen in the Fig. 2.25, signals generated when a high-energy beam of electrons interacts with a thin specimen [140]. These inelastic interactions between electrons and matter give different kinds of signals: secondary electrons, Auger electrons, X-rays, light and lattice vibrations. The X-ray energy corresponds to a difference between two energy levels of the electron cloud of an atom [141]. Most of these signals can be detected in different types of TEM. The directions shown for each signal do not always represent the physical direction of the signal, but indicate, in a relative manner, where the signal is strongest or where it is detected. In order to get the best signal out of the specimens one has to put the best signal in, and so the electron source is critical [140].

A transmission electron microscope is constituted of: (1) two or three condenser lenses to focus the electron beam on the sample, (2) an objective lens to form the diffraction in the back focal plane and the image of the sample in the image plane, (3) some intermediate lenses to magnify the image or the diffraction pattern on the screen [141].

A "light source" at the top of the microscope emits the electrons that travel through vacuum in the column of the microscope (Fig. 2.26). Instead of glass lenses focusing the light in the light microscope, the TEM uses electromagnetic lenses to focus the electrons into a very thin beam. The electron beam then travels through the specimen. Depending on the density of the material present, some of the electrons are scattered and disappear from the beam. At the bottom of the microscope the unscattered electrons hit a fluorescent screen, which gives rise to a "shadow image" of the specimen with its different parts displayed in varied darkness according to their density. The image can be studied directly by the operator or photographed with a camera [139].

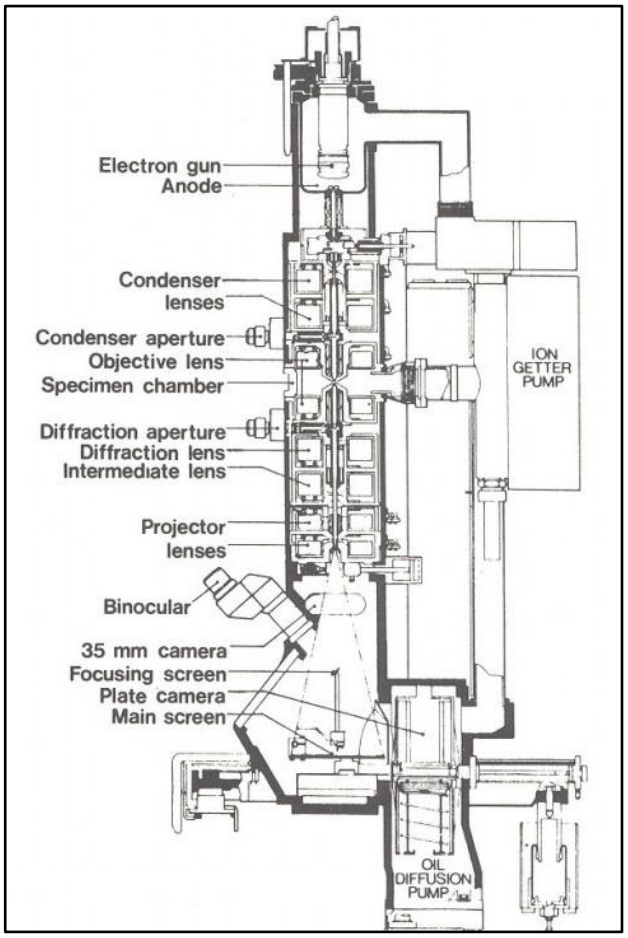

Figure 2.26 : Electron column of a TEM [142].

The amount and scale of the information which can be extracted by TEM depends critically on four parameters; the resolving power of the microscope (usually smaller than 0.3 nm); the energy spread of the electron beam (often several eV); the thickness of the specimen (almost always significantly less than 1 μm), and; the composition and stability of the specimen [138].

2.6 Applications of Magnetic Nanoparticles in Medicine

Iron oxide particles such as magnetite (Fe_3O_4) or its oxidized form maghemite (γ-Fe_2O_3) are by far the most commonly employed in biomedical applications since their biocompatibility has already been proven [17], (Fig. 2.27).

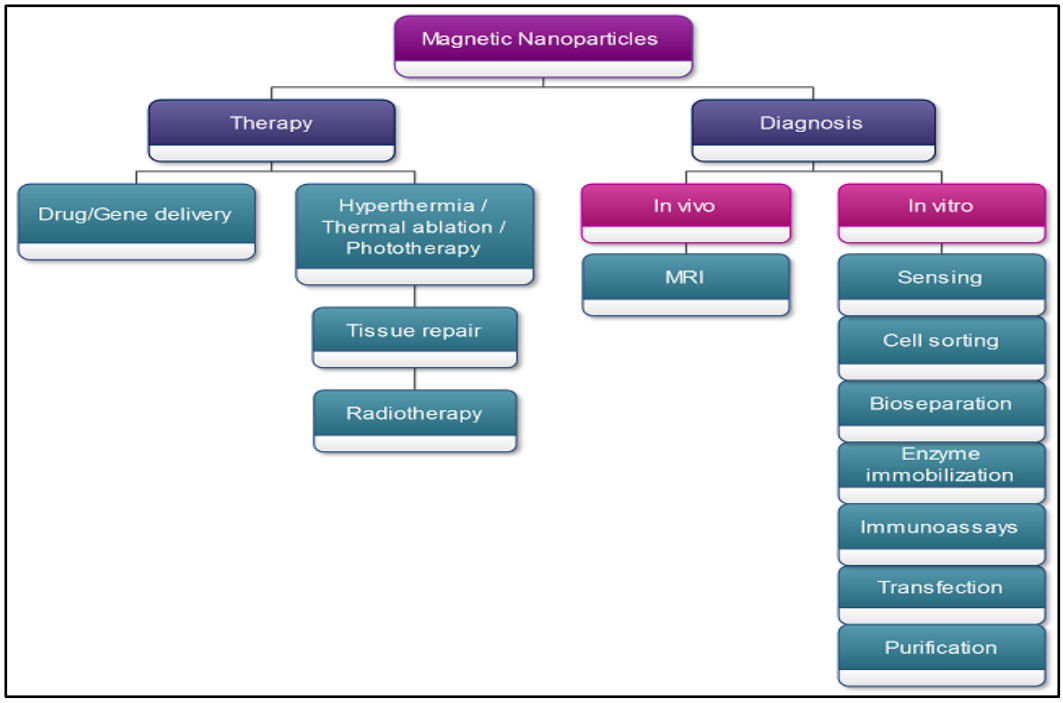

Figure 2.27 : General scheme of the different applications for magnetic nanoparticles (adapted from M. Arruebo et al., 2009) [143].

Fe_3O_4 has been widely studied in recent years due to its interesting magnetic properties and many potential applications, especially being an ideal candidate for biological applications [96]. In order that Fe_3O_4 nanoparticles exhibit required magnetic efficiency in biomedical applications, Fe_3O_4 nanoparticles should have the controlled size suitable for them because the magnetic properties depend strongly on the particle size. For example, Fe_3O_4 nanoparticles of about 10–20 nm are used for DDS (drug delivery system) and cancer therapy, and below 10 nm of superparamagnetic Fe_3O_4 nanoparticles with good dispersibility are needed for MRI

[49]. Though magnetic nanoparticles with different compositions, sizes and shapes have been developed for biomedical applications [16]. Thus, with these excellent properties, magnetite (Fe_3O_4) nanoparticles are suitable for biomedical applications, such as targeted drug delivery, MRI contrast enhancement, cancer diagnosis, hyperthermic treatment of tumors, and magnetically mediated separation of biomolecules [98].

2.6.1 Targeted drug delivery

Due to their small size, nanoparticles are particularly promising carriers for drug delivery systems used in cancer treatment. Such drug delivery systems increase the efficiency of chemotherapy and reduce the side effects [144].

The importance of targeted drug delivery and targeted drug therapy is to transport a drug directly to the centre of the disease under various conditions and thereby treat it deliberately, with no effects on the body [81]. Targeting of drugs by nanoparticles is intended to reduce drug wastage, frequency of drug administration, side effects providing prolonged, sustained drug delivery to desired targeted organ. Iron oxide magnetic nanoparticles present a higher performance in terms of chemical stability and biocompatibility compared with metallic nanoparticles. Nanoparticles have a large surface that may be properly modified to attach biological agents [145].

In magnetically targeted drug delivery, carriers comprising of coated magnetic nanoparticles loaded with anti-cancer drug are injected into the patient body via the human circulatory system. An external magnetic field is used to localize the drug loaded carriers at the tumor site and the drug can then be released from the carriers either via enzymatic activity or changes in physiological conditions such as pH, osmolality, or temperature and be taken up by tumor cells. Alexiou et al. showed that this magnetic targeted drug delivery caused complete tumor remission in tumor bearing rabbits without any negative side effects and the applied dose of drug reduced to 20 % of the regular systemic dose. A Phase-I human clinical trial with 4-epidoxorubicin showed encouraging results of the physiological tolerance of magnetic drug targeting by patients [146].

2.6.2 Hyperthermia cancer treatment

Magnetic nanoparticles can be utilized not only as carriers for drug delivery systems but also as heat sources for hyperthermia, which is a heat treatment for cancer that poses a low risk to the body and causes few side effects as compared to traditional cancer treatments such as surgery, chemotherapy, and radiation therapy [144].

Magnetic particles in a solution undergo two types of relaxation: Brownian relaxation, in which the entire particle rotates, and Néel relaxation, in which the moment rotates while the particle remains still [65]. When magnetic nanoparticles are subjected to an alternating magnetic field, heat can be generated by Néel relaxation, Brownian relaxation and hysteresis losses [146].

Hyperthermia is the heating of cells in the range of 41–47°C, which causes preferential death of tumor cells [146]. The method relies on the theory that any metallic objects when placed in an alternating magnetic field will have induced currents flowing within them. The amount of current is proportional to the size of the magnetic field and the size of the object. As these currents flow within the metal, the metal resists the flow of current and thereby heats, a process termed inductive heating. If the metal is magnetic, such as iron, the phenomenon is greatly enhanced. Therefore, when a magnetic fluid is exposed to an alternating magnetic field the particles become powerful heat sources, destroying the tumour cells. The magnetic fluids used are preferably suspensions of superparamagnetic particles, prepared much as described for MRI contrast agents, as these produce more heat per unit mass than larger particles. The level heating is simply controlled by the materials Marie Curie temperature, that is, the temperature above which materials lose their magnetic properties and thus their ability to heat [20].

The inevitable technical problem with hyperthermia is the difficulty in heating only the local tumor region to the intended temperature without damaging the surrounding healthy tissue. Fe_3O_4 nanoparticles have been used for hyperthermia treatment in an attempt to overcome this obstacle [96].

2.6.3 Magnetic resonance imaging (MRI)

The magnetic nanoparticles are especially useful in biomedicine when they are dispersed into water to form ferrofluids, which can be used, for example, as image contrast agents in magnetic resonance imaging (MRI) [147]. Fe_3O_4 MNPs possess

superparamagnetism which are suitable for MR contrast enhancement by alterations of proton relaxation in the tissue microenvironment [105].

MRI scans yield high-quality anatomical images for clinical diagnosis, pre-surgical assessment, and therapy monitoring. The technique works by applying a series of short-lived radio frequency (RF) pulses to a body placed within a constant magnetic field. Measured changes in the magnetization of hydrogen protons in water molecules are used to derive a picture of anatomical structures. So-called 'contrast agents', which alter the behavior of nearby molecules, can be administered to sharpen image detail [148].

In standard clinical MRI scans contrast agents travel through the bloodstream and tissues, increasing contrast wherever they go. Although the more commonly used MR contrast media are gadolinium (Gd) chelates, these tend to be non-specific with rapid accumulation in the liver, thus they only allow a short time imaging window. Colloidal iron oxides therefore play an important role as MRI contrast agents, as superparamagnetic iron oxide particles were the first liver-specific contrast agents used. It has been known for many years that the inclusion of magnetic particles within tissue enables a very large signal to be obtained from a MRI scanner [20].

MNPs can remain for longer periods in tissue than compared to common contrast agents. This has the added benefit of reducing the quantity of contrast agent to be administered to the patient thus minimizing any adverse toxic effects. In addition, it is possible to take more scans after administration resulting in an overall enhancement of the MRI contrast. Due to the polymer coating, MNPs possess longer blood circulation times which improve the efficiency of detection of the cancer cells. Furthermore, the possibility to add bioactive functional groups at the surface of the particles (such as enzymes, peptides, antibodies and various antagonists) allows the specific cell targeting of the MNPs in the organism. Finally, the MNPs are more selective and more specific than other contrast agents which improves MRI results [149].

2.6.4 Bioseparation processes

Separation of specific biological entities from their environments is very important in biochemical analysis and disease diagnosis [16]. Fe_3O_4 particles exhibit superparamagnetic behavior at room temperature. In other words, they magnetize

strongly under an applied magnetic field but retain no permanent magnetism once the field is removed [98]. This magnetic on/off switching behavior is extremely helpful for magnetic separation [16].

Magnetic separation is a well-developed method and can be used as an alternative to the conventional centrifugal separation method. A typical magnetic separation procedure mainly consists of four steps, and iron oxide particles are often used in magnetic separation. In the first step, magnetic microbeads are made by encasing iron oxide nanoparticles in a biocompatible coating, and the surface of the microbeads is functionalized with a special biological or chemical agent that can selectively bind to the target cells or molecules to be separated. In the second step, the functionalized microbeads are added to the solution containing the target cells or molecules, and the target cells or molecules are subsequently bound to the magnetic microbeads. In the third step, a permanent magnet is placed at the side of the solution, inducing a magnetic moment on the magnetic microbeads and establishing a magnetic field gradient which drives the magnetized microbeads to move along the field lines. Finally, the magnetized microbeads cluster together near the magnet, and thus the target cells or molecules bound to the magnetic microbeads are separated [16].

Various biological molecules such as antibodies, proteins, targeting ligands, etc., may also be bound to the polymer surfaces onto the nanoparticles by chemically coupling via amide or ester bonds to make the particles target specific [21], (Fig. 2.28).

When conjugated with biomolecules such as antibodies, biotin and enzyme and so on, the MNPs could form lock-and-key interactions with target molecules of antigen, streptavidin and substrate, respectively. Therefore, adequate amount of biomolecules and biological activity on the surface of MNPs is the key of their specific recognition and target capability [150].

MNPs can be further derivatised with non-specific moieties (ionic, hydrophobic, hydrogen bond), group specific (dye ligand, immobilized metal affinity chromatography, or chelating), or highly specific ligands (antigen-antibody, avidin-biotin, enzyme-inhibitor, etc). An overview of viable surface anchoring groups is represented in Fig. 2.29 [149].

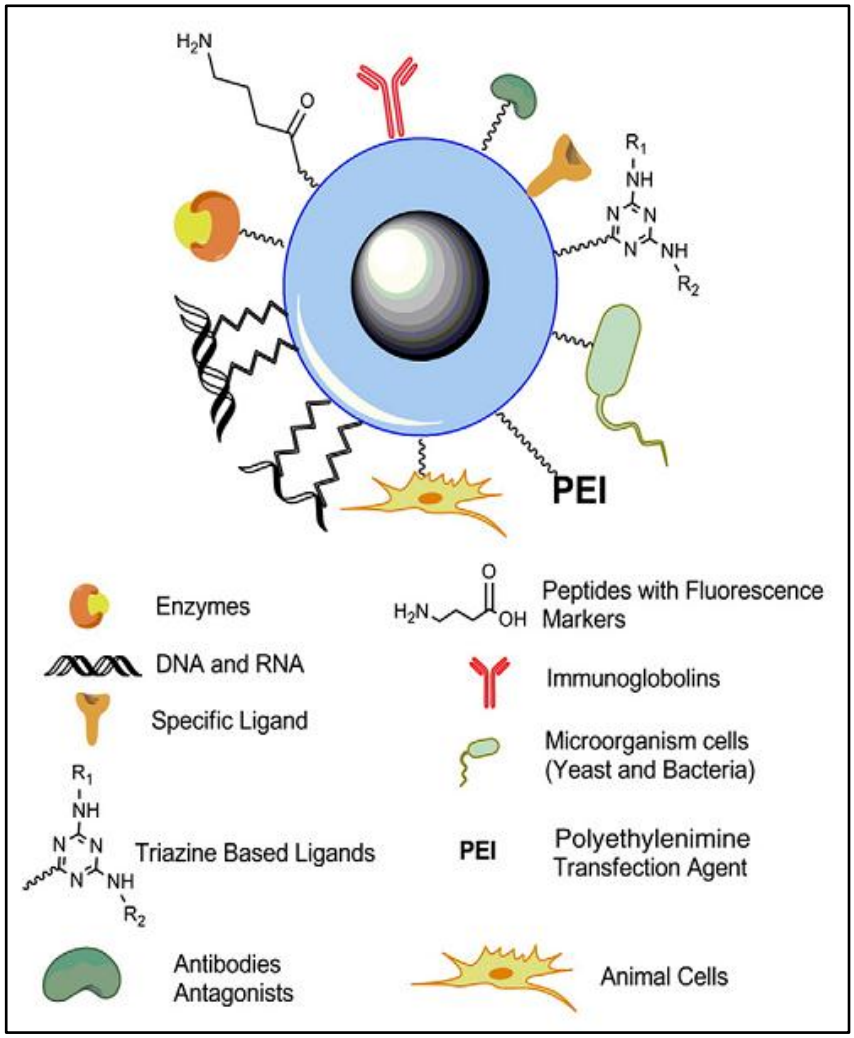

Figure 2.28 : Examples of magnetic nanoparticles coated with polysaccharides and decorated with multifunctional receptors [149].

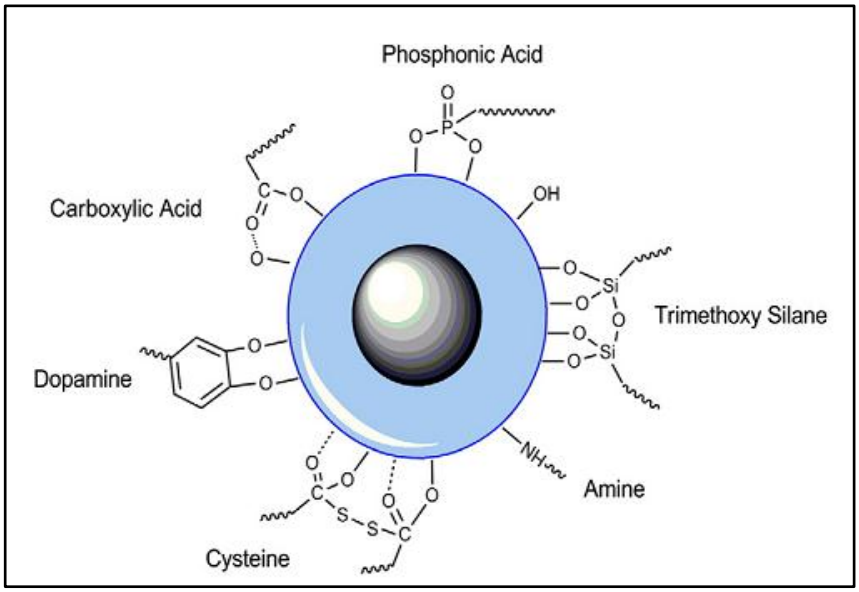

Figure 2.29 : Common chemical moieties for the anchoring of polymers and functional groups at the surface of magnetic nanoparticles [149].

The application of magnetic particles (sub-micron to 10 μm) in separation processes permits fast and cost effective separation of the target biomolecule from the reaction mixture without filtration or centrifugation, therefore representing a gentle, scalable, versatile and easy to automate separation process [149].

Magnetic separation has wide application in biotechnology and biomedicine, such as immunomagnetic cell separation and purification, immunoassays, isolation, purification and recognition of proteins. In molecular biology, it can be used for DNA/RNA purification. In addition, the isolation and detection of microorganisms is easily possible using magnetic separation [17].

2.6.4.1 Immunomagnetic separation

Immunomagnetic separation has become an essential tool for high-throughput and low-cost isolation of biomolecules and cells from heterogeneous samples [151]. With surface modification, magnetic nanoparticles have been labeled with a variety of biological molecules that have the ability to scavenge for targets of interest and separate them from complex biological media [152]. Antibodies, for example, specifically bind to their antigen, providing an effective means of tagging [65].

Antibodies are nanosize biological products that are part of the specific immune system. In addition to their own properties as pathogens or toxin neutralizers, as well as in the recruitment of immune elements (complement, improving phagocytosis, cytotoxicity antibody dependent by natural killer cells, etc.), they could carry several elements (toxins, drugs, fluorochroms, or even nanoparticles, etc.) and be used in several diagnostic procedures, or even in therapy to destroy a specific target [143].

A typical antibody molecule (the prototype class of immunoglobulin is IgG) is made up of four polypeptide chains with a molecular weight of about 150 kD. The four chains are divided into two identical light chains and two identical heavy chains [153], (Fig. 2.30).

A heavy chain has three regions that affect recognition, variable (V), diversity (D), and joining (J). A light chain has only the V and J regions. In humans, there are approximately one hundred different V genes, twelve D genes, and four J genes [154].

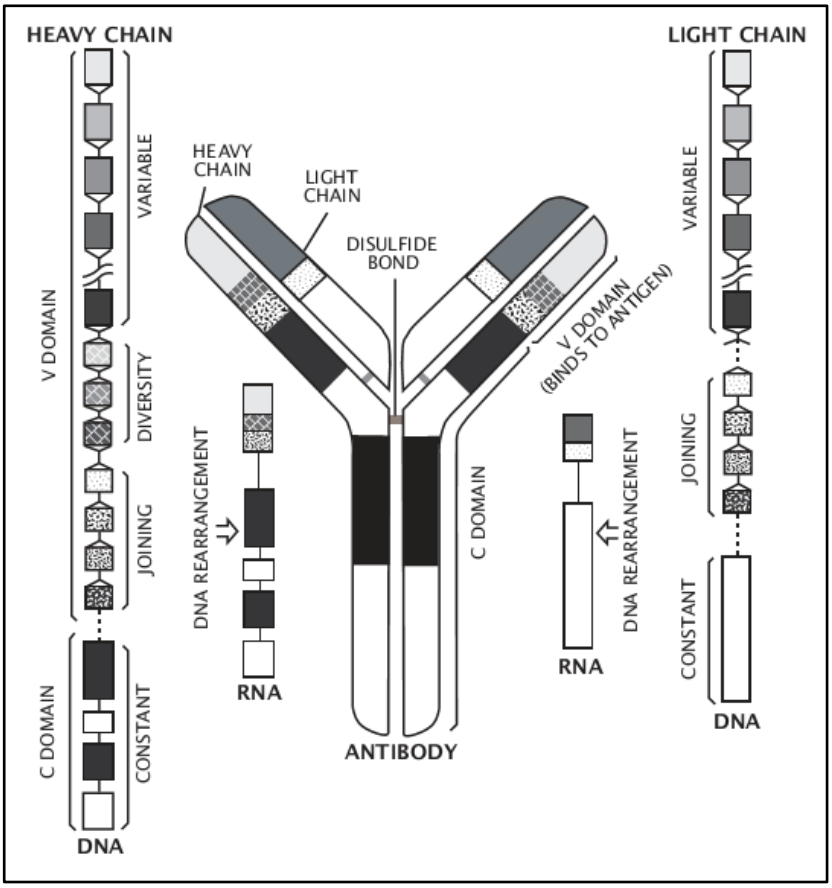

Figure 2.30 : The coding and assembly of antibody molecules [154].

An antibody molecule is Y-shaped, with two identical antigen-binding sites at the ends of the arms of the Y. The light and heavy chains contribute to the antigen-binding sites. Each antibody molecule can bind to two identical antigenic determinants. Where the arms meet, the stem of the Y is known as the hinge region. The hinge region allows segmental flexibility of the antibody molecule. The two antigen-binding ends (or amino-terminal ends) of the antibody molecule are called the Fab fragments (for fragment antigen binding), whereas the stem (or carboxyl-terminal end) of the Y is considered to be the Fc fragment (for fragment crystallizable). The Fc region of the antibody molecule is responsible for its biologic properties, which include activation of the complement system (leading to enhanced phagocytosis), placental transfer, and binding to cell-surface receptors [153].

Specific host immunity recognizes and binds to an epitope, which is a small molecular site within a larger parasite molecule. An antigen is a parasite molecule that stimulates a specific immune response because it contains one or more epitopes. For example, if one injects a large foreign protein into a host, the host recognizes thousands of different epitopes on the surface of the protein antigen [154].

In medical and clinical diagnostics, the interaction of antigens and antibodies is routinely used to measure concentrations of biological markers [155]. Most often, a monoclonal antibody (MAb) is used for immunomagnetic separation [156]. Monoclonal antibodies were the first targeting agents to exploit molecular recognition to deliver magnetic nanoparticles and continue to be widely used due to their high specificity [157].

Magnetic particles carrying specific antibody can be used for the capture of target cells and their separation from the environment [158]. Bioconjugation can take place by means of adsorption (at the isoelectrical point of the antibody via electrostatic interaction), by direct covalent linkage between the surface of the nanoparticle and the antibody. Optimal bioconjugation would involve the covalent attachment of the antibody through the Fc (fragment: crystallizable) region, leaving the antigen-binding site Fab (fragment: antigen binding) region oriented to the medium to preserve its full function, and in a ratio of one to one to allow a direct quantification. The conjugation of antibodies to nanoparticles can generate a product that combines the properties of both. For example, they can combine the small size of nanoparticles and their special thermal, imaging, drug carrier, or magnetic characteristics with the abilities of antibodies, such as specific and selective recognition [143].

A simple representation of immunomagnetic separation of targeted molecules is shown in Fig. 2.31.

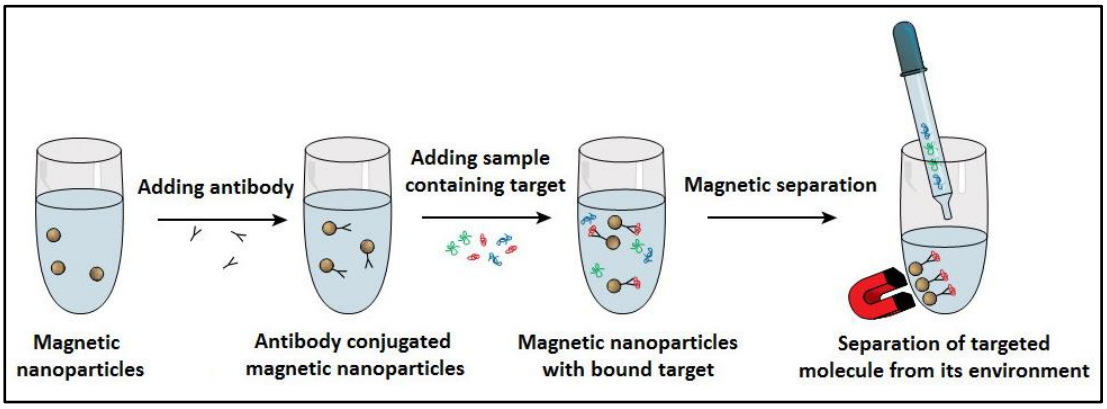

Figure 2.31 : Scheme diagram of immunomagnetic separation of targeted molecules (adapted from Dynal information booklet, 2010) [159].

As indicated in Fig. 2.31, immunomagnetic separation process mainly consists of three steps: first, the surface of the magnetic nanoparticles is anchored with antibodies which are against targeted antigens, and immunomagnetic nanoparticles

(antibody conjugated magnetic nanoparticles) are obtained. Second, these immunomagnetic nanoparticles are mixed with the suspension containing targeted molecules (antigens) to be separated. Finally, after forming antibody-antigen complexes, a magnetic field is applied to the suspension, and the immunomagnetic nanoparticles with the targeted molecules on them are separated from the rest of the sample. Then, all other substances are washed out easily. In the further step, a suitable solution to uncouple targeted molecules from antibodies is used together with a magnet, and the targeted molecules are obtained. The covalent bond between magnetic particle and antibody allows one to perform the regeneration of immunomagnetic nanoparticles without any significant loss of the binding capacity. So, after washing step, the immunomagnetic nanoparticles can be stored and used for further separation processes.

The number of papers in databases such as PubMed, employing the principle of immunomagnetic separation, is approaching 1000 and is rapidly increasing [156]. As an example, biotin-labelled polyclonal goat anti-*Escherichia coli* antibodies have been attached to streptavidin-coated magnetic nanoparticles, and used for the separation and selective quantification of *Escherichia coli* O157:H7 in ground beef in the presence of other bacteria [143].

H. Xu et al. demonstrated a highly efficient process using iron oxide magnetic nanoparticles-based immunomagnetic separation of tumor cells from fresh whole blood. The process involved polymer coated 30 nm iron oxide magnetic nanoparticles that was modified with antibodies (Ab) against human epithelial growth factor receptor 2 (anti-HER2 or anti-HER2/neu) forming iron oxide magnetic nanoparticles-antibody [160].

C.E. Probst et al. reported a rapid multitarget immunomagnetic separation technology that combined the extensive multiplexing capacity of DNA-antibody conjugates and the high selectivity, throughput, and simplicity of magnetic isolation by employing a unique approach involving strand-mediated displacement (SMD) of DNA linkers [151]. W. Chen et al. prepared immunomagnetic nanoparticles by covalently immobilizing anti-$CD34^+$ monoclonal antibodies to the surface of amino silane modified magnetic particles. The cell separation results showed that the synthesized immunomagnetic nanoparticles could rapidly and conveniently separate the $CD34^+$ cells with high efficiency and specificity than normal ones [161].

3. EXPERIMENTAL PART

3.1 Substances

Table 3.1 : Chemicals and reagents.

Name	Purity	Producer
Iron(II) sulfate heptahydrate, $FeSO_4.7H_2O$	≥ 99 %	Sigma-Aldrich, USA
Iron(III) chloride hexahydrate, $FeCl_3.6H_2O$	≥ 99 %	Sigma-Aldrich, USA
Ammonium hydroxide solution, NH_4OH	25 %	Lach-Ner, Czech Republic
Oleic acid, $C_{18}H_{34}O_2$	≥ 98 %	Lachema, Czech Republic
Chitosan	medium molecular weight	Aldrich, USA
Glutaric dialdehyde (Glutaraldehyde, $OHC(CH_2)_3CHO$)	50 % wt. solution in water	Sigma-Aldrich, USA
8-iso Prostaglandin $F_{2\alpha}$ EIA Antiserum	100 %	Cayman Chemical, USA
Cysteinyl Leukotriene EIA Monoclonal Antibody	LTC_4 – 100 % LTD_4 – 100 % LTE_4 – 79 %	Cayman Chemical, USA
Sodium dihydrogen phosphate monohydrate, $H_2NaO_4P.H_2O$	≥ 99 %	Fluka, USA
Sodium phosphate dibasic dihydrate, $Na_2HPO_4.2H_2O$	≥ 99.5 %	Riedel-deHaën, Germany
Sodium chloride, NaCl	≥ 99 %	Aldrich, USA
Albumin from bovine serum (BSA)	further purified Fraction V	Sigma, USA
alpha,alpha,alpha-Tris-(hydroxymethyl)-methylamin, $(HOCH_2)_3CNH_2$	≥ 99.9 %	Aldrich, USA
Sodium azide, NaN_3	≥ 99 %	Aldrich, USA
8-iso Prostaglandin $F_{2\alpha}$	> 99%	Cayman Chemical, USA
Cysteinyl-Leukotriene HPLC Mixture I (LTC_4, LTD_4, LTE_4)	≥ 98% for each compound	Cayman Chemical, USA
Glycine, $C_2H_5NO_2$	≥ 99 %	Sigma, USA
Dynabeads M-280 Tosylactivated	research grade	Dynal Biotech ASA, Norway

Table 3.1 (continued): Chemicals and reagents.

Name	Purity	Producer
Leukotriene C_4-d_5	≥ 99 %	Cayman Chemical, USA
Leukotriene D_4-d_5	≥ 99 %	Cayman Chemical, USA
Leukotriene E_4-d_5	≥ 99 %	Cayman Chemical, USA
8-iso Prostaglandin $F_{2\alpha}$-d_4	≥ 99 %	Cayman Chemical, USA

Table 3.2 : Solvents.

Name	Purity	Producer
Water	Deionized	Watrex, Czech Republic
Water	LC/MS quality	Fisher Scientific, USA
Nitric acid, HNO_3	65 %	Lach-Ner, Czech Republic
Acetone, C_3H_6O	99.97 %	Lach-Ner, Czech Republic
Acetic acid, $C_2H_4O_2$	99.8 %	Fisher Scientific, USA
Ethanol, C_2H_6O	HPLC quality	Merck, Germany
Hydrochloric acid, HCI	35 %	Lach-Ner, Czech Republic
Acetonitrile	99.9 %	Fisher Scientific, USA

Table 3.3 : Buffers.

Name	Preparation
Buffer A (0.1 M Phosphate Buffer, pH 7.4)	0.262 g $NaH_2PO_4.H_2O$ and 1.442 g $Na_2HPO_4.2H_2O$ are dissolved in 100 mL water
Buffer B (PBS Buffer, pH 7.4 with 0.1 % (w/v) BSA)	0.88 g NaCI and 0.1 g BSA are dissolved in 10 mL of 0.01 M phosphate buffer, and then diluted to 100 mL with water
Buffer C (0.2 M TRIS, pH 8.5 with 0.1 % (w/v) BSA)	2.42 g TRIS is dissolved in 50 mL water, and the pH is adjusted to 8.5 with 1 M HCI. Then, 0.1 g BSA is added and dissolved in the solution. Finally, it is diluted to 100 mL with water
Buffer D (PBS Buffer, pH 7.4 with 0.5 % (w/v) BSA)	0.88 g NaCI and 0.5 g BSA are dissolved in 50 mL of 0.01 M phosphate buffer, and diluted to 100 mL with water

Table 3.4 : Gases.

Name	Purity	Producer
Argon	technical 4.6	SIAD, Czech Republic
Nitrogen	technical 4.0	SIAD, Czech Republic
Air	technical	SIAD, Czech Republic

3.2 Instruments and Materials

3.2.1 Fourier transform infrared spectroscopy (FT-IR)

Infrared spectra were measured on FTIR spectrometer Nicolet 6700. Measuring technique was attenuated total reflectance (ATR) with single reflection ATR diamond crystal (GladiATR, PIKE Technologies, USA). The spectral range of the measurement was 4000 – 400 cm^{-1} with the resolution 4 cm^{-1} and number of spectra accumulation 64 and Happ-Genzel apodization. Spectra were processed by Omnic 7.3 (Nicolet Instruments Co., USA) program.

3.2.2 X-ray powder diffraction (XRD)

X-ray powder diffraction was measured on two types of instruments: (1) θ-θ powder difractometer X'Pert PRO (PANalytical, the Netherlands) and (2) θ-θ powder difractometer Bruker AXS D8 (Bruker AXS, USA). Measurement was done on θ-θ powder diffractometer X'Pert PRO in Bragg-Brentano parafocusing geometry with the use of CuK_α radiation (λ = 1.5418 Å, U = 40 kV, I = 30 mA) at room temperature. Data were scanned by ultrafast X'Celerator detector (or scintillation detector with secondary curved monochromator) in the angle range 5-60° (2θ) with the measuring step 0.02° (2θ) and frequency of measuring 0.3 s/step. Data were evaluated with the use of HighScore Plus program.

Data were also measured on θ-θ powder diffractometer Bruker AXS D8 in Bragg-Brentano parafocusing geometry with the use of CoK_α radiation (λ = 1.79021Å, U = 34 kV, I = 20 mA) at room temperature. Data were scanned by ultrafast LynxEye detector in the angle range 10-80° (2θ) with the measuring step 0.0196° (2θ) and frequency of measuring 19.2 s/step. Data were evaluated with the use of HighScore Plus program and the size of the particles was calculated from the width in the half of the peak.

3.2.3 Transmission electron microscopy (TEM)

Samples were viewed under a Philips CM100 electron microscope (FEI, formerly PEO Eindhoven, the Netherlands) at 80 kV**.** Digital images were recorded using a MegaView II slow scan camera (Olympus, formerly SiS GmbH, Germany) at a primary magnification ranging from 64,000× to 92,000× giving pixel size of 1 nm or 0.7 nm, respectively. Recorded images were processed in AnalySis 3.2 software.

3.2.4 Liquid chromatography–mass spectrometry (LC-MS)

The analysis of the substances were carried out on the LC-MS system consisting of degaser with pump and autosampler Accela (Thermo Fisher Scientific, USA) and mass spectrometer with triple stage quadrupole analyzer - TSQ Vantage (Thermo Fisher Scientific, USA) with electro-spray ionization (H-ESI). Fig. 3.1 shows the mass spectrometry combined with the liquid chromatography used in the laboratory.

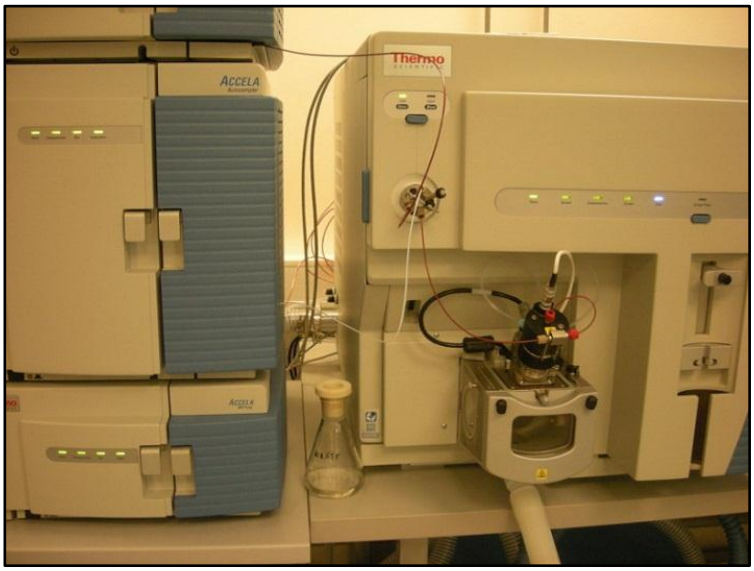

Figure 3.1 : LC-MS system.

3.2.5 Commercially available magnetic particles (Dynabeads M-280 Tosylactivated)

Dynabeads M-280 Tosylactivated are uniform, superparamagnetic, polystyrene beads coated with a polyurethane layer. They have diameters of 2.8 μm, a surface area of 4-8 m^2/g, a density of 1.4 g/cm^3 and an active chemical functionality of 0.1-0.2 mmol/g Dynabeads [162] (Fig. 3.2).

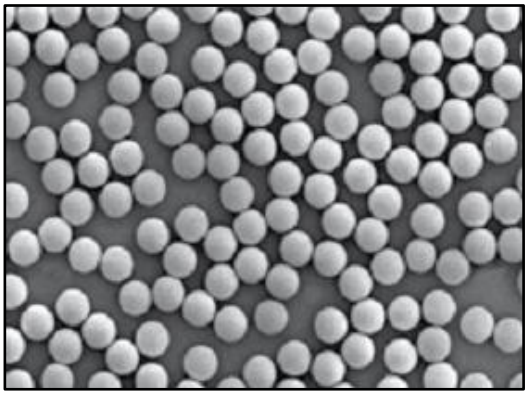

Figure 3.2 : Dynabeads M-280 Tosylactivated [159].

The hydroxy groups are activated by reaction with p-toluensulphonyl chloride. The resulting sulphonyl ester can subsequently react covalently with proteins or other ligands containing amino or sulfhydryl groups. Dynabeads M-280 Tosylactivated will bind proteins physically and chemically with an increasing number of covalent bonds with higher temperature and pH [162].

Dynabeads M-280 Tosylactivated is a solid-phase designed for biomagnetic separations. Any ligand (e.g. antibody, protein, peptide or glycoprotein) containing amino or sulfhydryl groups can be covalently coupled to the surface of the beads (Fig. 3.3) [162].

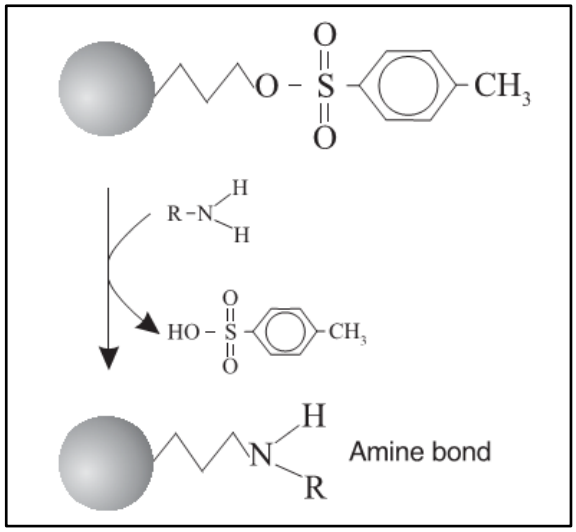

Figure 3.3 : Ligand coupling protocol for Dynabeads M-280 Tosylactivated [162].

The combination of specific antigens or antibodies and the superparamagnetic properties of the Dynabeads ensure rapid reaction kinetics both in the binding process and in the separation of the analyte [162].

In this study, apart from the synthesized magnetic Fe_3O_4–chitosan nanoparticles, antibodies were also conjugated to the Dynabeads M-280 Tosylactivated.

3.2.6 Other apparatus and equipments

- Overhead stirrer, IKA EUROSTAR power basic (IKA-Werke GmbH & Co. KG, Germany)
- Magnetic stirrer, IKA C-MAG HS 7 (IKA-Werke GmbH & Co. KG, Germany)
- Shaker, IKA MS 3 digital (IKA-Werke GmbH & Co. KG, Germany)
- Shaker, IKA KS 130 basic (IKA-Werke GmbH & Co. KG, Germany)

• Minishaker, IKA MS 2 (IKA-Werke GmbH & Co. KG, Germany)

• Magnet with 6 tube-holder plastic rack, Dynal MPC-S (Dynal Biotech ASA, Norway)

• Ultrasonic bath, Bandelin Sonorex Digitec DT 102 H (Bandelin GmbH & Co. KG, Germany)

• pH meter, CyberScan pH 510 (Eutech Instruments Pte Ltd, Singapore)

• Adjustable-volume pipettes in different sizes (Eppendorf AG, Germany)

• Eppendorf tubes (1.5-2 mL) and tips (Eppendorf AG, Germany)

3.3 Preparation of Magnetic Fe_3O_4 Nanoparticles with Oleic Acid

The magnetite, Fe_3O_4 ($FeO.Fe_2O_3$) magnetic nanoparticles were synthesized by co-precipitation of Fe(II) and Fe(III) solutions in base medium for using in the preparation of chitosan functionalized magnetic nanoparticles (Fe_3O_4–chitosan nanoparticles). Oleic acid was used for stabilization, preventing the agglomeration among the nanoparticles. Equation (3.1a) and (3.1b) show the overall reaction of Fe_3O_4:

$$FeSO_4 + 2FeCl_3 + 8NH_4OH \rightarrow Fe_3O_4 + (NH_4)_2SO_4 + 6NH_4Cl + 4H_2O \quad \textbf{(3.1a)}$$

$$Fe^{+2} + 2Fe^{+3} + 8OH^- \leftrightarrow Fe(OH)_2 + 2Fe(OH)_3 \rightarrow Fe_3O_4 + 4H_2O \quad \textbf{(3.1b)}$$

In the procedure, 0.9 g $FeSO_4.7H_2O$ was dissolved in 8.75 mL deionized water and 1.7 g $FeCl_3.6H_2O$ was dissolved in 10 mL deionized water with the mole ratio of Fe^{+2}/Fe^{+3} = 1/2. The iron solutions were mixed together and transferred into a 250 mL three-necked flask which was placed into an oil-bath. Then 4.4 mL of ammonium hydroxide solution (NH_4OH) and 0.4 mL oleic acid were added into the solution quickly under a vigorous stirring by a shaft mixer (overhead stirrer). The mixture was stirred for 1 hour at room temperature. After 1 hour the temperature was increased to 95°C. When 95°C was achieved and the reaction was completed, the flask was removed from the oil-bath and cooled to room temperature. The pH of the mixture was measured and adjusted to ~5 with HNO_3:H_2O (1:5) solution.

The supernatant was separated from the resulting black precipitates of magnetite by decantation with the help of a strong magnet, and the oleic acid modified magnetic Fe_3O_4 nanoparticles were collected through magnetic separation. Then the particles

were washed 4 times with deionized water and 4 times with acetone in order to remove non-binding components. The products were stored in acetone. Fig. 3.4 shows the flowchart of the synthesis of the oleic acid modified magnetic Fe_3O_4 nanoparticles by co-precipitation.

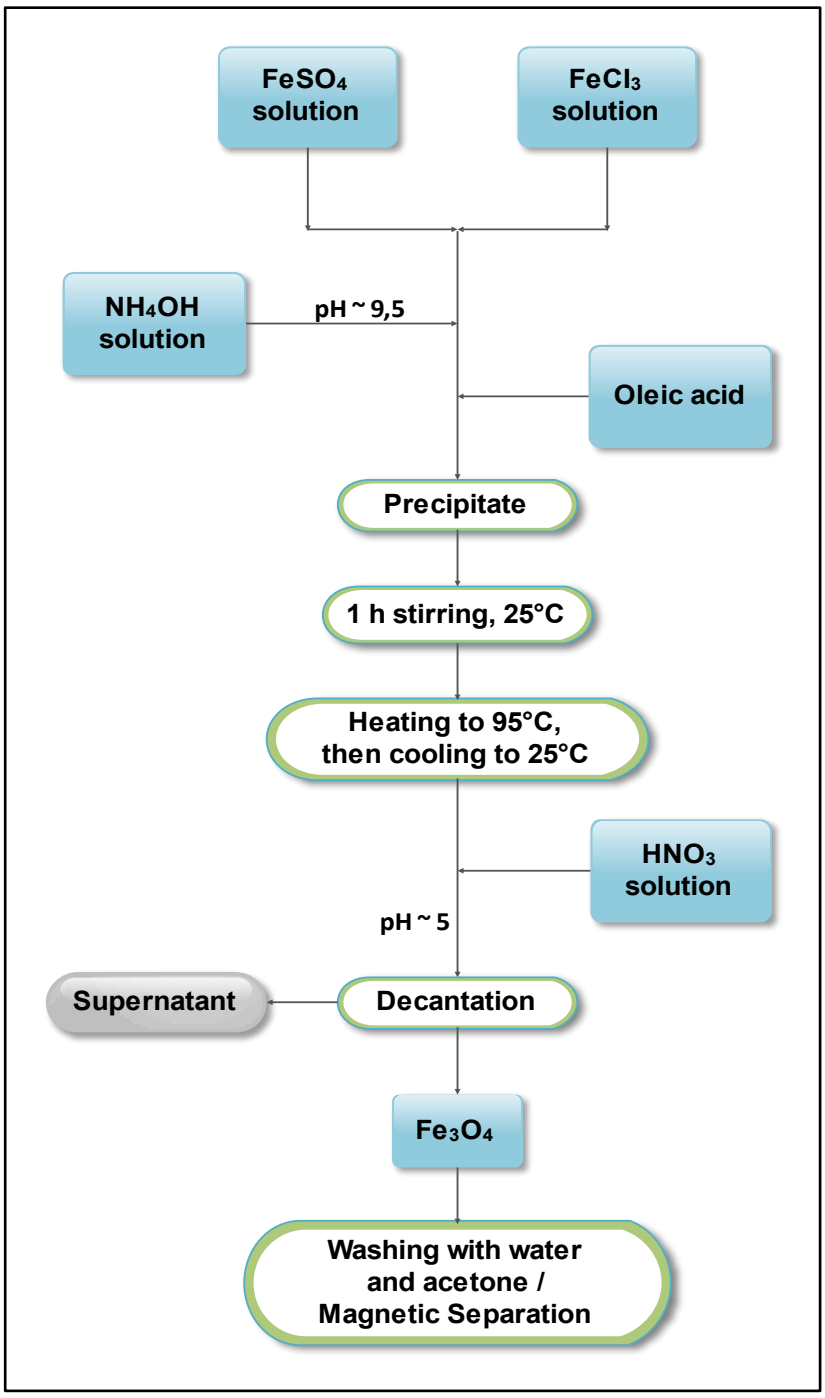

Figure 3.4 : Flowchart of the synthesis of the magnetic Fe_3O_4 nanoparticles by co-precipitation.

A schematic illustration for the formation of the oleic acid modified magnetic Fe_3O_4 nanoparticles is shown in Fig. 3.5.

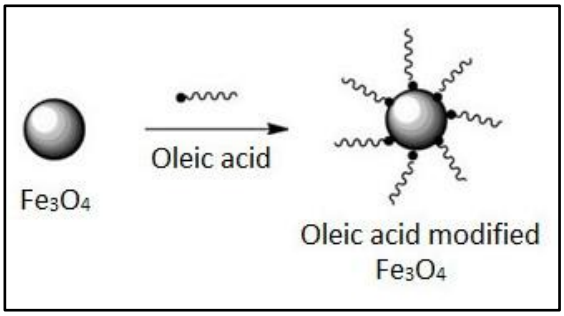

Figure 3.5 : Scheme for the oleic acid modified magnetic Fe_3O_4 nanoparticles (adapted from J. Qu et al., 2010) [89].

3.4 Functionalization of Fe_3O_4 Nanoparticles with Chitosan and Glutaraldehyde

For the functionalization of the magnetic Fe_3O_4 nanoparticles with chitosan and glutaraldehyde, first 0.25 g chitosan was dissolved in 50 mL of 1.0 wt% acetic acid solution and 0.75 g dry, oleic acid modified magnetic Fe_3O_4 nanoparticles were weighed. The Fe_3O_4 nanoparticles and the chitosan solution were added into a 100 mL flask. The flask was placed into an ultrasonic bath and the dispersion medium in the flask was treated with ultrasonic agitation for 10 min at room temperature. After 10 min, the flask was placed on a mechanical shaker and stirred for 20 min more. Then, an additional 1 mL of 25 wt% glutaraldehyde solution was added into the mixture as cross-linker, and the flask was placed into a water-bath which was set on a hot-plate magnetic stirrer. The cross-linking reaction between chitosan and glutaraldehyde was kept for 3 hours at 40°C under magnetic stirring. After the completion of the reaction, the supernatant was separated by decantation with the help of the magnet, and the magnetic Fe_3O_4–chitosan nanoparticles were collected through magnetic separation. Then the particles were washed 4 times with deionized water and 4 times with ethanol in order to remove non-binding components. The products were stored in ethanol. Fig. 3.6 shows the flowchart of the preparation of magnetic Fe_3O_4 nanoparticles functionalized with chitosan and glutaraldehyde.

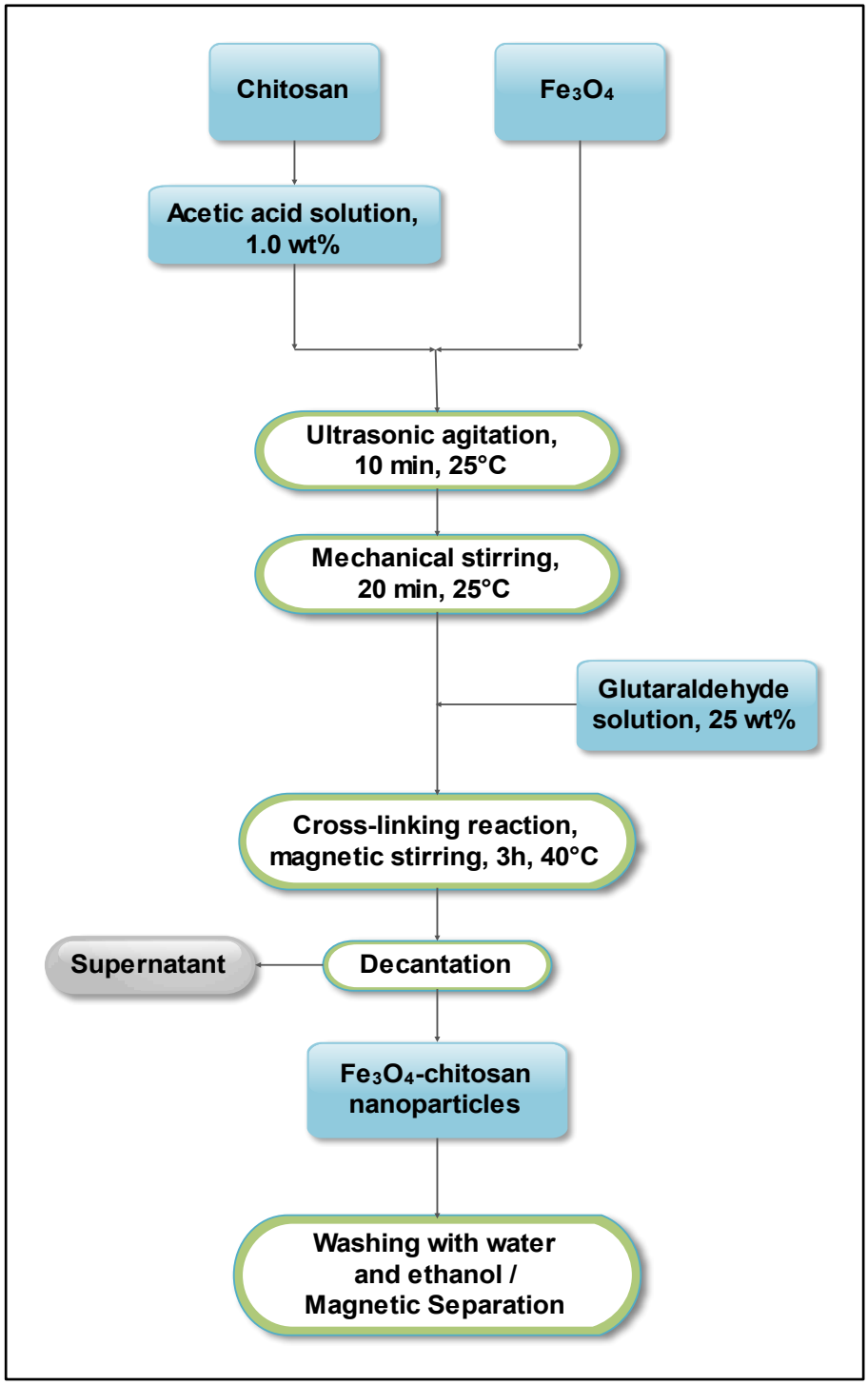

Figure 3.6 : Flowchart of the preparation of the magnetic Fe_3O_4–chitosan nanoparticles.

A schematic illustration for the formation of the magnetic Fe_3O_4–chitosan nanoparticles is shown in Fig. 3.7.

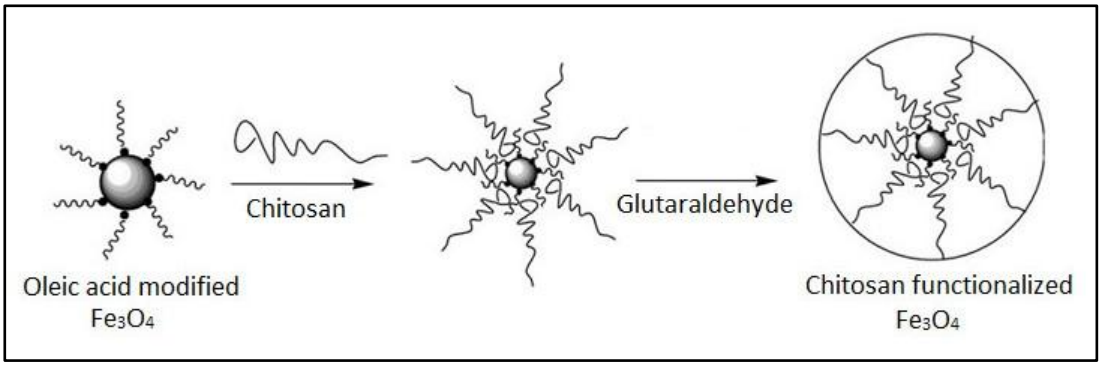

Figure 3.7 : Scheme for the chitosan functionalized magnetic Fe_3O_4 nanoparticles (adapted from J. Qu et al., 2010) [89].

3.5 Anchoring Antibody onto the Surface of Magnetic Fe_3O_4–Chitosan Nanoparticles

For immobilizing antibodies on the surface of the magnetic Fe_3O_4–chitosan nanoparticles, approximately 1 mg of magnetic Fe_3O_4–chitosan nanoparticles were weighed and put into an Eppendorf tube. To wash the particles, 200 µl of Buffer A was added into the tube and the tube was vortexed in a minishaker for 5 min. After 5 min, the tube was placed in the magnet (with holders) and the supernatant was removed by pipetting out and the particles were isolated from the liquid part. The washing procedure was repeated twice. After the washing step, 100 µl (could be at different amounts according to the experiment) antibody (against cysteinyl leukotrienes or 8-iso Prostaglandin $F_{2\alpha}$ according to the experiment) and 400 µl of Buffer A were added to the Fe_3O_4–chitosan nanoparticles. The tube was placed in the minishaker and vortexed for 20 hours. After 20 hours, the tube was placed in the magnet and the supernatant was removed by pipetting out, and the particles were washed in order to remove non-binding components. In the washing procedure, 200 µl of Buffer D was added into the tube and it was vortexed in the minishaker for 10 min. After 10 min, the tube was placed in the magnet and the supernatant was removed by pipetting out, and the antibody anchored magnetic Fe_3O_4–chitosan nanoparticles (immunomagnetic nanoparticles) were isolated from the liquid part. The washing procedure with Buffer D was repeated 4 times. The immunomagnetic nanoparticles were stored in 0.02 % sodium azide (NaN_3) solution prepared in Buffer A.

A schematic illustration for anchoring antibody onto the surface of the magnetic Fe_3O_4–chitosan nanoparticles is shown in Fig. 3.8.

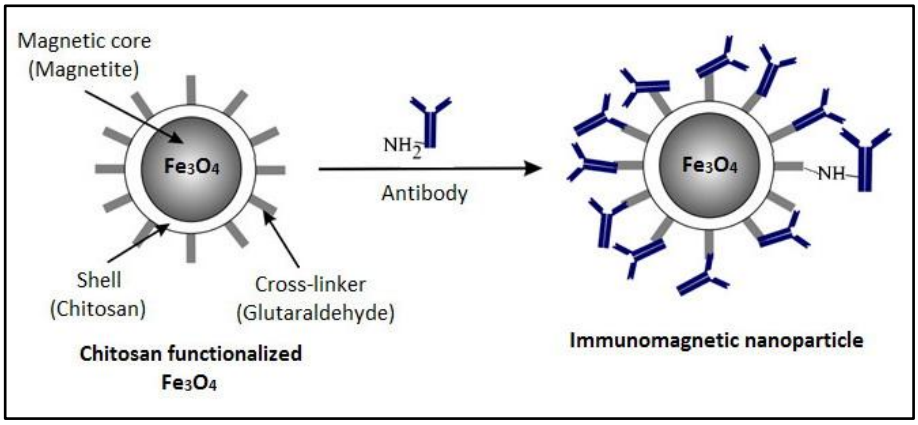

Figure 3.8 : Scheme for the formation of the immunomagnetic nanoparticles (adapted from K. Syslová et al.) [2].

3.6 Anchoring Antibody onto the Surface of Dynabeads M-280 Tosylactivated

The procedure for immobilizing antibodies on the surface of the Dynabeads M-280 Tosylactivated differs little from the procedure for immunomagnetic nanoparticles. To prepare antibody anchored Dynabeads, 30 µl (~42 mg) of Dynabeads solution was put into an Eppendorf tube and the tube was placed in the magnet (with holders) and the supernatant was removed by pipetting out, and the Dynabeads were isolated from its liquid part. To wash the particles, 200 µl of Buffer A was added into the tube and the tube was vortexed in the minishaker for 5 min. After 5 min, the tube was placed in the magnet and the supernatant was removed again, and the particles were isolated from the liquid part. The washing procedure was repeated 3 times. After the washing step, 100 µl antibody against Cys-LTs and 400 µl of Buffer A was added to these washed Dynabeads. The tube was placed in the minishaker and vortexed for 24 hours. After 24 hours, the tube was placed in the magnet and the supernatant was removed, and the particles were washed in order to remove non-binding components. In the washing procedure, the Dynabeads were first washed 2 times with 200 µl of Buffer B, each vortexing for 5 min. After removing the second supernatant, 200 µl of Buffer C was added into the tube and it was vortexed for 4 hours. After 4 hours, the tube was placed in the magnet and the supernatant was removed. As the final washing step 200 µl of Buffer B was added into the tube and it was vortexed for 5 min. After 5 min, the tube was placed in the magnet and the supernatant was removed, and the antibody anchored magnetic Dynabeads were isolated from the liquid part. The resulting immunomagnetic Dynabeads were stored in 0.02 % sodium azide (NaN_3) solution prepared in Buffer B.

3.7 Formation of Antibody-Antigen Complexes

The immunomagnetic particles were used to separate Cys-LTs and 8-iso $PGF_{2\alpha}$ (essential biomarkers of asthma and oxidative stress, respectively) from biological matrices like exhaled breath condensate (EBC). These biomarker molecules were treated like antigens in this study. The principle of the immunomagnetic separation method was based on forming antibody-antigen (antibody-biomarker) complexes on the surface of the particles and isolating these complexes by applying an external magnetic field. In the procedure, first the immunomagnetic particles, which were already in the Eppendorf tubes, were washed 3 times with 500 µl of Buffer A, each vortexing for 5 min. After the washing step, the tube was placed in the magnet and the supernatant was removed by pipetting out. A sample containing biomarkers (Cys-LTs or 8-iso $PGF_{2\alpha}$, at different concentrations according to the experiment) was prepared and added to the particles. Then the tube was vortexed in the minishaker for 1 hour. After 1 hour vortexing, antibody-antigen complexes were formed. The tube was placed in the magnet and the supernatant was removed by pipetting out, and the particles were washed 3 times with 1 mL of HPLC quality water in order to remove non-binding components (each vortexing for 5 min). After the last washing step, the supernatant was removed again by pipetting out and the immunomagnetic particles with the antibody-antigen complexes on them were isolated from the liquid part.

A schematic illustration for forming antibody-antigen complexes on the immunomagnetic nanoparticles is shown in Fig. 3.9.

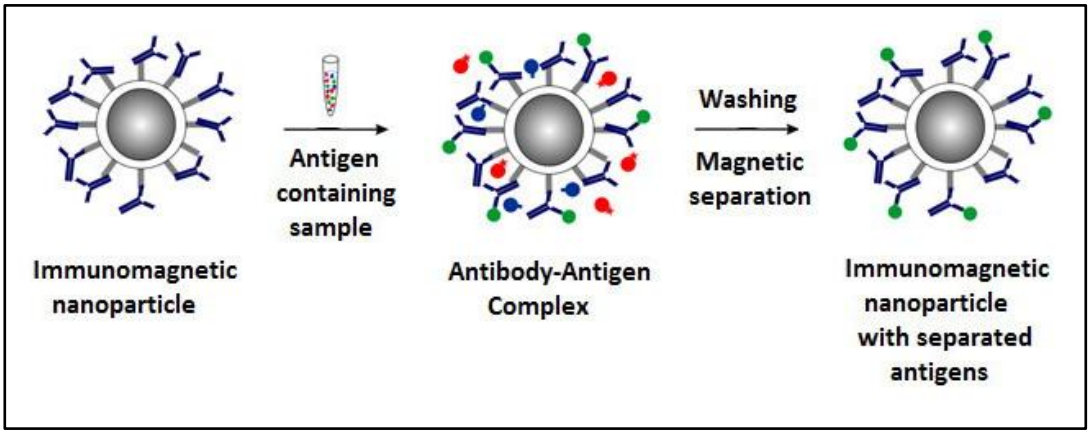

Figure 3.9 : Scheme for formation of antibody-antigen complexes (adapted from K. Syslová et al.) [2].

3.8 Separation of Antigens from Antibody-Antigen Complexes

In order to uncouple the antigens (Cys-LTs and 8-iso $PGF_{2\alpha}$) from the antibodies (and thus from the immunomagnetic nanoparticles or the immunomagnetic Dynabeads) by breaking the bonds between them, 100 mmol/L glycine solution was used. To prepare this solution 0.075 g glycine was weighed and dissolved in 10 mL water. 100 µl of this solution was added to the immunomagnetic particles having antibody-biomarker complexes on them. The tube was vortexed in the minishaker for 10 min. After 10 min, the biomarkers (Cys-LTs/8-iso $PGF_{2\alpha}$) were uncoupled from the antibodies and released to the liquid part (glycine solution). The tube was placed in the magnet once again, but this time the liquid part containing Cys-LTs/8-iso $PGF_{2\alpha}$ was separated from the immunomagnetic particles by pipetting out. The amount of the biomarkers in this sample was measured by LC-MS. After washing, the immunomagnetic particles were regenerated and stored in the fridge for next immunomagnetic separations.

A schematic illustration for separating antigens from antibody-antigen complexes is shown in Fig. 3.10.

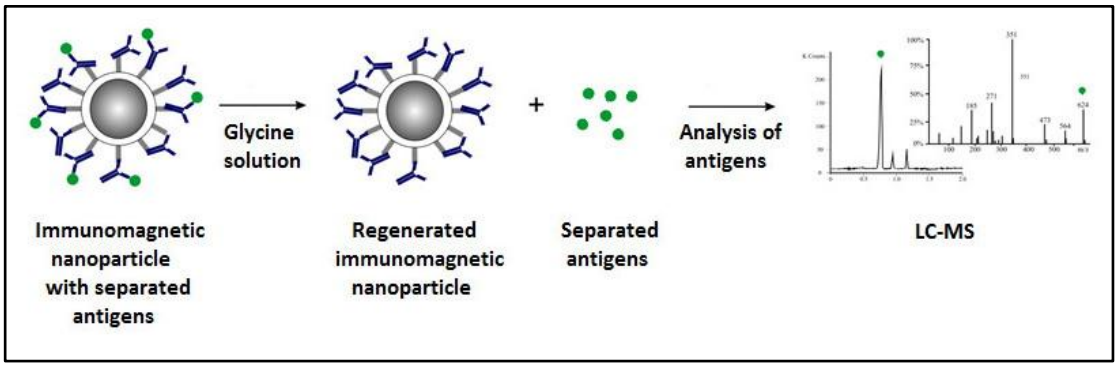

Figure 3.10 : Scheme for separation of antigens from antibody-antigen complexes (adapted from K. Syslová et al.) [2].

The summary of the principle of the immunomagnetic separation method applied in this study can be seen in Fig. 3.11.

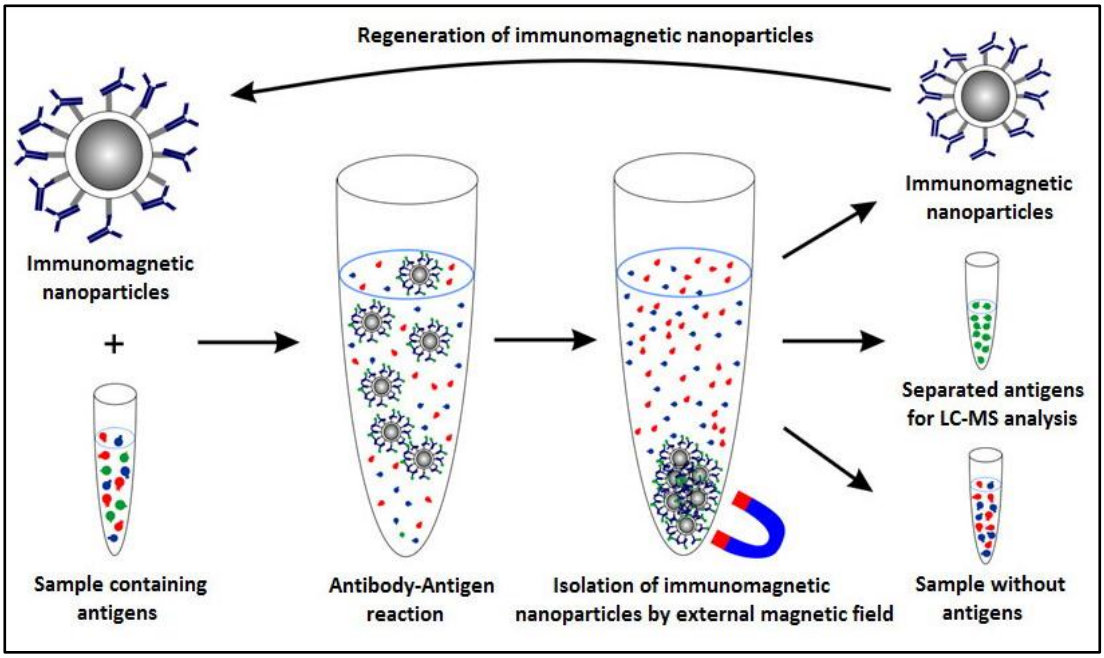

Figure 3.11 : Scheme for the principle of the immunomagnetic separation method (adapted from K. Syslová et al.) [2].

3.9 LC-ESI-MS/MS Analysis

In LC-ESI-MS/MS (liquid chromatography combined with electrospray ionization tandem mass spectrometry), isocratic mobile phase composition of acetonitrile:water (70:30 v/v) was used for the separation of Cys-LTs and 8-iso $PGF_{2\alpha}$. Flow of the mobile phase was 150 µl/min. For the determination of the Cys-LTs and 8-iso $PGF_{2\alpha}$ and their deuterium labelled analogues (LTC_4-d_5, LTD_4-d_5, LTE_4-d_5 and 8-iso $PGF_{2\alpha}$-d_4) by the mass spectrometer, negative electrospray ionization (ESI^-) in selective reaction monitoring (SRM) mode with collision-induced dissociation (CID) was used. In particular, the selected reaction monitoring mode was used for its extremely high degree of selectivity. Monitoring reactions were: LTC_4 624 (precursor ion) → 271 (product ion) (collision energy: 24 eV), LTD_4 495 → 176 (21 eV), LTE_4 438 → 333 (21 eV), and 8-iso Prostaglandin $F_{2\alpha}$ 353 → 193 (27 eV). Conditions on the mass spectrometer were optimized to values as follows: spray voltage -2500V (negative ion mode), capillary (ion transfer tube) temperature 300°C, HESI vaporizer temperature 300°C, sheath gas (nitrogen) pressure 35 psi, auxiliary gas flow (nitrogen) 10 ArbU. The data were acquired and processed using the software Xcalibur 2.1.0 (Thermo Scientific, USA).

3.10 Collection of Exhaled Breath Condensate

The commercially available condenser EcoScreen (Jaeger, Germany) was used to collect the samples of exhaled breath condensate (EBC). All clinical samples were collected between 8-12 a.m. The subjects (patients diagnosed with sub-types of bronchial asthma and the control group of healthy non-smokers) were encouraged to perform a tidal breathing through a mouthpiece connected to the condenser (-20°C) for 5-10 minutes (volume of exhaled air was held at a constant level of 120 l) while wearing a nose-clip. The acquired volumes of EBC samples ranged between 1-2 ml. The EBC sample (1.0 ml) was immediately spiked with 250 pg of each deuterium labelled internal standard (LTC_4-d_5, LTD_4-d_5, LTE_4-d_5 and 8-iso $PGF_{2\alpha}$-d_4) and consecutively frozen to -80°C. The storage period was not exceeded one month.

3.11 Preparation of Samples for LC-ESI-MS/MS Analysis – Separation of Substances from Exhaled Breath Condensate

Anti-Cys-LTs/*Anti*-8-iso $PGF_{2\alpha}$ coated magnetic Fe_3O_4–chitosan nanoparticles (approx. 1 mg) stored in Buffer A with sodium azide were washed two times with Buffer B (400 μl) and re-suspended in 1 ml EBC. The suspension was incubated under shaking for 1 h and supernatant was removed. The nanoparticles were washed five times in Buffer B (400 μl). The supernatant was removed and the nanoparticles were treated with 50 μl of glycine solution for 1 min, which caused elution of Cys-LTs/8-iso $PGF_{2\alpha}$ from the antibody-antigen complex on the surface of the magnetic nanoparticles. The resulting supernatant was collected immediately and the sample prepared in this way was analyzed by HPLC-ESI-MS/MS. The nanoparticles were washed five times in Buffer B (400 μl) and the regenerated immunomagnetic nanoparticles were stored at 4°C in Buffer A (400 μl) with 0.1 % sodium azide (w/v) for next immunomagnetic separations.

3.12 Validation of the Method

3.12.1 Standard preparation and calibration procedure

The Cys-LTs and 8-iso $PGF_{2\alpha}$ stock solutions (20 ng/ml) were prepared by diluting biomarker standards in the mobile phase (acetonitrile:water). It was used for the preparation of a series of calibration samples with following concentrations: 5, 10,

25, 50, 100, 250 and 500 pg/50 µl water (each calibration sample was spiked with 250 pg of each internal standards (LTC_4-d_5, LTD_4-d_5, LTE_4-d_5 and 8-iso $PGF_{2\alpha}$-d_4)). The peak area of a particular substance with the assigned internal standard was used as the function to quantify the concentration.

3.12.2 Accuracy and precision

The "EBC blank matrix" was prepared by combining EBC samples from healthy subjects and immunomagnetic separation of Cys-LTs and 8-iso $PGF_{2\alpha}$ was repeated up to the time where the amount of each particular substance was below limit of detection (= LOD; determined by LC-ESI-MS/MS). The aliquot (1 ml) of the "EBC blank matrix" was spiked with four different amounts of individual Cys-LTs and 8-iso $PGF_{2\alpha}$ (25, 50, 100 and 250 pg). Each sample was prepared repeatedly (n = 5). These samples were pre-treated by the immunomagnetic separation procedure and quantified by LC-ESI-MS/MS. The limits of detection (LOD) and quantification (LOQ) were determined using the assay of the "EBC blank matrix" (n = 5). The values of LOD and LOQ were calculated as the mean value of the "EBC blank matrix" treble signals, three times the amount of the standard deviation for LOD and ten times the amount of the standard deviation for LOQ, respectively. Subsequently, the mean of each set of concentrations, the standard deviation (SD) and the relative standard deviation (RSD) were calculated and the value of the precision parameter was determined. The accuracy of the method was calculated as the difference between the standards (corresponding concentration level of a particular substrate was dissolved in mobile phase and analyzed by LC-ESI-MS/MS) and the samples worked out by the pre-treatment procedure. The relative error (RE) and the recovery were calculated on this basis.

3.13 Clinical Study

The objective of the clinical study was to verify the possibility of using immunomagnetic separation procedure as a pre-treatment method in combination with LC-ESI-MS/MS for the evaluation of clinical samples. Exhaled breath condensate (EBC) samples were collected from persons with two sub-types of bronchial asthma (occupational asthma (30 subjects) and hard-to-treat asthma (32 subjects)). The control group for occupational asthma was represented by 20 healthy

subjects with identical average age (45-54 years) and gender (male). The control group for hard-to-treat asthma was also represented by 20 subjects with identical average age (20-25 years) and gender (male) without bronchial asthma diagnosis (healthy subjects). The samples collected during the clinical study were worked out by the above-mentioned immunomagnetic separation method and the concentration levels of Cys-LTs and 8-iso $PGF_{2\alpha}$ were determined by LC-ESI-MS/MS.

4. RESULTS AND DISCUSSION

4.1 Preparation of Immunomagnetic Nanoparticles

The magnetic Fe_3O_4 nanoparticles were firstly synthesized by co-precipitation method and oleic acid was used for stabilization. Oleic acid was chemically adsorbed onto the surface of the nanoparticles. Then chitosan was added to coat on the surface of the Fe_3O_4 nanoparticles as a polymeric shell. The magnetic Fe_3O_4–chitosan nanoparticles were functionalized by cross-linking the amino groups on the chitosan using glutaraldehyde. X-ray diffraction pattern indicated that the magnetic nanoparticles were pure Fe_3O_4 with an average diameter of about 5.7 nm. Transmission electron microscopy showed that the magnetic Fe_3O_4–chitosan nanoparticles were quasi-spherical with a mean diameter of about 8.4 nm. The binding of chitosan and glutaraldehyde onto the surface of the magnetic Fe_3O_4 nanoparticles was also demonstrated by the measurement of Fourier transform infrared spectra.

After these procedures, antibody conjugated magnetic Fe_3O_4–chitosan nanoparticles (immunomagnetic nanoparticles) were prepared. TEM images demonstrated that the magnetic Fe_3O_4–chitosan nanoparticles were anchored with antibodies. These immunomagnetic nanoparticles were used to form antibody-antigen complexes on them and separate biomarkers from biological complexes like EBC.

In this study, cysteinyl leukotrienes (Cys-LTs) and 8-iso Prostaglandin $F_{2\alpha}$ (8-iso $PGF_{2\alpha}$) were treated like antigens and they were uncoupled from the formed complexes by glycine solution through magnetic separation. The resulting samples of these molecules were measured by liquid chromatography combined with mass spectrometry. The mass spectrometry results showed that the measured samples contained Cys-LTs and 8-iso $PGF_{2\alpha}$, proving that the isolation of these molecules from the complexes, and thus from the immunomagnetic nanoparticles was successful and the prepared immunomagnetic nanoparticles actually worked. The whole process applied in this study is summarized in Fig. 4.1.

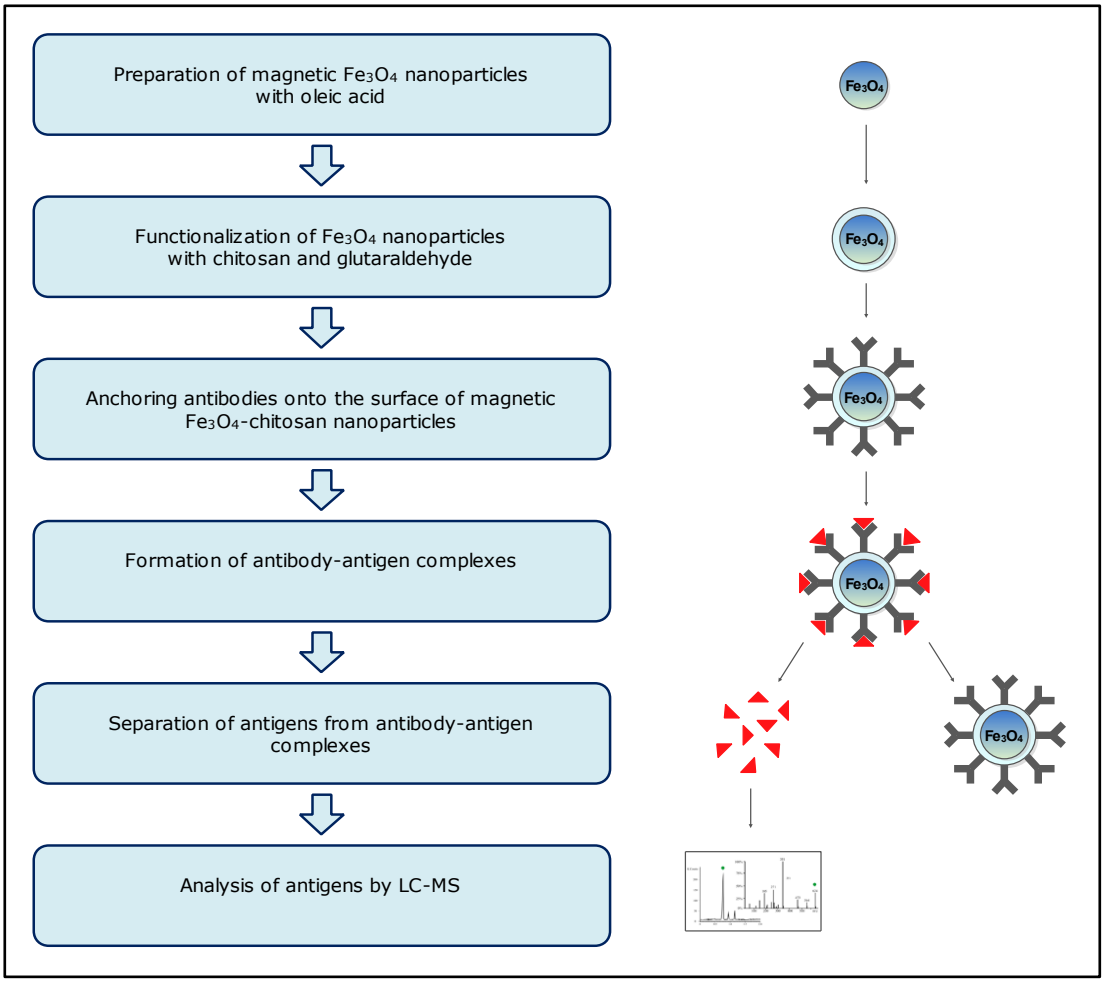

Figure 4.1 : Summary of the whole process applied in the study.

4.2 Characterization of Magnetic Nanoparticles

4.2.1 Fourier transform infrared spectroscopy (FT-IR)

For the measurement of infrared spectra, the sample of particles was dispersed in acetone and spreaded on a crystal. The solvent evaporated very quickly and the spectrum was measured for determination of the presence of oleic acid, chitosan and glutaraldehyde on the surface of the magnetic nanoparticles.

Fourier transform infrared measurements were carried out on the pure oleic acid, chitosan, glutaraldehyde solution, magnetic Fe_3O_4 nanoparticles stabilized with oleic acid and magnetic Fe_3O_4 nanoparticles functionalized with chitosan and glutaraldehyde. The spectra can be seen in Fig. 4.2–6. Under the Fig. 4.2, 4.3 and 4.4 there are tables (4.1, 4.2 and 4.3) with absorption bands identifying the substances.

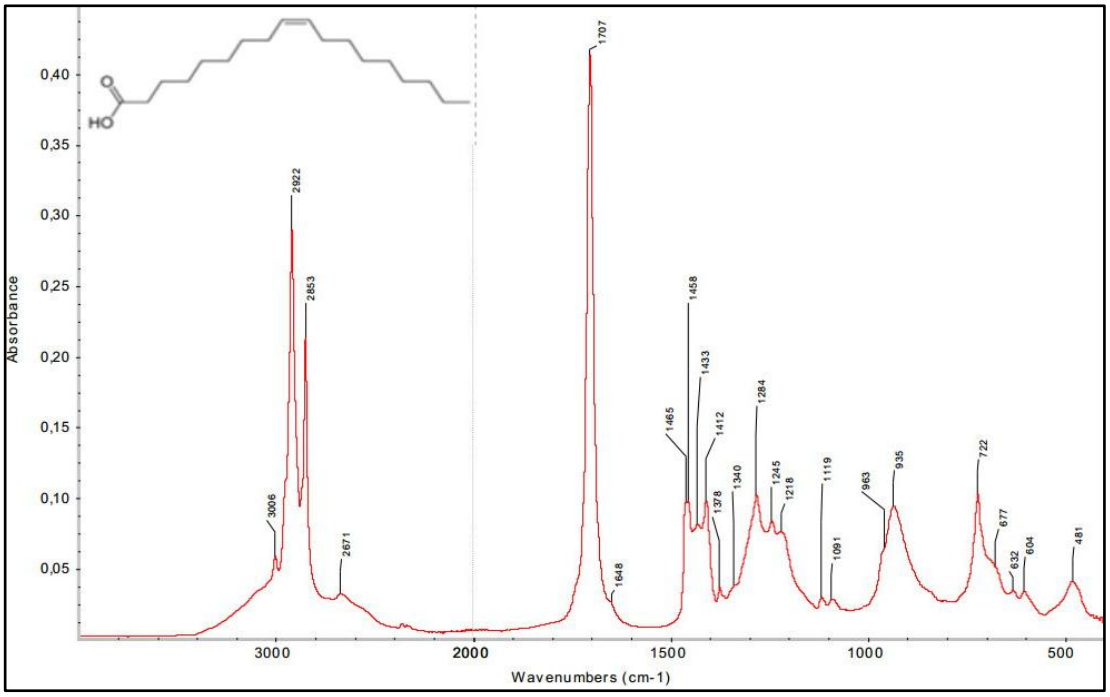

Figure 4.2 : The infrared spectrum of pure oleic acid.

Table 4.1 : Identification of the functional groups of oleic acid[2].

Wave number [cm^{-1}], intensity	Present band	Assignment	Functional group
3050-2995; m	3006	ν (CH)	=CH-
1685-1620; w-m	1648	ν (C=C)	>C=C<, >C=CH_2
1415-1340; w	1340	δ (CH)	-CH=CH-, *cis*
730-665; m	677	γ (CH)	R-CH=CH-R', *cis*
2955-2915; m	2922	ν_{as} (CH_2)	-(C)-CH_2-, -(O)-CH_2
2880-2830; m	2853	ν_s (CH_2)	-(C)-CH_2-, -(O)-CH_2
1470-1440; m	1458	δ (CH_2)	-(C)-CH_2-, -(O)-CH_2
735-720; w-m	722	ρ (CH_2)	$(CH_2)_n$-(C)-, n>3
1480-1440; m	1465	δ_d (CH_3)	-(C)-CH_3, -(O)-CH_3
1395-1345; m-s	1378	δ_s (CH_3)	-(C)-CH_3, -(O)-CH_3
3300-2500; m, br	wide bandwidth of 3300-2500	ν $(OH)^+$	-COOH
1725-1700; vs	1707	ν (C=O)	-COOH, dimeric form
1440-1395; w	1433	δ $(OH)^+$, ν (CO)	-COOH, dimeric form
1320-1210; m-s	1284	ν (CO)	-COOH, dimeric form, sometimes doublet
955-915; m, br	935	γ (OH)	-COOH, dimeric form

[2] Abbreviations used in the tables: w: weak, m: medium, s: strong, vs: very strong, v: variable, br: broad; ν: stretching, ν_{as}: asymmetric stretching, ν_s: symmetric stretching, δ: bending, γ: out-of-plane bending, δ_s: in-plane bending (scissoring), ρ: in-plane bending (rocking).

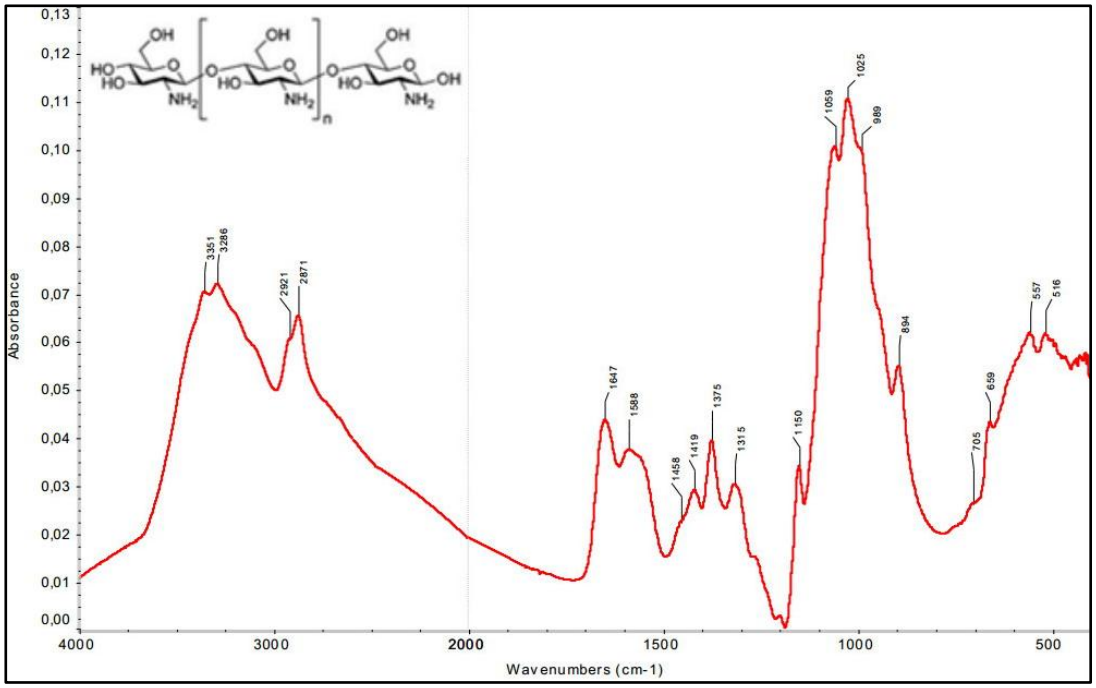

Figure 4.3 : The infrared spectrum of chitosan.

Table 4.2 : Identification of the functional groups of chitosan[3].

Wave number [cm^{-1}], intensity	Present band	Assignment	Functional group
3450-3300; w-m, br	3351	ν_{as} (NH_2)	-NH_2
3400-3250; w-m, br	3286	ν_s (NH_2)	-NH_2
1650-1580; s-m	1647	δ (NH_2)	-NH_2
1100-1000; w-m	covered	ν (CN)	R-NH_2, often covered by other bands
900- 650; s, br	894	γ (NH)	-NH_2
2955-2915; m	2921	ν_{as} (CH_2)	-(C)-CH_2-, -(O)-CH_2
2880-2830; m	2871	ν_s (CH_2)	-(C)-CH_2-, -(O)-CH_2
1470-1440; m	1458	δ (CH_2)	-(C)-CH_2-, -(O)-CH_2
785- 750; w-m	covered	ρ (CH_2)	-CH_2-CH_x, $x \neq 2$
1155-1050; s	1150	ν_{as} (COC)	-O-, aliphatic ethers
1140- 900; s	1025	ν_s (COC)	-O-, =C-O-C, aliphatic ethers
3550-3230; m-s, br	Wide bandwidth of 3500-2600	ν (OH)	-OH, dimeric and polymeric intermol. H-bond
3200-2500; v, br		ν (OH)	-OH, intramol. chelating H-bond
1440-1310; m-s	1375	δ (COH)	tert.-OH, Ar-OH
1130-1055; s	1059	ν (CO)	R_2CH-OH, (second.)

[3] Abbreviations as in Table 4.1.

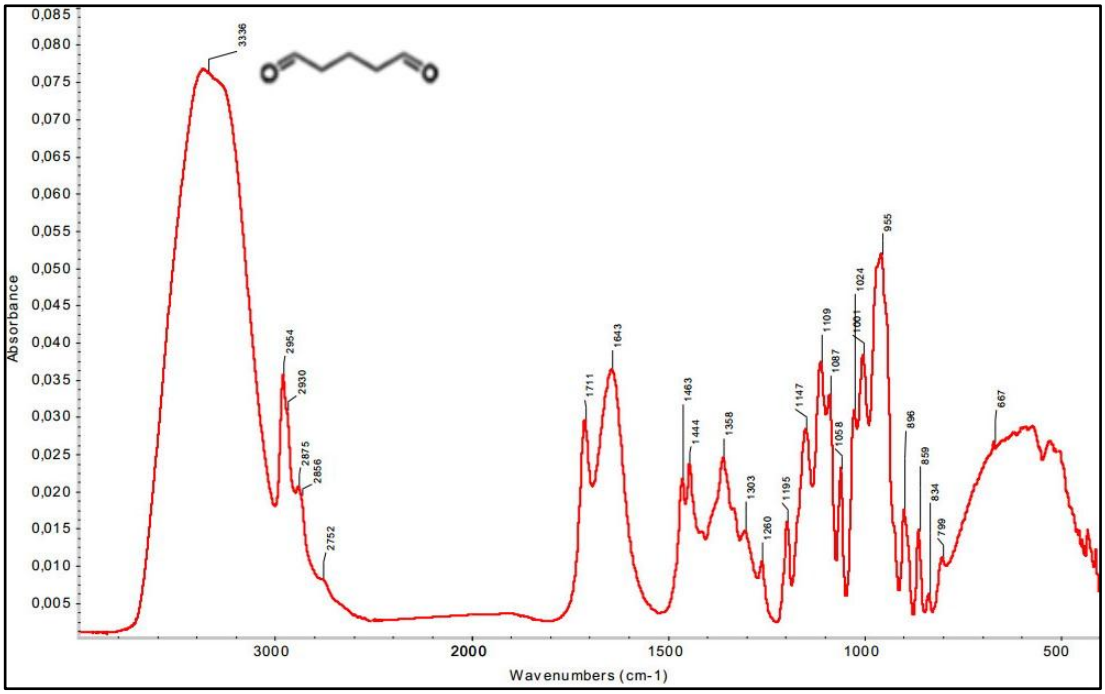

Figure 4.4 : The infrared spectrum of 50 % of glutaraldehyde solution.

Table 4.3 : Identification of the functional groups of glutaraldehyde[4].

Wave number [cm^{-1}], intensity	Present band	Assignment	Functional group
3600-3100; s, br	3336	ν_{as} (H_2O)	H_2O in the solvent
1645-1615; v	1643	δ (H_2O)	H_2O
2955-2915; m	2954, 2930	ν_{as} (CH_2)	-(C)-CH_2-, -(O)-CH_2
2880-2830; m	2875	ν_s (CH_2)	-(C)-CH_2-, -(O)-CH_2
1470-1440; m	1463, 1444	δ (CH_2)	-(C)-CH_2-, -(O)-CH_2
785- 750; w-m	covered	ρ (CH_2)	-CH_2-CH_x, x≠2
2755-2650; w	2752	ν $(CH)^+$	-CHO
1745-1650; vs	1711	ν (C=O)	-CHO
1440-1325; m	1358	δ (CH)	-CHO
975- 780; w	834	γ (CH)	-CHO

[4] Abbreviations as in Table 4.1.

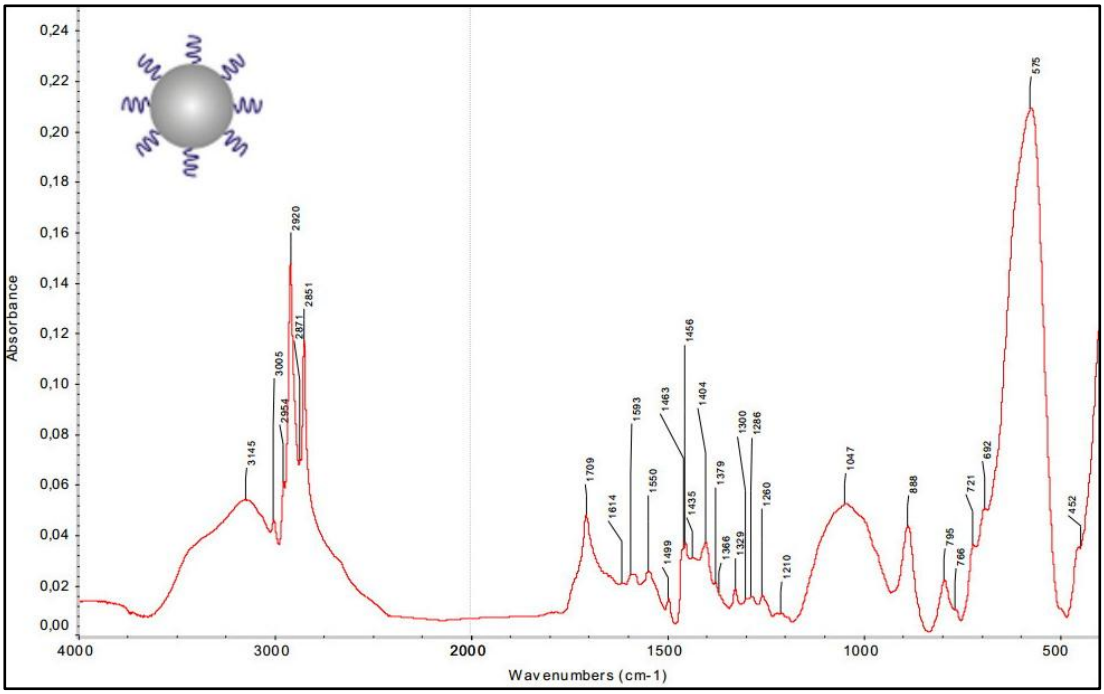

Figure 4.5 : The infrared spectrum of oleic acid modified magnetic Fe_3O_4 nanoparticles.

Fig. 4.5 shows the FT-IR spectrum of the oleic acid modified Fe_3O_4 nanoparticles. The sharp intense peak at 575 cm^{-1} corresponded to the vibration of the Fe–O bond in the crystalline lattice of Fe_3O_4. This characteristic peak demonstrated that the nanoparticles were Fe_3O_4. The oleic acid molecules in the adsorbed state were subjected to the solid surface of Fe_3O_4 nanoparticles. In the infrared spectrum of the pure oleic acid, two sharp bands at 2922 and 2853 cm^{-1} were attributed to the asymmetric CH_2 stretch and the symmetric CH_2 stretch, respectively. In the infrared spectrum of Fe_3O_4 nanoparticles coated with oleic acid, these asymmetric CH_2 stretch and the symmetric CH_2 stretch shifted to 2920 and 2851 cm^{-1}, respectively. The characteristic band at 1709 cm^{-1} was derived from the existence of the stretching vibration of C=O of the carboxyl group in oleic acid. A strong absorption band at 1047 cm^{-1} exhibited the presence of the C–O single bond stretching. At 1550 and 1593 cm^{-1}, two new bands appeared, which were characteristic vibration bands of the symmetric ν_s(-COO-) and asymmetric ν_{as}(-COO-) stretches, respectively. These results demonstrated that oleic acid was chemically adsorbed onto the surface of Fe_3O_4 nanoparticles.

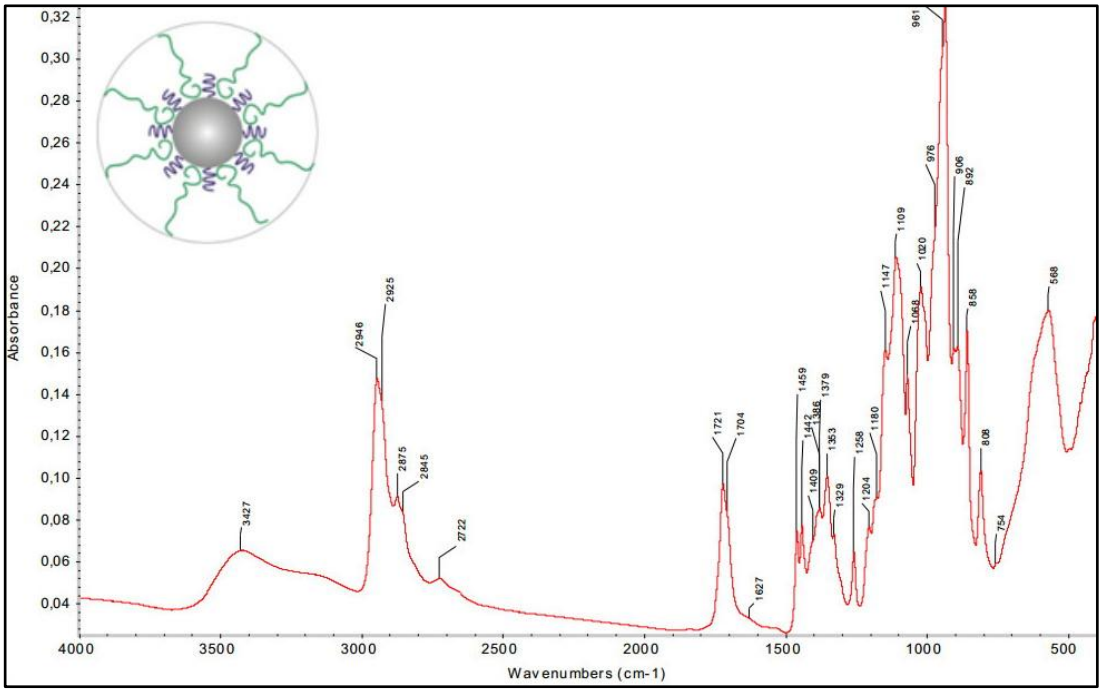

Figure 4.6 : The infrared spectrum of magnetic Fe_3O_4 nanoparticles stabilized with oleic acid and functionalized with chitosan and glutaraldehyde.

Fig. 4.6 shows the FT-IR spectrum of oleic acid modified, chitosan and glutaraldehyde functionalized Fe_3O_4 nanoparticles. The peak at 568 cm^{-1} related to the Fe–O bond in the Fe_3O_4 nanoparticles. The infrared bands for the symmetric and the asymmetric CH_2 stretches in oleic acid could be observed as shifted to 2875 and 2946 cm^{-1}, respectively. The band at 1721 cm^{-1} belonged to the stretching vibration of C=O of the carboxyl group in oleic acid. The absorption band at 3427 cm^{-1} represented the presence of the hydrogen bonded OH group in chitosan. The functional group bands between 900-1200 cm^{-1} could be assignable to the vibration of C–O–C in chitosan. The peak at 1627 cm^{-1}, which was related to the imine bonds (C=N) formed in the cross-linking process, indicated that chitosan reacted with glutaraldehyde to form the Schiff base[5]. These results demonstrated that chitosan and glutaraldehyde were coated onto the surface of the oleic acid modified magnetic Fe_3O_4 nanoparticles successfully.

4.2.2 X-ray powder diffraction (XRD)

The compositions of the sample of the nanoparticles were determined by measuring the powder diffraction and comparing the reflextions in diffractogram with the library of spectra. Reflextions of the prepared particles corresponded to magnetite

[5] Compounds containing an azomethine group (-C=N-) are known as Schiff bases [163].

with all characteristic peaks of standard Fe_3O_4. Diffraction maxima (reflextions) of magnetite for Co anode were 2θ = 21.3°, 35.1°, 41.5°, 50.6°, 63.3°, 67.4° and 74.4°. They could be marked by Miller indexes as (111), (220), (311), (400), (422), (511) and (440), respectively. Besides, the evaluating program was able to calculate the size of the particles which were in crystalline form. The mean size of the Fe_3O_4 nanoparticles was determined to be about 5.7 nm. This was the size of the magnetic core in diameter, the shell formed by oleic acid cannot be determined by XRD. The calculation of size was not affected by agglomeration of the particles. All significant reflections for magnetite can be seen in Fig. 4.7.

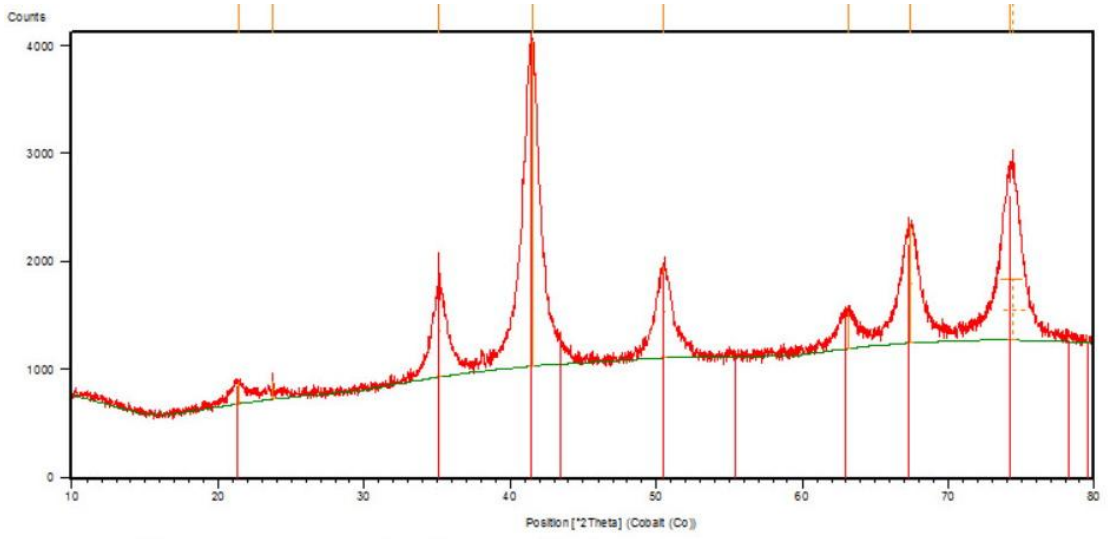

Figure 4.7 : Diffractogram of magnetic Fe_3O_4 nanoparticles.

4.2.3 Transmission electron microscopy (TEM)

For the preparation of the sample of the magnetic nanoparticles or immunomagnetic nanoparticles for TEM, first glow discharge-activated carbon-coated grids were prepared. To make the surface more accessible to water, the carbon grid needs to be made hydrophilic. Hence, Polaron sputter-coater modified for activation of carbon support films for electron microscopy by glow discharge [164] was used and the surface of the grid was made hydrophilic. Then a small drop of the sample of the nanoparticles (~5 μL) was placed on this hydrophilic grid and the particles were let adsorbing for 60 s. The grid needs to be stained if the sample on it contains organic material as proteins. For normal electron microscope viewing, samples are stained with a heavy metal salt (uranyl acetate or ammonium molybdate; staining with these heavy atoms is called "negative staining") that readily absorbs electrons. For that purpose, the samples of the magnetic nanoparticles was negatively stained with 1 %

ammonium molybdate and 0.1 % of trehalose in double distilled water on the glow discharge-activated carbon-coated grids. After staining, the grids were air-dried on a filter paper and the samples prepared in this way were viewed under the electron microscope [165].

Fig. 4.8–13 show the TEM images for the magnetic Fe_3O_4–chitosan nanoparticles, antibody anchored magnetic Fe_3O_4–chitosan nanoparticles and antibody anchored Dynabeads M-280 Tosylactivated. The images showed that the magnetic Fe_3O_4–chitosan nanoparticles were quasi-spherical with a mean diameter of about 8.4 nm, and the size of the Dynabeads M-280 Tosylactivated was about 2.9 μm in diameter.

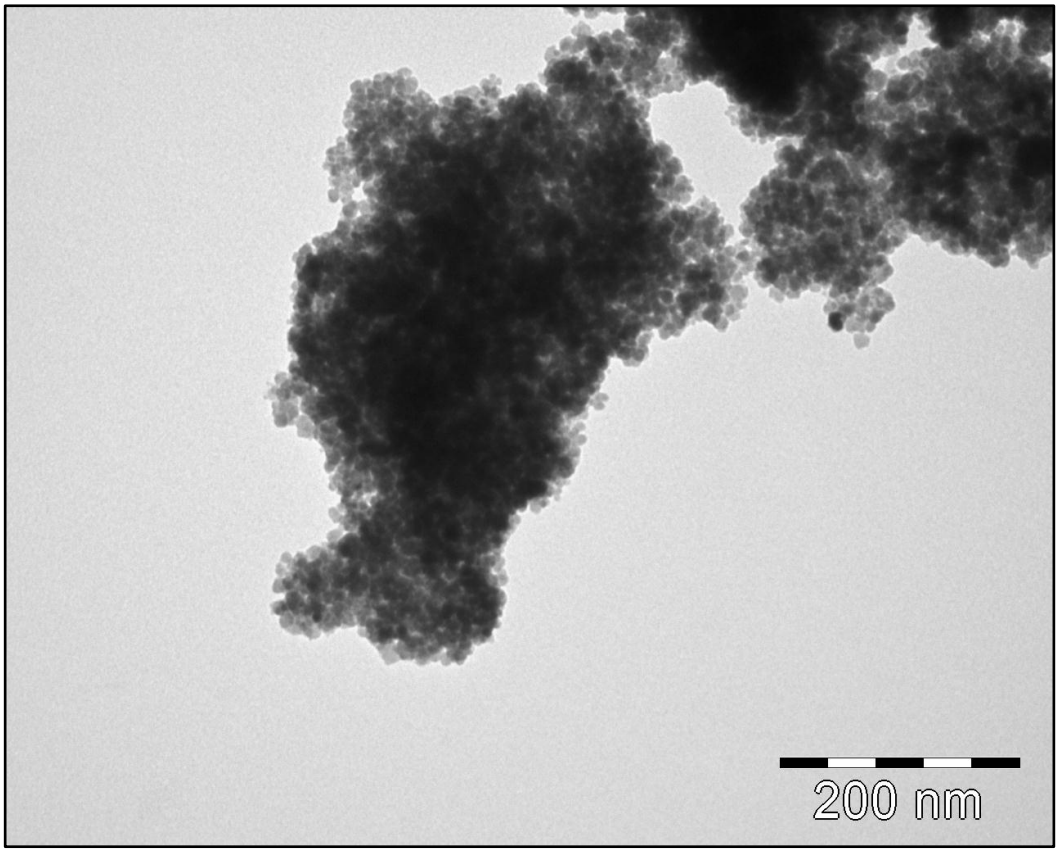

Figure 4.8 : TEM image of the magnetic Fe_3O_4–chitosan nanoparticles.

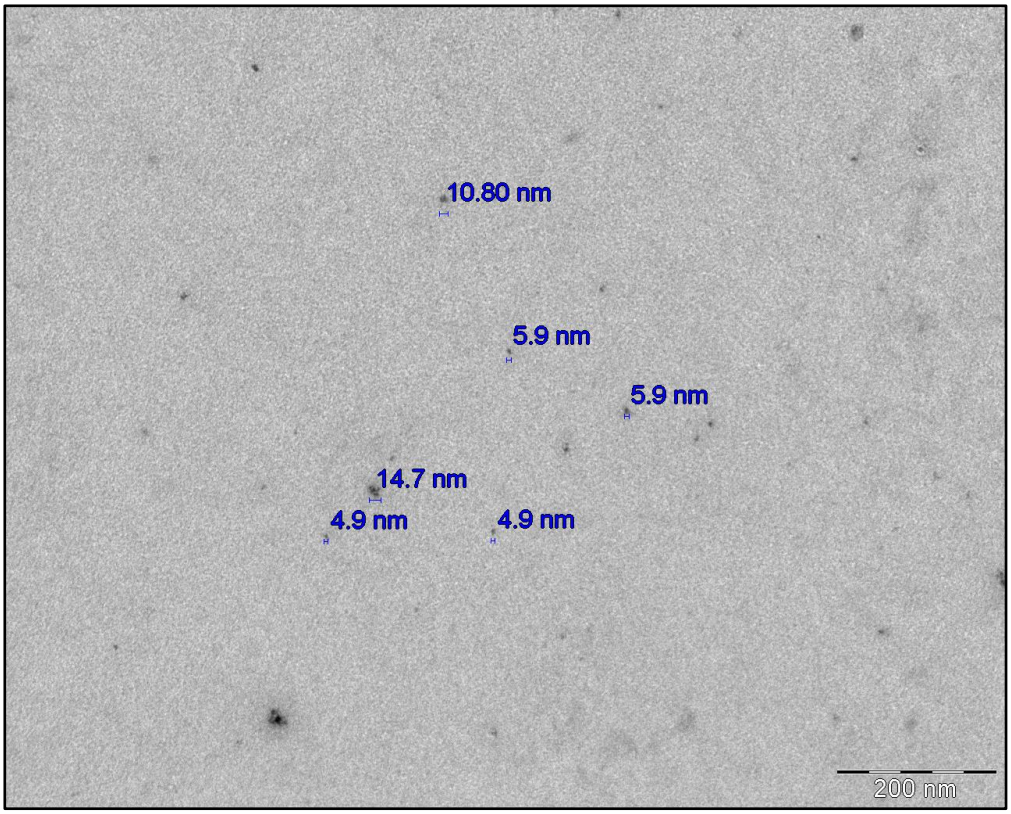

Figure 4.9 : TEM image of the magnetic Fe_3O_4–chitosan nanoparticles and their sizes in diameter.

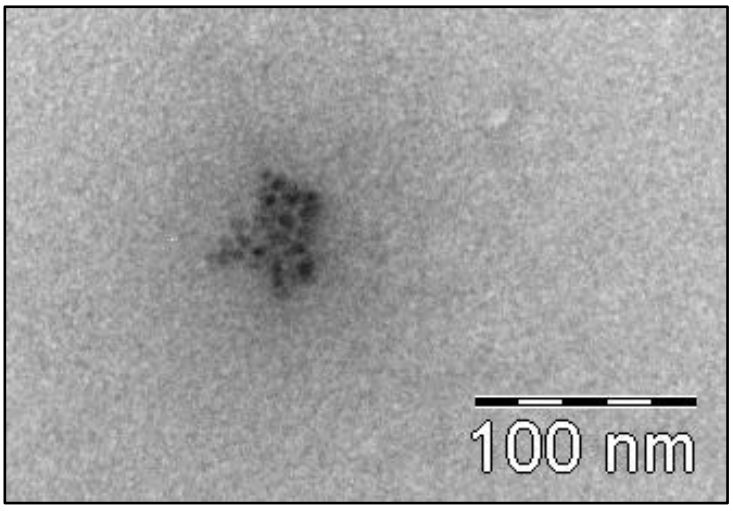

Figure 4.10 : TEM image of the antibody anchored magnetic Fe_3O_4–chitosan nanoparticles.

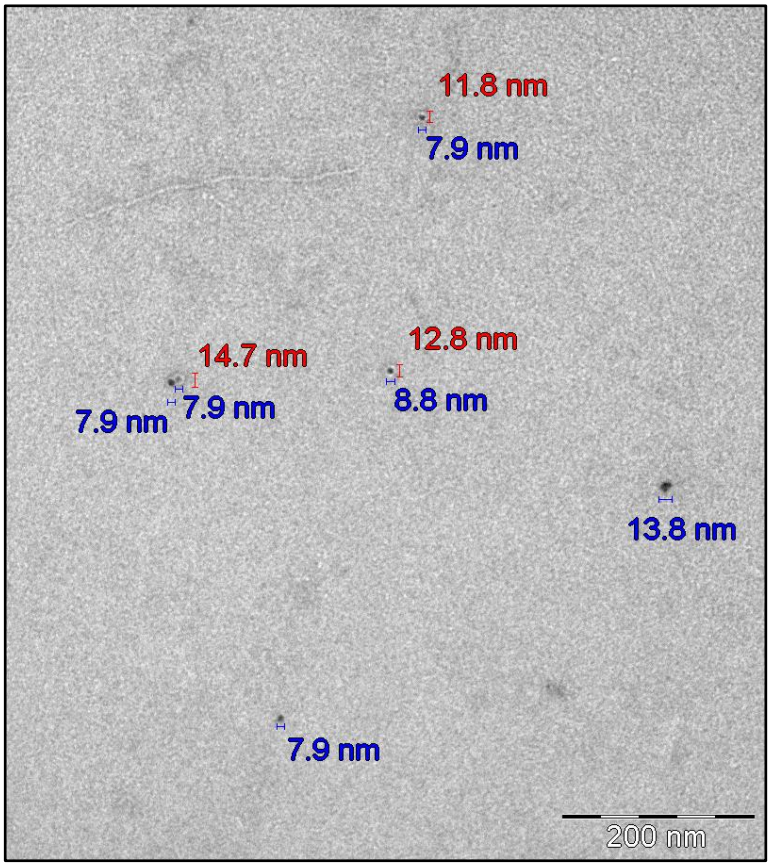

Figure 4.11 : TEM image of the antibody anchored magnetic Fe_3O_4–chitosan nanoparticles and their sizes in diameter (The blue color was used to show the core sizes and the red was used for showing the whole particle size including antibody).

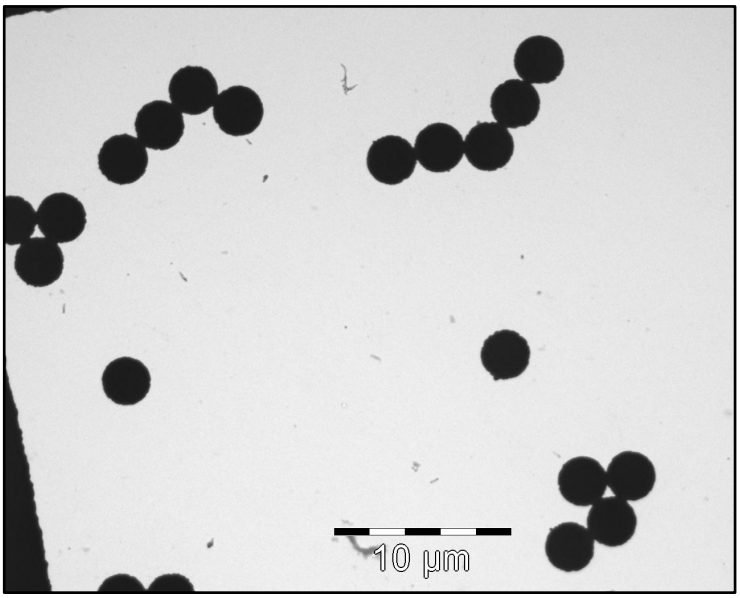

Figure 4.12 : TEM image of the antibody anchored Dynabeads M-280 Tosylactivated.

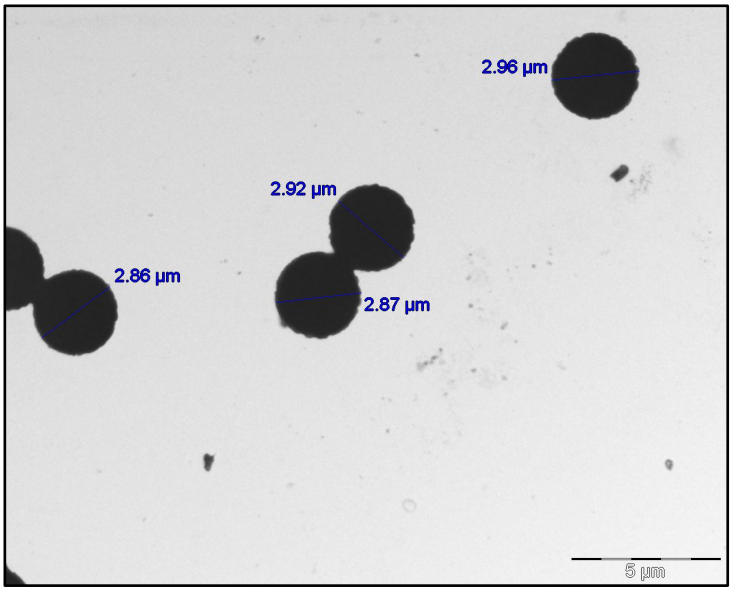

Figure 4.13 : TEM image of the antibody anchored Dynabeads M-280 Tosylactivated and their sizes in diameter.

4.3 HPLC-ESI-MS/MS Analysis

Kinetex C18 (2.7 µm) column was used for chromatographic separation of the substances. The mobile phase consisted of water and acetonitrile (30:70 v/v) and isocratic elution at the flow rate 150 µl/min was used. Mass-spectrometric detection was realized using negative electrospray ionization (ESI^-) in a very selective SRM mode. Product spectra for each substance are in Figures 4.14–17.

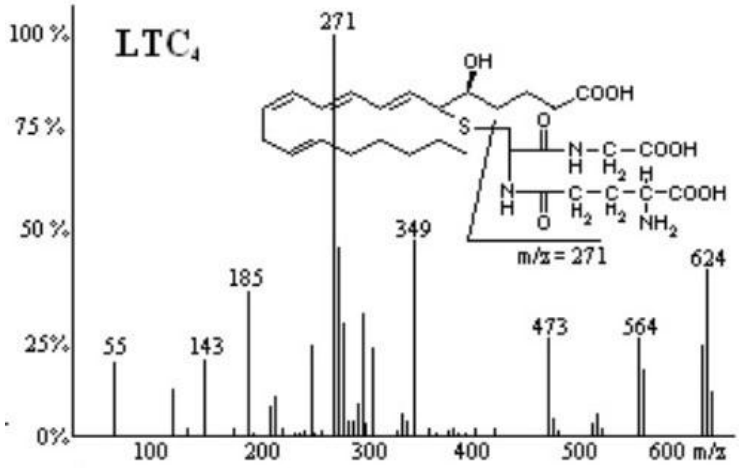

Figure 4.14 : MS/MS spectrum of LTC_4.

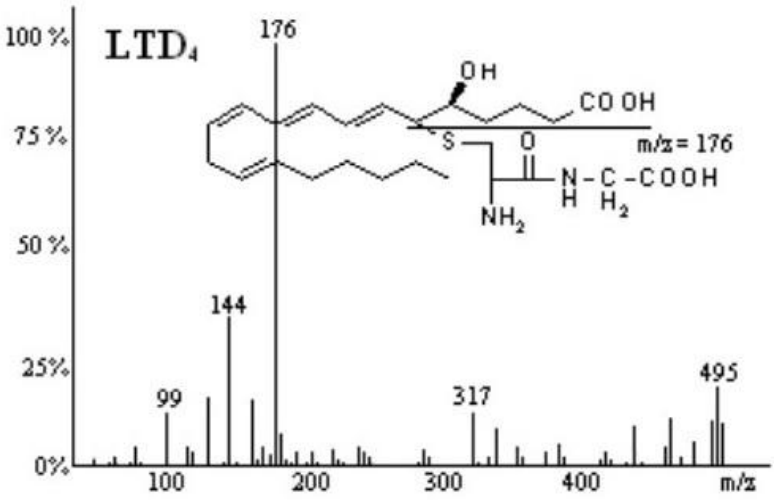

Figure 4.15 : MS/MS spectrum of LTD_4.

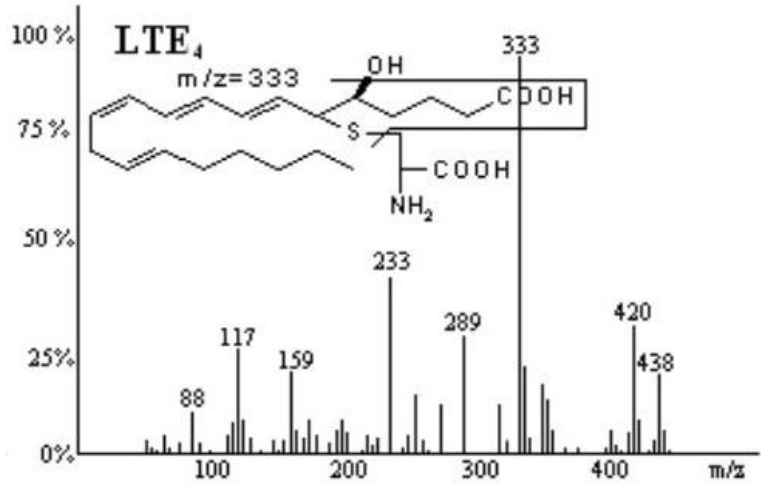

Figure 4.16 : MS/MS spectrum of LTE_4.

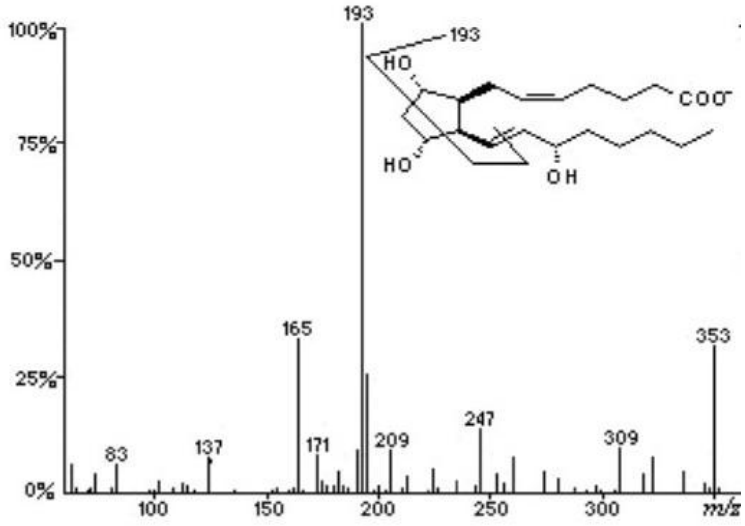

Figure 4.17 : MS/MS spectrum of 8-iso $PGF_{2\alpha}$.

4.4 Calibration Curves and Validation of the Method

The calibration graphs for Cys-LTs and 8-iso $PGF_{2\alpha}$ were constructed for EBC (originally free of Cys-LTs and 8-iso $PGF_{2\alpha}$). The calibration was created from artificially prepared samples with increasing amounts of Cys-LTs and 8-iso $PGF_{2\alpha}$ and their corresponding internal standards (250 pg of particular internal standard in 1 ml EBC) after the pre-treatment by immunomagnetic nanoparticles with *anti*-LTC_4, *anti*-LTD_4, *anti*-LTE_4 and *anti*-8-iso $PGF_{2\alpha}$ antibodies. The samples were immediately analyzed by HPLC/MS in MRM mode. Calibration graphs were formed using the ratio of a particular biomarker peak area to the corresponding internal standard peak area (axis x) *versus* the biomarker concentration in mobile phase (axis y). The calibration curve was evaluated by the least square regression in the form $y = ax + b$. The results are summarized in Table 4.4. All substances exhibited a linear dependence within the range starting at the LOQ to 5000 pg with the Pearson's correlation coefficients (R^2) higher than 0.992 for all the analytes (the acceptable value of R^2 for each calibration curve was $R^2 \geq 0.99$).

Table 4.4 : Linear regression analysis of calibration curves (n = 10) for Cys-LTs and 8-iso $PGF_{2\alpha}$.

Analyte	Slope	Intercept	SD	RSD [%]	R^2
LTC_4	59.013	-72.624	1.579	2.676	0.9982
LTD_4	172.440	-250.54	4.289	2.487	0.9926
LTE_4	60.229	-144.87	1.382	2.295	0.9950
8-iso $PGF_{2\alpha}$	362.320	-40.81	7.121	1.965	0.9988

The validation parameters of the method such as the accuracy (RE) and the precision (RSD) were assessed by analyzing four various concentration levels of the Cys-LTs and 8-iso $PGF_{2\alpha}$. The LOD and LOQ were estimated by the analysis of the blank matrix (n = 5) for each particular biomarker. All the values are summarized in Table 4.5.

Table 4.5 : Validation parameters for Cys-LTs and 8-iso $PGF_{2\alpha}$ in exhaled breath condensate (n = 5).

Analyte	LOD (pg/ml)	LOQ (pg/ml)	Precision RSD (%)	Accuracy RE (%)	Recovery (%)
LTC_4	3	7	8.2	17.8	82.2
LTD_4	2	5	10.4	18.5	81.5
LTE_4	2	4	11.2	17.6	82.4
8-iso $PGF_{2\alpha}$	2	6	28.7	19.2	80.8

4.5 Repeatability of Immunomagnetic Nanoparticles

For the repeatability of the magnetic Fe_3O_4–chitosan nanoparticles with anchored antibodies against Cys-LTs or 8-iso $PGF_{2\alpha}$, it was tried to determine that after one performed immunomagnetic separation, if these immunomagnetic nanoparticles could be used for further separations of Cys-LTs and 8-iso $PGF_{2\alpha}$ from samples or not.

For that purpose, 5 same samples of Cys-LTs were prepared at concentration of 100 ng Cys-LTs/100 µl water. The concentration of the stock solution of Cys-LTs was 5 µg of each leukotriene in 250 µl ethanol. To prepare 100 ng Cys-LTs/100 µl water concentration value, 5 µl of the stock solution of Cys-LTs and 95 µl of water were put into an Eppendorf tube. The tube was vortexed in the minishaker for 1 min. 5 samples were prepared in this way. As immunomagnetic nanoparticles, magnetic Fe_3O_4–chitosan nanoparticles with 100 µl of anchored antibodies against Cys-LTs were used. They were treated with these prepared Cys-LTs samples, respectively.

Similarly, 8-iso $PGF_{2\alpha}$ samples were prepared at concentration of 200 ng 8-iso $PGF_{2\alpha}$/100 µl water. The concentration of the stock solution of 8-iso $PGF_{2\alpha}$ was 1 µg/1 µl. To prepare 200 ng 8-iso $PGF_{2\alpha}$/100 µl water concentration value, 2 µl of the stock solution of 8-iso $PGF_{2\alpha}$ and 998 µl of water were put into an Eppendorf tube. The tube was vortexed in the minishaker for 1 min. As immunomagnetic nanoparticles, magnetic Fe_3O_4–chitosan nanoparticles with 50 µl of anchored antibodies against 8-iso $PGF_{2\alpha}$ were used. In each five separation process, the particles were treated with 100 µl of the prepared 8-iso $PGF_{2\alpha}$ samples, respectively.

The procedures for formation of antibody-antigen interactions and separation of Cys-LTs and 8-iso $PGF_{2\alpha}$ from the complexes were followed as described in Section 3.7 and 3.8. Table 4.6 shows the recovery of Cys-LTs and 8-iso $PGF_{2\alpha}$ in the samples measured by LC-MS.

Table 4.6 : Recovery of Cys-LTs and 8-iso $PGF_{2\alpha}$ in the samples.

Analyte	**Recovery (%)**				
	1	**2**	**3**	**4**	**5**
LTC_4	99.3	98.7	96.1	94.9	92.0
LTD_4	99.5	99.1	97.2	95.7	94.1
LTE_4	99.1	98.6	96.8	94.2	91.9
8-iso $PGF_{2\alpha}$	98.9	98.1	96.9	93.6	90.9

As can be seen from the results, after 5 performed separations, the immunomagnetic nanoparticles worked without any significant change to bind Cys-LTs or 8-iso $PGF_{2\alpha}$ (loss of ability ≤ 10%). So, it was concluded that the magnetic Fe_3O_4–chitosan nanoparticles with anchored antibodies against Cys-LTs/8-iso $PGF_{2\alpha}$ could be used for immunomagnetic separations efficiently at least 5 times in a row.

4.6 Capacity of Immunomagnetic Nanoparticles

To determine the capacity of *anti*-Cys-LTs antibody anchored magnetic nanoparticles, samples of Cys-LTs were prepared at different concentration values: 5, 10, 25, 50, 75, 100, 150, 200, 500, 1000, 1500, 2500, 3500, 5500, and 7500 pg Cys-LTs each in 100 µl water. As immunomagnetic nanoparticles, magnetic Fe_3O_4–chitosan nanoparticles with 100 µl of anchored antibodies against Cys-LTs were used. They were treated with these prepared Cys-LTs samples, respectively.

The procedures for formation of antibody-antigen interactions and separation of Cys-LTs from the complexes were followed as described in Section 3.7 and 3.8. Fig. 4.18 shows the capacity of immunomagnetic nanoparticles to isolate LTC_4, LTD_4, and LTE_4.

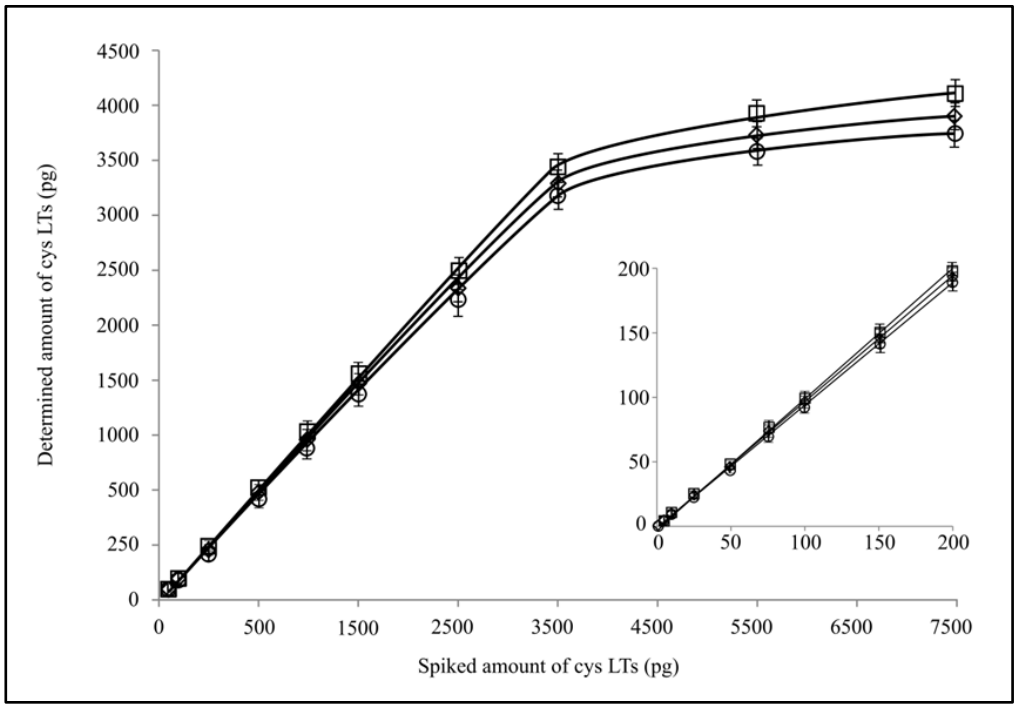

Figure 4.18 : Capacity of immunomagnetic nanoparticles to isolate LTC_4 (□), LTD_4 (◇) and LTE_4 (○).

As can be seen from the Fig. 4.18, at first, as the initial concentration values of Cys-LTs (LTC_4, LTD_4, and LTE_4) in the samples increased, the amount of Cys-LTs separated by the antibodies after the immunomagnetic separations also increased. But after a while (after the subsequent separations), the amount of separated Cys-LTs became constant showing the maximum binding capacity of the *anti*-Cys-LTs antibodies. After this point, it was pointless to add more Cys-LTs to the samples as antigens, because the amount of molecules more than the maximum binding capacity of antibodies could not be detected.

4.7 Mixing of Immunomagnetic Nanoparticles

One of the main goals of this study was to investigate if the magnetic nanoparticles conjugated with different antibodies (*anti*-Cys-LTs/*anti*-8-iso $PGF_{2\alpha}$) could work together when they were prepared by different ways. For this purpose, two different immunomagnetic separations were carried out. For the first separation process, magnetic Fe_3O_4–chitosan nanoparticles conjugated with 50 µl of antibodies against Cys-LTs (MN–Cys-LTs) and magnetic Fe_3O_4–chitosan nanoparticles conjugated with 50 µl of antibodies against 8-iso $PGF_{2\alpha}$ (MN–8-iso $PGF_{2\alpha}$) were mixed together (These immunomagnetic nanoparticles were separately prepared and then mixed together).

For the second separation process, 50 µl of antibodies against Cys-LTs and 50 µl of antibodies against 8-iso $PGF_{2\alpha}$ were added to the same magnetic Fe_3O_4–chitosan nanoparticles at the same time (Cys-LTs–MN–8-iso $PGF_{2\alpha}$) (Section 3.5).

For both of the immunomagnetic separations, same samples containing both Cys-LTs and 8-iso $PGF_{2\alpha}$ were prepared at concentration of 100 ng/100 µl water. The first sample was added to the first immunomagnetic nanoparticles ((MN–Cys-LTs)+(MN–8-iso $PGF_{2\alpha}$)) and the second sample was added to the second immunomagnetic nanoparticles (Cys-LTs–MN–8-iso $PGF_{2\alpha}$). The procedures for formation of antibody-antigen complexes and separation of Cys-LTs and 8-iso $PGF_{2\alpha}$ from these complexes were followed as described in Section 3.7 and 3.8. Table 4.7 shows the recovery of Cys-LTs and 8-iso $PGF_{2\alpha}$ performed by the immunomagnetic nanoparticles prepared by two different ways.

Table 4.7 : Recovery of Cys-LTs and 8-iso $PGF_{2\alpha}$ in the samples performed by the immunomagnetic nanoparticles prepared by two different ways.

(MN–Cys-LTs)+(MN–8-iso $PGF_{2\alpha}$)		**(Cys-LTs–MN–8-iso $PGF_{2\alpha}$)**	
∑Cys-LTs	**8-iso $PGF_{2\alpha}$**	**∑Cys-LTs**	**8-iso $PGF_{2\alpha}$**
97.3 %	85.1 %	21.3 %	15.4 %

As the results also indicate that the immunomagnetic nanoparticles prepared for the first separation process ((MN–Cys-LTs)+(MN–8-iso $PGF_{2\alpha}$)) worked better than the other immunomagnetic nanoparticles (Cys-LTs–MN–8-iso $PGF_{2\alpha}$) in separating Cys-LTs and 8-iso $PGF_{2\alpha}$ from the samples. The reason might be either the antibodies on the Cys-LTs–MN–8-iso $PGF_{2\alpha}$ couldn't be immobilized on the surface of the nanoparticles, or they did, but this time the orientation of them were not good enough for binding Cys-LTs and 8-iso $PGF_{2\alpha}$. Another reason might arise from the surface competition between the different antibodies (*anti*-Cys-LTs and *anti*-8-iso $PGF_{2\alpha}$) for the same binding sites on the nanoparticles.

4.8 Dynabeads M-280 Tosylactivated with Anchored Antibodies Against Cysteinyl Leukotrienes

Antibodies were also conjugated to the Dynabeads M-280 Tosylactivated to compare with the immunomagnetic Fe_3O_4–chitosan nanoparticles. They were prepared with 100 µl of antibodies against Cys-LTs as described in Section 3.6. The samples to be added to these immunomagnetic Dynabeads were prepared at concentration of 100 ng Cys-LTs/100 µl water. The immunomagnetic Dynabeads were treated with these five Cys-LTs samples, respectively. The procedures for formation of antibody-antigen interactions and separation of Cys-LTs from the complexes were followed as described in Section 3.7 and 3.8.

From the results, it was concluded that 99.8 % of Cys-LTs could be separated by the *anti*-Cys-LTs antibody (100 µl) anchored Dynabeads. Compared to the results of magnetic Fe_3O_4–chitosan nanoparticles with 100 µl of anchored antibodies against Cys-LTs, Dynabeads M-280 Tosylactivated with the same amount of anchored antibody against Cys-LTs showed similar results.

4.9 Clinical Study

The aim of the clinical study was to evaluate the concentration levels of cysteinyl leukotrienes and 8-iso Prostaglandin $F_{2\alpha}$ in exhaled breath condensate (EBC) of patients with two types of asthma: occupational asthma and hard-to-treat asthma. The concentrations were compared with control groups. The groups of patients differed in age; occupational asthma patients were older than hard-to-treat-asthma patients (See Section 3.13 in Experimental Part), therefore two different control groups were chosen.

The data were processed statistically (Fig. 4.19–22). A difference between concentration levels of each biomarker could be observed. The difference between the group of patients with hard-to-treat asthma and the control group was more significant than the same for occupational asthma. This could be arised from the differences in age of subjects, because the biomarkers are also present in the body of healthy people and their concentration increases with ageing.

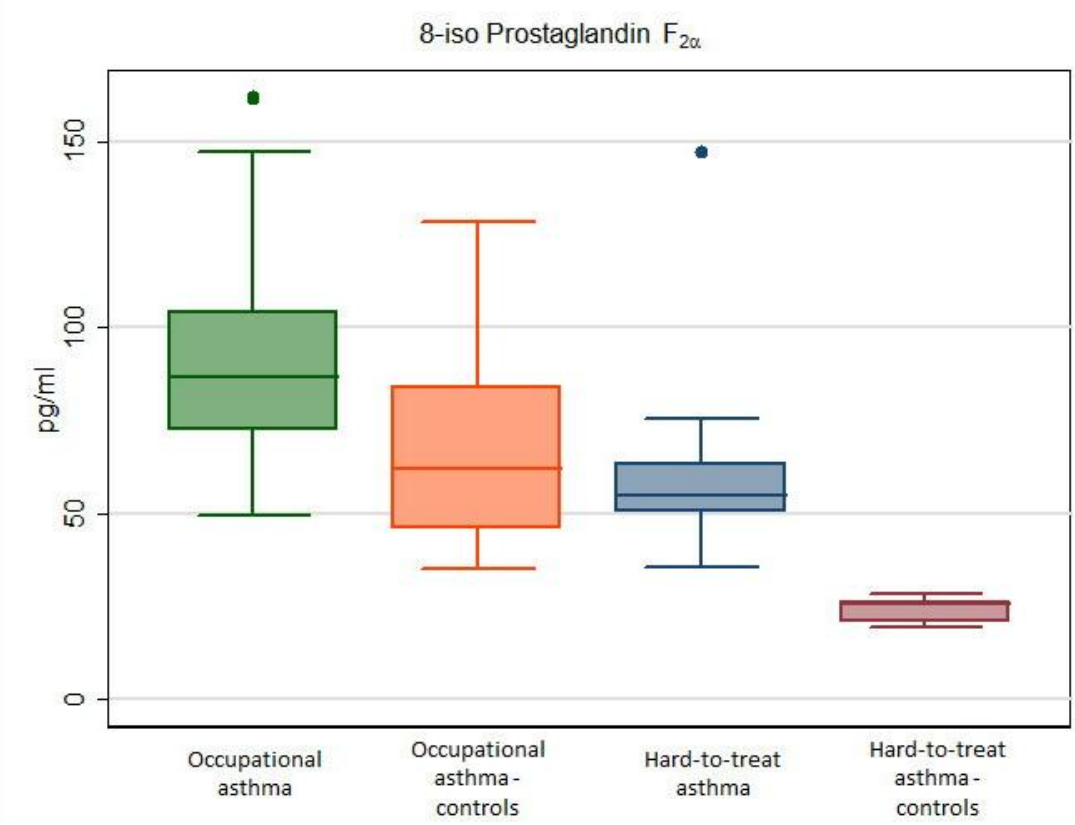

Figure 4.19 : Concentration of 8-iso Prostaglandin $F_{2\alpha}$ in EBC in clinical study.

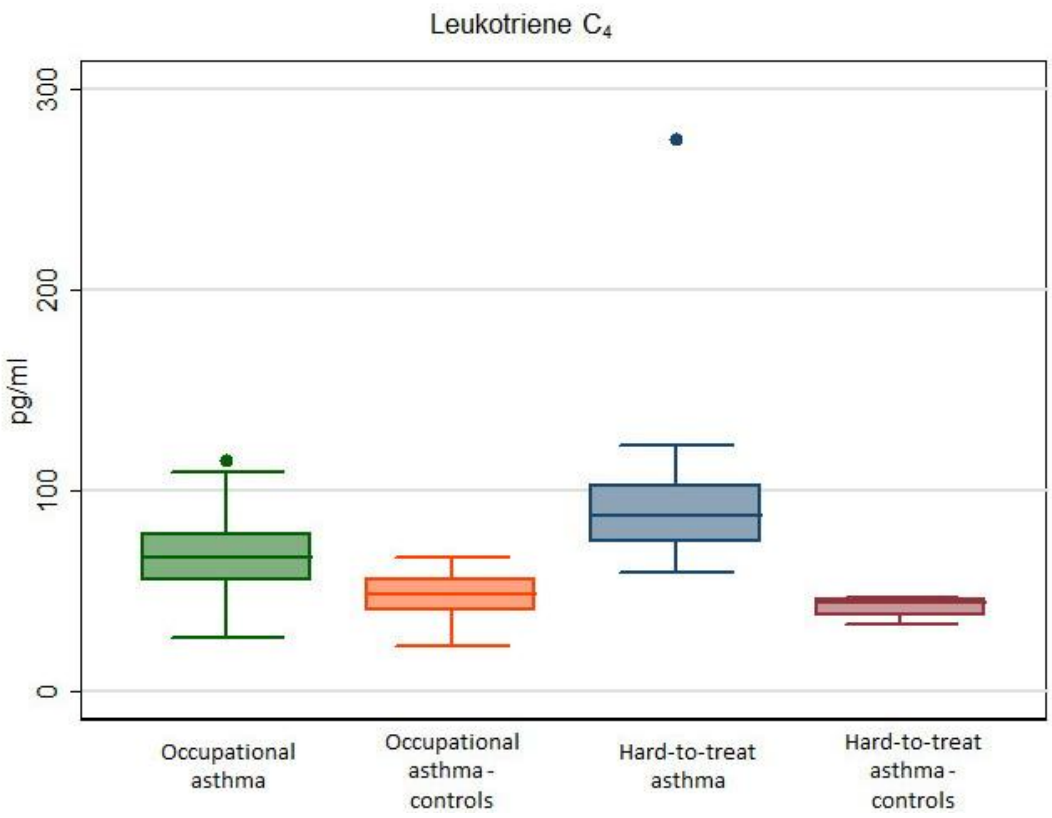

Figure 4.20 : Concentration of LTC_4 in EBC in clinical study.

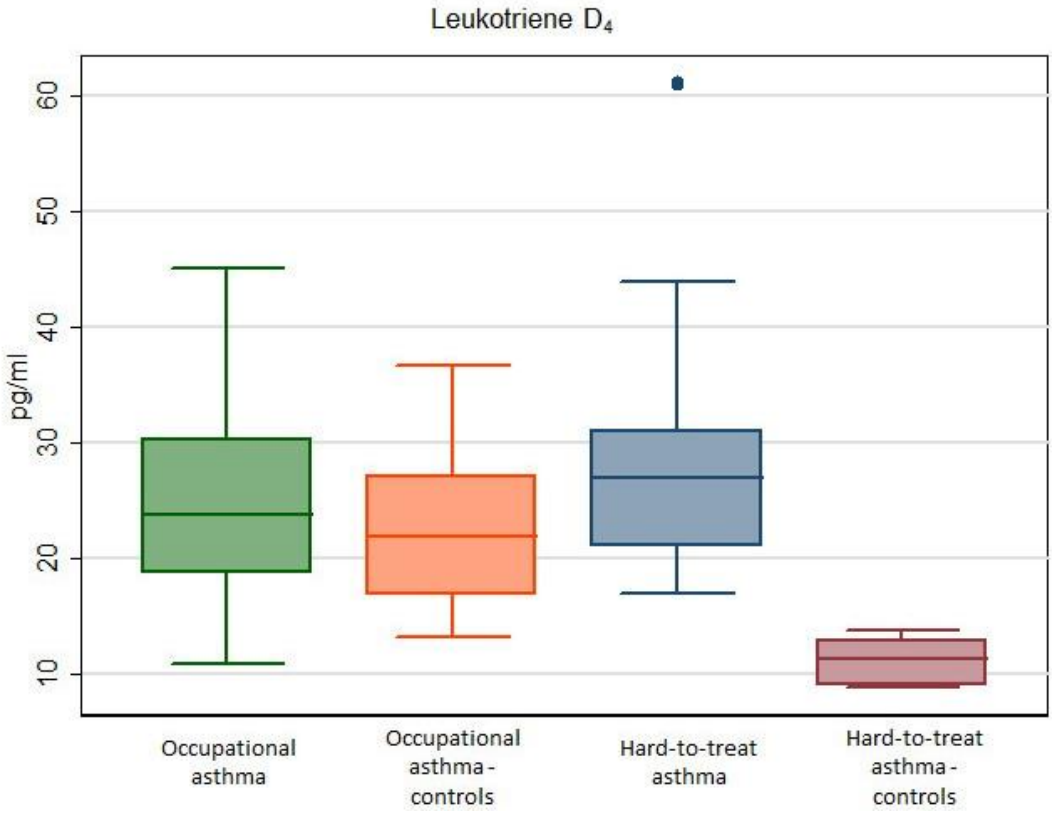

Figure 4.21 : Concentration of LTD_4 in EBC in clinical study.

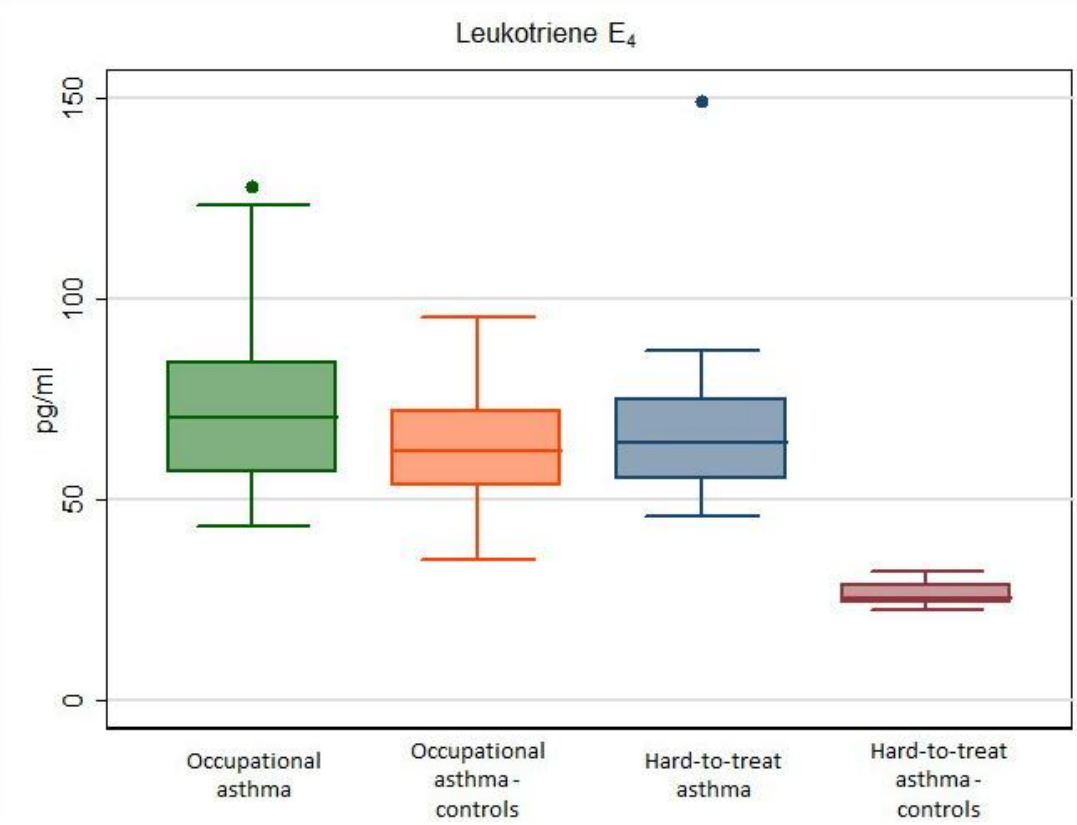

Figure 4.22 : Concentration of LTE_4 in EBC in clinical study.

5. CONCLUSIONS

The oleic acid modified magnetic Fe_3O_4 nanoparticles were synthesized from ferrous and ferric iron solutions by co-precipitation method with a mean diameter of about 5.7 nm. The magnetic nanoparticles were coated and functionalized with chitosan and glutaraldehyde. These Fe_3O_4–chitosan nanoparticles had an average size of 8.4 nm diameter. Antibodies against cysteinyl leukotrienes and 8-iso Prostaglandin $F_{2\alpha}$ were conjugated to these magnetic Fe_3O_4–chitosan nanoparticles, and the prepared immunomagnetic nanoparticles were used to separate biomarkers (Cys-LTs and 8-iso $PGF_{2\alpha}$) from biological matrix of EBC by immunomagnetic separation method. The amounts of the separated molecules were determined by a highly selective and sensitive detection method: mass spectrometry combined with high-performance liquid chromatography (HPLC-MS).

The results showed that the clinic using of these immunomagnetic nanoparticles for separation of biomarkers (LTC_4, LTD_4, LTE_4 and 8-iso $PGF_{2\alpha}$) in EBC of patients with sub-types of bronchial asthma (occupational and hard-to-treat) and healthy subjects, where reasonable differences in Cys-LTs and 8-iso $PGF_{2\alpha}$ concentration levels were found, was efficient. The performed clinical study confirmed the possibility of differential diagnosis of bronchial asthma using the developed pre-treatment method. The detection of elevated inflammatory and oxidative stress mediators (Cys-LTs and 8-iso $PGF_{2\alpha}$) in EBC of subjects with relatively asymptomatic asthma and normal pulmonary function tests could offer a novel way for monitoring the lung inflammation and perhaps initiating treatment in an earlier stage. The simplicity, rapidity, and robustness of the whole method make it suitable for use as a high-throughput assay in routine clinical biochemical laboratories.

REFERENCES

[1] **Voynow, J.A. and Kummarapurugu, A.** (2011). Review: Isoprostanes and asthma. *Biochimica et Biophysica Acta*, ***1810,*** 1091–1095.

[2] **Syslová, K., Demirbağ, E., Pankrácová, A., Gajdošová, M., Šimková, K., Kuzma, M., Pelclová, D. and Kačer, P.** (in press). Immunomagnetic Molecular Probe with LC-MS: A way for Bronchial Asthma Diagnostics Based on Quantification of Cysteinyl Leukotrienes (A Method for Routine Practice). *Journal of Chromatography A.*

[3] **Global Initiative for Asthma,** (2011). *Global Strategy for Asthma Management and Prevention (Updated 2011)*. Date retrieved: 05.01.2012, Address: http://www.ginasthma.org/

[4] **Diamant, Z., Boot, J.D., Mantzouranis, E., Flohr, R., Sterk, P.J. and Gerth van Wijk, R.** (2010). Review: Biomarkers in asthma and allergic rhinitis. *Pulmonary Pharmacology & Therapeutics*,***23,*** 468-481.

[5] **Syslová, K., Kačer P., Vilhanová, B., Kuzma, M., Lipovová, P., Fenclová, Z., Lebedová, J. and Pelclová, D.** (2011). Determination of cysteinyl leukotrienes in exhaled breath condensate: Method combining immunoseparation with LC–ESI-MS/MS. *Journal of Chromatography B,* ***879,*** 2220-2228.

[6] **Syslová, K., Kačer, P., Kuzma, M., Klusáčková, P., Fenclová, Z., Lebedová, J. and Pelclová, D.** (2008). Determination of 8-iso-prostaglandin $F_{2\alpha}$ in exhaled breath condensate using combination of immunoseparation and LC–ESI-MS/MS. *Journal of Chromatography B,* ***867,*** 8–14.

[7] **Montuschi, P. and Barnes, P.J.** (2006). Isoprostanes and asthma. *Drug Discovery Today: Therapeutic Strategies, Respiratory diseases,* Vol. ***3,*** No. 3.

[8] **Syslová, K., Kačer, P., Kuzma, M., Najmanová, V., Fenclová, Z., Vlčková, Š., Lebedová, J. and Pelclová, D.** (2009). Rapid and easy method for monitoring oxidative stress markers in body fluids of patients with asbestos or silica-induced lung diseases. *Journal of Chromatography B,* ***877,*** 2477–2486.

[9] **Zanconato, S., Carraro, S., Corradi, M., Alinovi, R.,** et al. (2004). Leukotrienes and 8-isoprostane in exhaled breath condensate of children with stable and unstable asthma. *Journal of Allergy and Clinical Immunology*, Vol. ***113,*** Issue 2, 257-263.

[10] **8-Isoprostane EIA Kit,** (2012). Information booklet of *Cayman Chemical Company*, U.S.A. Address: https://www.caymanchem.com/pdfs/516351.pdf

[11] **Montuschi, P.** (2007). Review: Analysis of exhaled breath condensate in respiratory medicine: methodological aspects and potential clinical applications. *Therapeutic Advances in Respiratory Disease, **1(1),*** 5–23.

[12] **National Nanotechnology Initiative,** official web-site: http://www.nano.gov/

[13] **Yih, T.C. and Wei, C.** (2005). Nanomedicine in cancer treatment. *Nanomedicine: Nanotechnology, Biology, and Medicine, **1,*** 191–192.

[14] **The National Nanotechnology Initiative Strategic Plan** (2004). National Science and Technology Council Executive Office of the President of the United States, Washington, DC. Address: http://www.whitehouse.gov/administration/eop/ostp/nstc /docsreports/archives

[15] **Gubin, S.P.** (2009). Magnetic Nanoparticles, Wiley-VCH Verlag GmbH & Co. KGaA, Weinheim.

[16] **Varadan, V.K., Chen, L. and Xie, J.** (2008). Nanomedicine: Design and Applications of Magnetic Nanomaterials. Nanosensors and Nanosystems, John Wiley & Sons, Ltd., United Kingdom.

[17] **Ma, Z. and Liu, H.** (2007). Synthesis and surface modification of magnetic particles for application in biotechnology and biomedicine. *China Particuology, **5,*** 1–10.

[18] **Cornell, R.M. and Schwertmann**, **U.** (2003). The Iron Oxides: Structure, Properties, Reactions, Occurences and Uses, 2nd Edition, Wiley-VCH Verlag GmbH & Co. KGaA, Weinheim.

[19] **Jolivet, J-P., Chanéac, C. and Tronc, E.** (2004). Iron oxide chemistry. From molecular clusters to extended solid networks. *Chem. Commun.*, 481-487.

[20] **Berry, C.C. and Curtis**, **A.S.G.** (2003). Topical Review: Functionalisation of magnetic nanoparticles for applications in biomedicine. *Journal of Physics D: Applied Physics, **36,*** R198–R206.

[21] **Gupta, A.K. and Gupta, M.,** (2005). Review: Synthesis and surface engineering of iron oxide nanoparticles for biomedical applications. *Biomaterials, **26,*** 3995–4021.

[22] **Jolivet, J-P., Tronc, E. and Chanéac**, **C.** (2006). Iron oxides: From molecular clusters to solid. A nice example of chemical versatility. *C. R. Geoscience, **338,*** 488–497.

[23] **Teja, A.S. and Koh, P-Y.** (2009). Synthesis, properties, and applications of magnetic iron oxide nanoparticles. *Progress in Crystal Growth and Characterization of Materials, **55,*** 22-45.

[24] **Hu, M., Ji, R-P. and Jiang, J-S.** (2010). Hydrothermal synthesis of magnetite crystals: From sheet to pseudo-octahedron, *Materials Research Bulletin, **45,*** 1811–1815.

[25] **Laurent, S., Forge, D., Port, M., Roch, A., Robic, C., Elst, L.V. and Muller, R.N.** (2008). Magnetic Iron Oxide Nanoparticles: Synthesis, Stabilization, Vectorization, Physicochemical Characterizations, and Biological Applications. *Chemical Reviews,* Vol. ***108,*** No. 6, 2064–2110.

[26] **Jolivet, J-P., Tronc, É. and Chanéac, C.** (2002). Synthesis of iron oxide-based magnetic nanomaterials and composites. *C. R. Chimie, **5,*** 659–664.

[27] **Donadel, K., Felisberto, M.D.V., Fávere, V.T., Rigoni, M., Batistela, N.J., Laranjeira, M.C.M.,** (2008). Synthesis and characterization of the iron oxide magnetic particles coated with chitosan biopolymer. *Materials Science and Engineering, C **28,*** 509–514.

[28] **Tronc, E., Belleville, P., Jolivet, J-P. and Livage, J.** (1992). Transformation of Ferric Hydroxide into Spinel by Fe^{II} Adsorption. *Langmuir,* Vol. ***8,*** No. 1, 313-319.

[29] **Hribernik, S., Sfiligoj-Smole, M., Bele, M., Gyergyek, S., Jamnik, J. And Stana-Kleinschek, K.** (2012). Synthesis of magnetic iron oxide particles: Development of an in situ coating procedure for fibrous materials. *Colloids and Surfaces A: Physicochem. Eng. Aspects, **400,*** 58–66.

[30] **Jolivet, J-P. and Tronc, E.** (1988). Interfacial Electron Transfer in Colloidal Spinel Iron Oxide. Conversion of Fe_3O_4-γFe_2O_3 in Aqueous Medium. *Journal of Colloid and Interface Science,* Vol. ***125,*** No. 2.

[31] **Willard, M.A., Kurihara, L.K., Carpenter, E.E., Calvin, S. and Harris, V.G.** (2004). Chemically prepared magnetic nanoparticles. *International Materials Reviews,* Vol. ***49,*** No. 3–4, 125-170.

[32] **Lu, A-H., Salabas, E.L. and Schüth, F.** (2007). Magnetic Nanoparticles: Synthesis, Protection, Functionalization, and Application. *Angew. Chem. Int. Ed., **46,*** 1222–1244.

[33] **Khalafalla, S.E. and Reimers**, **G.W.** (1980). Preparation of Dilution-Stable Aqueous Magnetic Fluids. *IEEE Transactions on Magnetics,* Vol. Mag-***16,*** No. 2.

[34] **Massart**, **R.** (1981). Preparation of Aqueous Magnetic Liquids in Alkaline and Acidic Media. *IEEE Transactions on Magnetics,* Vol. Mag-***17,*** No. 2, 1247-1248.

[35] **Tronc, E., Jolivet, J.P. and Massart, R.** (1982). Defect Spinel Structure in Iron Oxide Colloids. *Mat. Res. Bull.,* Vol. ***17,*** 1365-1369.

[36] **Tao, K., Dou, H. and Sun, K.** (2008). Interfacial coprecipitation to prepare magnetite nanoparticles: Concentration and temperature dependence. *Colloids and Surfaces A: Physicochem. Eng. Aspects, **320,*** 115–122.

[37] **Jolivet, J.P., Belleville, P., Tronc, E. and Livage, J.** (1992). Influence of Fe(II) on the formation of the Spinel Iron Oxide in Alkaline Medium. *Clays and Clay Minerals,* Vol. ***40,*** No. 5, 531-539.

[38] **Babes, L., Denizot, B., Tanguy, G., Jeune, J.J.L. and Jallet**, **P.** (1999). Synthesis of Iron Oxide Nanoparticles Used as MRI Contrast Agents: A Parametric Study. *Journal of Colloid and Interface Science,* ***212,*** 474–482.

[39] **Jolivet, J-P., Froidefond, C., Pottier, A., Chaneac, C., Cassaignon, S., Tronc, E. And Euzen, P.** (2004). Size tailoring of oxide nanoparticles by precipitation in aqueous medium. A semi-quantitative modelling. *J. Mater. Chem.*, ***14,*** 3281-3288.

[40] **Qiu, X-P.** (2000). Synthesis and characterization of magnetic nanoparticles. *Chinese Journal of Chemistry,* Vol. ***18,*** Issue 6, 834–837.

[41] **Woo, K., Hong, J. and Ahn**, **J-P.** (2005). Synthesis and surface modification of hydrophobic magnetite to processible magnetite@silica-propylamine. *Journal of Magnetism and Magnetic Materials*, ***293,*** 177–181.

[42] **Sun, S., Zeng, H., Robinson, D.B., Raoux, S., Rice, P.M., Wang, S.X. and Li, G.** (2004). Monodisperse MFe_2O_4 (M = Fe, Co, Mn) Nanoparticles. *J. Am. Chem. Soc.*, Vol. ***126,*** No. 1, 273-279.

[43] **Sun, S. and Zeng, H.** (2002). Size-Controlled Synthesis of Magnetite Nanoparticles. *J. Am. Chem. Soc.*, Vol. ***124,*** No. 28, 8204-8205.

[44] **Euliss, L.E., Grancharov, S.G., O'Brien, S., Deming, T.J., Stucky, G.D., Murray, C.B. and Held, G.A.** (2003). Cooperative Assembly of Magnetic Nanoparticles and Block Copolypeptides in Aqueous Media. *Nano Lett.*, Vol. ***3,*** No. 11, 1489-1493.

[45] **Li, Z., Chen, H., Bao, H. and Gao, M.** (2004). One-Pot Reaction to Synthesize Water-Soluble Magnetite Nanocrystals. *Chem. Mater.*, Vol. ***16,*** No. 8, 1391-1393.

[46] **Li, Z., Sun, Q. and Gao, M.** (2005). Preparation of Water-Soluble Magnetite Nanocrystals from Hydrated Ferric Salts in 2-Pyrrolidone: Mechanism Leading to Fe_3O_4. *Angew. Chem. Int . Ed.,* ***44,*** 123–126.

[47] **Jun, Y-w., Huh, Y-M., Choi, J-s., Lee, J-H., Song, H-T., Kim, S., Yoon, S., Kim, K-S., Shin, J-S., Suh, J-S. and Cheon, J.** (2005). Nanoscale Size Effect of Magnetic Nanocrystals and Their Utilization for Cancer Diagnosis via Magnetic Resonance Imaging. *J. Am. Chem. Soc.*, Vol. ***127,*** No. 16, 5732-5733.

[48] **Haw, C.Y., Mohamed, F., Chia, C.H., Radiman, S., Zakaria, S., Huang, N.M., Lim, H.N.** (2010). Hydrothermal synthesis of magnetite nanoparticles as MRI contrast agents. *Ceramics International,* ***36,*** 1417–1422.

[49] **Mizutani, N., Iwasaki, T., Watano, S., Yanagida, T. and Kawai, T.** (2010). Size control of magnetite nanoparticles in hydrothermal synthesis by coexistence of lactate and sulfate ions. *Current Applied Physics,* ***10,*** 801–806.

[50] **Yitai, Q., Yi, X., Chuan, H., Jing, L. and Zuyao, C.** (1994). Hydrothermal Preparation and Characterization of Ultrafine Magnetite Powders. *Materials Research Bulletin,* Vol. ***29,*** No. 9, 953-957.

[51] **Chen, D. and Xu, R.** (1998). Hydrothermal Synthesis and Characterization of Nanocrystalline Fe_3O_4 Powders. *Materials Research Bulletin,* Vol. ***33,*** No. 7, 1015–1021.

[52] **Konishi, Y., Kawamura, T. and Asai**, **S.** (1993). Preparation and Characterization of Fine Magnetite Particles from Iron(III) Carboxylate Dissolved in Organic Solvent. *Ind. Eng. Chem. Res.,* Vol. ***32,*** No. 11, 2888-2891.

[53] **Si, S., Li, C., Wang, X., Yu, D., Peng, Q. and Li, Y.** (2005). Magnetic Monodisperse Fe_3O_4 Nanoparticles. *Crystal Growth & Design,* Vol. ***5,*** No. 2, 391-393.

[54] **Xuan, S., Hao, L., Jiang, W., Gong, X., Hu, Y. and Chen, Z.** (2007). Preparation of water-soluble magnetite nanocrystals through hydrothermal approach. *Journal of Magnetism and Magnetic Materials, **308,*** 210–213.

[55] **Fan, R., Chen, X.H., Gui, Z., Liu, L. and Chen, Z.Y.** (2001). A new simple hydrothermal preparation of nanocrystalline magnetite Fe_3O_4. *Materials Research Bulletin, **36,*** 497–502.

[56] **Lin, X-M. and Samia, A.C.S.** (2006). Synthesis, assembly and physical properties of magnetic nanoparticles. *Journal of Magnetism and Magnetic Materials, **305,*** 100–109.

[57] **Capek, I.** (2004). Preparation of metal nanoparticles in water-in-oil (w/o) microemulsions. *Advances in Colloid and Interface Science, **110,*** 49–74.

[58] **Holmberg, K., Jönsson, B., Kronberg, B. and Lindman, B.** (2003). Surfactants and Polymers in Aqueous Solution, 2nd Edition, John Wiley & Sons, Ltd., England.

[59] **Eastoe, J., Hollamby, M.J. and Hudson, L.** (2006). Recent advances in nanoparticle synthesis with reversed micelles. *Advances in Colloid and Interface Science, **128–130,*** 5–15.

[60] **Gupta, A.K. and Wells, S.** (2004). Surface-Modified Superparamagnetic Nanoparticles for Drug Delivery: Preparation, Characterization, and Cytotoxicity Studies. *IEEE Transactions on Nanobioscience,* Vol. ***3,*** No. 1.

[61] **Lee, Y., Lee, J., Bae, C.J., Park, J-G., Noh, H-J., Park, J-H. and Hyeon, T.** (2005). Large-scale synthesis of uniform and crystalline magnetite nanoparticles using reverse micelles as nanoreactors under reflux conditions. *Adv. Funct. Mater., **15,*** No. 3, 503-509.

[62] **Vidal-Vidal, J., Rivas, J. and Lopez-Quintela, M.A.** (2006). Synthesis of monodisperse maghemite nanoparticles by the microemulsion method. *Colloids and Surfaces A: Physicochem. Eng. Aspects, **288,*** 44–51.

[63] **Jia, Z., Yujun, W., Yangcheng, L., Jingyu, M. and Guangsheng, L.** (2006). In situ preparation of magnetic chitosan/Fe_3O_4 composite nanoparticles in tiny pools of water-in-oil microemulsion. *Reactive & Functional Polymers, **66,*** 1552–1558.

[64] **Dresco, P.A., Zaitsev, V.S., Gambino, R.J. and Chu, B.** (1999). Preparation and Properties of Magnetite and Polymer Magnetite Nanoparticles. *Langmuir,* Vol. ***15,*** No. 6, 1945-1951.

[65] **Sellmyer, D. and Skomski, R.** (2006). Advanced Magnetic Nanostructures, Springer Science+Business Media, Inc., the United States of America.

[66] **Zhu, A., Yuan, L. and Liao, T.** (2008). Suspension of Fe_3O_4 nanoparticles stabilized by chitosan and *o*–carboxymethylchitosan. *International Journal of Pharmaceutics, **350,*** 361–368.

[67] **Vayssieres, L., Chaneac, C., Tronc, E. and Jolivet, J.P.** (1998). Size Tailoring of Magnetite Particles Formed by Aqueous Precipitation: An Example of Thermodynamic Stability of Nanometric Oxide Particles. *Journal of Colloid and Interface Science, **205,*** 205–212.

[68] **Bönnemann, H. and Richards, R.M.** (2001). Nanoscopic Metal Particles - Synthetic Methods and Potential Applications. *Eur. J. Inorg. Chem.,* 2455-2480.

[69] **Jingjinga, W. and Dengxin, L.** (2011). Preparation and Characterization of Magnetic Fe_3O_4 Nanoparticles Coated by Oleic Acid. *Energy Procedia, **11,*** 4794–4802.

[70] **Yang, K., Peng, H., Wen, Y. and Li, N.** (2010). Re-examination of characteristic FTIR spectrum of secondary layer in bilayer oleic acid-coated Fe_3O_4 nanoparticles. *Applied Surface Science, **256,*** 3093–3097.

[71] **Wang, Y., Wong, J.F., Teng, X., Lin, X.Z. and Yang, H.** (2003). "Pulling" Nanoparticles into Water: Phase Transfer of Oleic Acid Stabilized Monodisperse Nanoparticles into Aqueous Solutions of α-Cyclodextrin. *Nano Lett.,* Vol. ***3,*** No. 11, 1555-1559.

[72] **Shen, L., Laibinis, P.E. and Hatton, T.A.** (1999). Bilayer Surfactant Stabilized Magnetic Fluids: Synthesis and Interactions at Interfaces. *Langmuir,* Vol. ***15,*** No. 2, 447-453.

[73] **Maity, D. and Agrawal, D.C.** (2007). Synthesis of iron oxide nanoparticles under oxidizing environment and their stabilization in aqueous and non-aqueous media. *Journal of Magnetism and Magnetic Materials, **308,*** 46–55.

[74] **Wei, Y., Han, B., Hu, X., Lin, Y., Wang, X. and Deng, X.** (2012). Synthesis of Fe_3O_4 nanoparticles and their magnetic properties. *Procedia Engineering, **27,*** 632–637.

[75] **Sahoo, Y., Pizem, H., Fried, T., Golodnitsky, D., Burstein, L., Sukenik, C.N. and Markovich, G.** (2001). Alkyl Phosphonate/Phosphate Coating on Magnetite Nanoparticles: A Comparison with Fatty Acids. *Langmuir,* Vol. ***17,*** No. 25, 7907-7911.

[76] **Tural, B., Özkan, N. and Volkan, M.** (2009). Preparation and characterization of polymer coated superparamagnetic magnetite nanoparticle agglomerates. *Journal of Physics and Chemistry of Solids, **70,*** 860–866.

[77] **Zhang, H., Wang, R., Zhang, G. and Yang, B.** (2003). A covalently attached film based on poly(methacrylic acid)-capped Fe_3O_4 nanoparticles. *Thin Solid Films,* ***429,*** 167–173.

[78] **Lee, J., Isobe, T. and Senna, M.** (1996). Preparation of Ultrafine Fe_3O_4 Particles by Precipitation in the Presence of PVA at High pH. *Journal of Colloid and Interface Science,* ***177,*** 490–494.

[79] **Andrade, A.L., Valente, M.A., Ferreira, J.M.F. and Fabris, J.D.** (2012). Preparation of size-controlled nanoparticles of magnetite. *Journal of Magnetism and Magnetic Materials,* ***324,*** 1753–1757.

[80] **Santra, S., Tapec, R., Theodoropoulou, N., Dobson, J., Hebard, A. and Tan, W.** (2001). Synthesis and Characterization of Silica-Coated Iron Oxide Nanoparticles in Microemulsion: The Effect of Nonionic Surfactants. *Langmuir,* Vol. ***17,*** No. 10, 2900-2906.

[81] **Chomoucka, J., Drbohlavova, J., Huska, D., Adam, V., Kizek, R. and Hubalek, J.** (2010). Review: Magnetic nanoparticles and targeted drug delivering. *Pharmacological Research,* ***62,*** 144–149.

[82] **Čampelj, S., Makovec, D. and Drofenik, M.** (2009). Functionalization of magnetic nanoparticles with 3-aminopropyl silane. *Journal of Magnetism and Magnetic Materials,* ***321,*** 1346–1350.

[83] **Shubayev, V.I., Pisanic II, T.R. and Jin, S.** (2009). Magnetic nanoparticles for theragnostics. *Advanced Drug Delivery Reviews,* ***61,*** 467–477.

[84] **Hong, R.Y., Li, J.H., Qu, J.M., Chen, L.L. and Li, H.Z.** (2009). Preparation and characterization of magnetite/dextran nanocomposite used as a precursor of magnetic fluid. *Chemical Engineering Journal,* ***150,*** 572–580.

[85] **Li, G-y., Huang, K-l., Jiang, Y-r., Ding, P. and Yang, D-l.** (2008). Preparation and characterization of carboxyl functionalization of chitosan derivative magnetic nanoparticles. *Biochemical Engineering Journal,* ***40,*** 408–414.

[86] **Jia, Z., Yujun, W. and Guangsheng, L.** (2005). Adsorption of diuretic furosemide onto chitosan nanoparticles prepared with a water-in-oil nanoemulsion system. *Reactive & Functional Polymers,* ***65,*** 249–257.

[87] **Baroni, P., Vieira, R.S., Meneghetti, E., da Silva, M.G.C. and Beppu, M.M.** (2008). Evaluation of batch adsorption of chromium ions on natural and crosslinked chitosan membranes. *Journal of Hazardous Materials,* ***152,*** 1155–1163.

[88] **Wan Ngah, W.S., Ab Ghani, S. and Kamari**, **A.** (2005). Adsorption behaviour of Fe(II) and Fe(III) ions in aqueous solution on chitosan and cross-linked chitosan beads. *Bioresource Technology,* ***96,*** 443–450.

[89] **Qu, J., Liu, G., Wang, Y. and Hong, R.** (2010). Preparation of Fe_3O_4–chitosan nanoparticles used for hyperthermia. *Advanced Powder Technology,* ***21,*** 461–467.

[90] **Dash, M., Chiellini, F., Ottenbrite, R.M. and Chiellini, E.** (2011). Chitosan-A versatile semi-synthetic polymer in biomedical applications. *Progress in Polymer Science,* ***36,*** 981–1014.

[91] **Hong, S., Chang, Y. and Rhee, I.** (2010). Chitosan-coated Ferrite (Fe_3O_4) Nanoparticles as a T_2 Contrast Agent for Magnetic Resonance Imaging. *Journal of the Korean Physical Society,* Vol. ***56,*** No. 3, 868-873.

[92] **Mcconnell, E.L., Murdan, S. and Basit, A.W.** (2008). An Investigation into the Digestion of Chitosan (Noncrosslinked and Crosslinked) by Human Colonic Bacteria. *Journal of Pharmaceutical Sciences,* Vol. ***97,*** No. 9, 3820-3829.

[93] **Wan Ngah, W.S., Endud, C.S. and Mayanar, R.** (2002). Removal of copper(II) ions from aqueous solution onto chitosan and cross-linked chitosan beads. *Reactive & Functional Polymers, **50,*** 181–190.

[94] **Gonçalves, V.L., Laranjeira, M.C.M., Fávere, V.T. and Pedrosa, R.C.** (2005). Effect of Crosslinking Agents on Chitosan Microspheres in Controlled Release of Diclofenac Sodium. *Polímeros: Ciência e Tecnologia,* Vol. ***15,*** No.1, 6-12.

[95] **Li, G-y., Jiang, Y-r., Huang, K-l., Ding, P. and Chen, J.** (2008). Preparation and properties of magnetic Fe_3O_4–chitosan nanoparticles. *Journal of Alloys and Compounds, **466,*** 451–456.

[96] **Zhao, D-L., Wang, X-X., Zeng, X-W., Xia, Q-S. and Tang, J-T.** (2009). Preparation and inductive heating property of Fe_3O_4–chitosan composite nanoparticles in an AC magnetic field for localized hyperthermia. *Journal of Alloys and Compounds, **477,*** 739–743.

[97] **Kim, E.H., Ahn, Y. and Lee, H.S.,** (2007). Biomedical applications of superparamagnetic iron oxide nanoparticles encapsulated within chitosan. *Journal of Alloys and Compounds **434–435,*** 633–636.

[98] **Feng, B., Hong, R.Y., Wu, Y.J., Liu, G.H., Zhong, L.H., Zheng, Y., Ding, J.M. and Wei, D.G.** (2009). Synthesis of monodisperse magnetite nanoparticles via chitosan–poly (acrylic acid) template and their application in MRI. *Journal of Alloys and Compounds, **473,*** 356–362.

[99] **Bautista, M.C., Bomati-Miguel, O., Morales, M.d.P., Serna, C.J. and Veintemillas-Verdaguer, S.** (2005). Surface characterisation of dextran-coated iron oxide nanoparticles prepared by laser pyrolysis and coprecipitation. *Journal of Magnetism and Magnetic Materials, **293,*** 20–27.

[100] **Pitarresi, G., Palumbo, F.S., Giammona, G., Casadei, M.A. and Moracci, F.M.** (2003). Biodegradable hydrogels obtained by photocrosslinking of dextran and polyaspartamide derivatives. *Biomaterials, **24,*** 4301–4313.

[101] **Mornet, S., Vasseur, S., Grasset, F. and Duguet, E.** (2004). Magnetic nanoparticle design for medical diagnosis and therapy. *Journal of Materials Chemistry, **14,*** 2161–2175.

[102] **Ding, J., Tao, K., Li, J., Song, S. and Sun, K.** (2010). Cell-specific cytotoxicity of dextran-stabilized magnetite nanoparticles. *Colloids and Surfaces B: Biointerfaces, **79,*** 184–190.

[103] **Bai, H., Liu, Z. and Sun, D.D.** (2011). Highly water soluble and recovered dextran coated Fe_3O_4 magnetic nanoparticles for brackish water desalination. *Separation and Purification Technology,* ***81,*** 392–399.

[104] **Hradil, J., Pisarev, A., Babič, M. and Horák, D.** (2007). Dextran-modified iron oxide nanoparticles. *China Particuology,* ***5,*** 162–168.

[105] **Hong, R.Y., Feng, B., Chen, L.L., Liu, G.H., Li, H.Z., Zheng, Y. and Wei**, **D.G.** (2008). Synthesis, characterization and MRI application of dextran-coated Fe_3O_4 magnetic nanoparticles. *Biochemical Engineering Journal,* ***42,*** 290–300.

[106] **Liu, G., Hong, R.Y., Guo, L., Li, Y.G. and Li**, **H.Z.** (2011). Preparation, characterization and MRI application of carboxymethyl dextran coated magnetic nanoparticles. *Applied Surface Science,* ***257,*** 6711–6717.

[107] **Gupta, A.K. and Curtis A.S.G.** (2004). Surface modified superparamagnetic nanoparticles for drug delivery: Interaction studies with human fibroblasts in culture. *Journal of Materials Science: Materials in Medicine,* ***15,*** 493-496.

[108] **Kanatt, S.R., Rao, M.S., Chawla, S.P. and Sharma A.** (2012). Active chitosan-polyvinyl alcohol films with natural extracts. *Food Hydrocolloids,* ***29,*** 290-297.

[109] **Udrea, L.E., Hritcu, D., Popa, M.I. and Rotariu O.** (2011). Preparation and characterization of polyvinyl alcohol-chitosan biocompatible magnetic microparticles. *Journal of Magnetism and Magnetic Materials,* ***323,*** 7–13.

[110] **Petri-Fink, A., Chastellain, M., Juillerat-Jeanneret, L., Ferrari, A. and Hofmann, H.** (2005). Development of functionalized superparamagnetic iron oxide nanoparticles for interaction with human cancer cells. *Biomaterials,* ***26,*** 2685–2694.

[111] **D'Souza, A.J.M., Schowen, R.L. and Topp, E.M.** (2004). Polyvinylpyrrolidone – drug conjugate: synthesis and release mechanism. *Journal of Controlled Release,* ***94,*** 91–100.

[112] **Zhang, Y., Liu, J-Y., Ma, S., Zhang, Y-J., Zhao, X., Zhang, X-D. and Zhang, Z-D.** (2010). Synthesis of PVP-coated ultra-small Fe_3O_4 nanoparticles as a MRI contrast agent. *J Mater Sci: Mater Med,* ***21,*** 1205–1210.

[113] **Xu, Y-Y., Zhou, M., Geng, H-J., Hao, J-J., Ou, Q-Q., Qi, S-D., Chen, H-L. and Chen, X-G.** (2012). A simplified method for synthesis of Fe_3O_4@PAA nanoparticles and its application for the removal of basic dyes. *Applied Surface Science,* ***258,*** 3897–3902.

[114] **Mahmoudi, M., Sant, S., Wang, B., Laurent, S. and Sen, T.** (2011). Superparamagnetic iron oxide nanoparticles (SPIONs): Development, surface modification and applications in chemotherapy. *Advanced Drug Delivery Reviews,* ***63,*** 24–46.

[115] **Im, S.H., Herricks, T., Lee, Y.T. and Xia, Y.** (2005). Synthesis and characterization of monodisperse silica colloids loaded with superparamagnetic iron oxide nanoparticles. *Chemical Physics Letters,* ***401,*** 19–23.

[116] **Bruce, I.J. and Sen, T.** (2005). Surface Modification of Magnetic Nanoparticles with Alkoxysilanes and Their Application in Magnetic Bioseparations. *Langmuir,* Vol. ***21,*** No. 15, 7029-7035.

[117] **Roca, A.G., Costo, R., Rebolledo, A.F., Veintemillas-Verdaguer, S., Tartaj, P., González-Carreno, T., Morales, M.P. and Serna, C.J.** (2009). Topical Review: Progress in the preparation of magnetic nanoparticles for applications in biomedicine. *Journal of Physics D: Applied Physics,* ***42,*** 224002 (11pp).

[118] **Lu, Y., Yin, Y., Mayers, B.T. and Xia, Y.** (2002). Modifying the Surface Properties of Superparamagnetic Iron Oxide Nanoparticles through A Sol−Gel Approach. *Nano Lett.,* Vol. ***2,*** No. 3, 183-186.

[119] **Chang, J.H., Kang, K.H., Choi, J. and Jeong, Y.K.** (2008). High efficiency protein separation with organosilane assembled silica coated magnetic nanoparticles. *Superlattices and Microstructures,* ***44,*** 442–448.

[120] **Ashtari, K., Khajeh, K., Fasihi, J., Ashtari, P., Ramazani, A. and Vali, H.** (2012). Silica-encapsulated magnetic nanoparticles: Enzyme immobilization and cytotoxic study. *International Journal of Biological Macromolecules,* ***50,*** 1063–1069.

[121] **Kang, K., Choi, J., Nam, J.H., Lee, S.C., Kim, K.J., Lee, S-W. and Chang J.H.** (2009). Preparation and Characterization of Chemically Functionalized Silica-Coated Magnetic Nanoparticles as a DNA Separator. *J. Phys. Chem. B,* Vol. ***113,*** No. 2, 536–543.

[122] **Yu, C.H., Tam, K.Y., Lo, C.C.H. and Tsang, S.C.** (2007). Functionalized Silica Coated Magnetic Nanoparticles With Biological Species for Magnetic Separation. *IEEE Transactions on Magnetics,* Vol. ***43,*** No. 6, 2436-2438.

[123] **Goon, I.Y., Lai, L.M.H., Lim, M., Munroe, P., Gooding, J.J. and Amal, R.** (2009). Fabrication and Dispersion of Gold-Shell-Protected Magnetite Nanoparticles: Systematic Control Using Polyethyleneimine. *Chem. Mater.,* Vol. ***21,*** No. 4, 673–681.

[124] **Kim, D.K., Mikhailova, M., Toprak, M., Zhang, Y., Bjelke, B., Kehr, J. and Muhammed, M.** (2002). In-situ gold coating of superparamagnetic nanoparticles by microemulsion method. *Materials Research Society Symp. Proc.,* Vol. ***704.***

[125] **Salgueirino-Maceira, V., Correa-Duarte, M.A., Farle, M., López-Quintela, A., Sieradzki, K. and Diaz, R.** (2006). Bifunctional Gold-Coated Magnetic Silica Spheres. *Chem. Mater.,* Vol ***18,*** No. 11, 2701-2706.

[126] **Wu, A., Yang, X. and Yang, H.** (2012). Magnetic properties of carbon coated Fe, Co and Ni nanoparticles. *Journal of Alloys and Compounds,* ***513,*** 193–201.

[127] **He, N.Y., Guo, Y.F., Deng, Y., Wang, Z.F., Li, S. and Liu, H.N.** (2007). Carbon encapsulated magnetic nanoparticles produced by hydrothermal reaction. *Chinese Chemical Letters,* ***18,*** 487–490.

[128] **Zhang, S., Niu, H., Hu, Z., Cai, Y. and Shi, Y.** (2010). Preparation of carbon coated Fe_3O_4 nanoparticles and their application for solid-phase extraction of polycyclic aromatic hydrocarbons from environmental water samples. *Journal of Chromatography A,* ***1217,*** 4757–4764.

[129] **Hojati-Talemi, P., Azadmanjiri, J. and Simon, G.P.,** (2010). A simple microwave-based method for preparation of Fe_3O_4/carbon composite nanoparticles. *Materials Letters,* ***64,*** 1684–1687.

[130] **Introduction to Fourier Transform Infrared Spectrometry,** (2001). Information Booklet of *Thermo Nicolet Corporation,* U.S.A. Address: http://mmrc.caltech.edu/FTIR/FTIRintro.pdf

[131] **Materials Characterization,** (2012). Information Booklet of *Evans Analytical Group (EAG),* U.S.A. Address: http://www.eaglabs.com/

[132] **Derrick, M.R., Stulik, D. and Landry, J.M.** (1999). Infrared Spectroscopy in Conservation Science, Scientific Tools for Conservation. The Getty Conservation Institute, Los Angeles, the United States of America.

[133] **Handbook of Analytical Methods For Materials,** (2010). *Materials Evaluation and Engineering, Inc.*, the United States of America. Address: http://www.mee-inc.com/hamm72d.pdf

[134] **FT-IR Spectroscopy,** (2011). Quick Guide of *Thermo Fisher Scientific,* U.S.A. Address: http://www.thermofisher.com.au /Uploads/file/ENewsAU/FTIR-Spectroscopy-Quick-guides.pdf

[135] **Moudgil, H.K.** (2010). Textbook of Physical Chemistry, PHI Learning Private Limited, New Delhi.

[136] **Basics of X-ray Diffraction,** (1999). Information Booklet of *Scintag Inc.*, U.S.A. Address: http://epswww.unm.edu/xrd/xrdbasics.pdf

[137] **http://**web.pdx.edu/~pmoeck/phy381/Topic5a-XRD.pdf

[138] **Brydson, R.** (2011). Aberration-Corrected Analytical Transmission Electron Microscopy (Chapter 1: General Introduction to Transmission Electron Microscopy (TEM), Goodhew, P.), 1st Edition, John Wiley & Sons, Ltd.

[139] **The Nobel Prize** official web site: http://www.nobelprize.org/educational /physics/microscopes/tem/index.html

[140] **Williams, D.B. and Carter, C.B.** (2009). Transmission Electron Microscopy, A Textbook for Materials Science, Springer Science+Business Media, LLC. Inc., the United States of America.

[141] **http://**cbe.ivic.ve/mic250/pdf/thesebook-chap3.pdf

[142] **http://**micron.ucr.edu/public/manuals/Tem-intro.pdf

[143] **Arruebo, M., Valladares, M. and González-Fernández, Á.** (2009). Review Article: Antibody-Conjugated Nanoparticles for Biomedical Applications. *Journal of Nanomaterials,* Vol. ***2009,*** 1-24.

[144] **Tomitaka, A., Koshi, T., Hatsugai, S., Yamada, T. and Takemura, Y.** (2011). Magnetic characterization of surface-coated magnetic nanoparticles for biomedical application. *Journal of Magnetism and Magnetic Materials,* ***323,*** 1398–1403.

[145] **Indira, T.K. and Lakshmi, P.K.** (2010). Magnetic Nanoparticles – A Review, *International Journal of Pharmaceutical Sciences and Nanotechnology,* Vol. ***3,*** Issue 3, 1035-1042.

[146] **Kayal, S. and Ramanujan, R.V.** (2010). Doxorubicin loaded PVA coated iron oxide nanoparticles for targeted drug delivery. *Materials Science and Engineering,* C ***30,*** 484–490.

[147] **Lu, J., Yang, S., Ng, K.M., Su, C-H., Yeh, C-S., Wu, Y-N. and Shieh, D-B.** (2006). Solid-state synthesis of monocrystalline iron oxide nanoparticle based ferrofluid suitable for magnetic resonance imaging contrast application. *Nanotechnology,* ***17,*** 5812–5820.

[148] **Gould, P.** (2004). Nanoparticles probe biosystems. *Materials Today,* Vol. ***7,*** Issue 2, 36–43.

[149] **Dias, A.M.G.C., Hussain, A., Marcos, A.S. and Roque, A.C.A.** (2011). A biotechnological perspective on the application of iron oxide magnetic colloids modified with polysaccharides. *Biotechnology Advances,* ***29,*** 142–155.

[150] **Zhang, S., Bian, Z., Gu, C., Zhang, Y., He, S., Gu, N. and Zhang, J.** (2007). Preparation of anti-human cardiac troponin I immunomagnetic nanoparticles and biological activity assays. *Colloids and Surfaces B: Biointerfaces,* ***55,*** 143–148.

[151] **Probst, C.E., Zrazhevskiy, P. and Gao, X.** (2011). Rapid Multitarget Immunomagnetic Separation through Programmable DNA Linker Displacement. *Journal of the American Chemical Society,* ***133,*** 17126–17129.

[152] **Smith, J.E., Sapsford, K.E., Tan, W. and Ligler, F.S.** (2011). Optimization of antibody-conjugated magnetic nanoparticles for target preconcentration and immunoassays. *Analytical Biochemistry,* ***410,*** 124–132.

[153] **Elgert, K.D.** (1996). Immunology: Understanding the Immune System, John Wiley & Sons, Inc., US.

[154] **Frank, S.A.** (2002). Immunology and Evolution of Infectious Disease, Princeton University Press, New Jersey.

[155] **Neuberger, T., Schöpf, B., Hofmann, H., Hofmann, M. and Rechenberg, B.v.** (2005). Review: Superparamagnetic nanoparticles for biomedical applications: Possibilities and limitations of a new drug delivery system. *Journal of Magnetism and Magnetic Materials,* ***293,*** 483–496.

[156] **Šafařík, I. and Šafaříková, M.** (1999). Review: Use of magnetic techniques for the isolation of cells. *Journal of Chromatography B,* ***722,*** 33–53.

[157] **Sun, C., Lee, J.S.H. and Zhang, M.** (2008). Magnetic nanoparticles in MR imaging and drug delivery. *Advanced Drug Delivery Reviews,* ***60,*** 1252–1265.

[158] **Španová, A., Rittich, B., Horák, D., Lenfeld, J., Prodělalová, J., Sučiková, J. and Štrumcová, S.** (2003). Immunomagnetic separation and detection of Salmonella cells using newly designed carriers. *Journal of Chromatography A, **1009,*** 215–221.

[159] **Magnetic Separation Technology, Surface-activated Dynabeads,** (2010). Information Booklet of *Dynal Biotech ASA,* Oslo, Norway. Address: http://tools.invitrogen.com/content/sfs/brochures/Surface_Activated_ Dynabeads.PDF

[160] **Xu, H., Aguilar, Z.P., Yang, L., Kuang, M., Duan, H., Xiong, Y., Wei, H. and Wang, A.** (2011). Antibody conjugated magnetic iron oxide nanoparticles for cancer cell separation in fresh whole blood. *Biomaterials, **32,*** 9758-9765.

[161] **Chen, W., Shen, H., Li, X., Jia, N. and Xu, J.** (2006). Synthesis of immunomagnetic nanoparticles and their application in the separation and purification of $CD34^+$ hematopoietic stem cells. *Applied Surface Science, **253,*** 1762–1769.

[162] **Dynabeads M-280 Tosylactivated,** (2004). Information Booklet of *Dynal Biotech ASA,* Oslo, Norway. Address: http://www.bioon.com.cn/picture/20085/200856133737988.pdf

[163] **Mohammed, M.Q.** (2011). Synthesis and characterization of new Schiff bases and evaluation as Corrosion inhibitors. *Journal of Basrah Researches (Sciences),* Vol. ***37,*** No: 4 A/15, 116-130.

[164] **Benada, O. and Pokorný, V.** (1990). Modification of the polaron sputter-coater unit for glow-discharge activation of carbon support films. *Journal of Electron Microscopy Technique, **16(3),*** 235-239.

[165] **Benada, O.** (2012). Personal communication. Laboratory of Molecular Structure Characterization, Electron Microscopy Group, Institute of Microbiology, Academy of Sciences of the Czech Republic, v.v.i., Vídeňská 1083, CZ-142 20 Prague 4, Czech Republic.

CURRICULUM VITAE

Name Surname: Elvan DEMİRBAĞ

Place and Date of Birth: İstanbul, 12.06.1986

E-Mail: elvandemirbag@gmail.com

B.Sc.: Yıldız Technical University, Chemical Engineering Department (2008)

PUBLICATIONS/PRESENTATIONS ON THE THESIS

- Syslová, K., **Demirbağ, E.,** Pankrácová, A., Gajdošová, M., Šimková, K., Kuzma, M., Pelclová, D. and Kačer, P. "Immunomagnetic Molecular Probe with LC-MS: A way for Bronchial Asthma Diagnostics Based on Quantification of Cysteinyl Leukotrienes (A Method for Routine Practice)". *Journal of Chromatography A* (in press).